T.R.
ONDOKUZ MAYIS UNIVERSITY
INSTITUTE OF GRADUATE STUDIES
DEPARTMENT OF MECHANICAL ENGINEERING

INVESTIGATION OF PERFORMANCE IN THE DIFFUSION ABSORPTION REFRIGERATION SYSTEMS DRIVEN BY A LOW GENERATOR TEMPERATURE

PhD Thesis

Muhammed MEHYO

Supervisor

Prof. Dr. Hakan ÖZCAN

II. Supervisor

Assist. Prof. Dr. Engin ÖZBAŞ

SAMSUN
2021

ACCEPTANCE AND APPROVAL OF THE THESIS

The study entitled **"Investigation of Performance in The Diffusion Absorption Refrigeration Systems Driven by a Low Generator Temperature"** prepared by **Muhammed MEHYO** and supervised by. **Prof. Dr. Hakan ÖZCAN** was found successful and unanimously accepted by committee members as PhD thesis of the Department of Mechanical Engineering, following the examination on the date 05/07/2021.

	Title Name Surname **University** **Department**	**Signature**	**Final decision**
Chairman **(supervisor)**	Prof. Dr. Hakan ÖZCAN Ondokuz Mayis University Department of Mechanical Engineering		☒ Acception ☐ Rejection
Member:	Assoc. Prof. Dr. Mustafa ÖZBEY Ondokuz Mayis University Department of Mechanical Engineering		☒ Acception ☐ Rejection
Member:	Assist. Prof. Dr. İbrahim İNANÇ Ondokuz Mayis University Department of Metallurgy and Materials Engineering		☒ Acception ☐ Rejection
Member:	Assist. Prof. Dr. Bilal SUNGUR Samsun University Department of Mechanical Engineering		☒ Acception ☐ Rejection
Member:	Assist. Prof. Dr. Mahmut KAPLAN Amasya University Department of Mechanical Engineering		☒ Acception ☐ Rejection

This thesis has been approved by the committee members that already stated above and determined by the Institute Executive Board.

CONFIRMATION
… / … / …
Prof. Dr. Ali BOLAT
Head of Institute of Graduate Studies

DECLARATION OF COMPLIANCE WITH SCIENTIFIC ETHIC

I hereby declare and undertake that I complied with scientific ethics and academic rules in all stages of my PhD thesis, that I have referred to each quotation that I use directly or indirectly in the study and that the works I have used consist of those shown in the sources, that it was written in accordance with the institute writing guide and that the situations stated in the article 3, section 9 of the Regulation for TÜBİTAK Research and Publication Ethics Board were not violated.

July/2021

Muhammed MEHYO

DECLARATION OF THE THESIS STUDY ORIGINAL REPORT

Thesis Title: Investigation Of Performance in The Diffusion Absorption Refrigeration Systems Driven by a Low Generator Temperature.

As a result of the originality report taken by me from the plagiarism detection program on 03.06.2021 for the thesis titled above;

Similarity ratio : % 19

Single resource rate : % 2 has been released.

07/07/2021

Prof. Dr. Hakan ÖZCAN

ÖZET

DÜŞÜK JENERATÖR SICAKLIĞI İLE ÇALIŞAN DİFÜZYON ABSORBSİYONLU SOĞUTMA SİSTEMLERİNİN PERFORMANSININ İNCELENMESİ

Muhammed MEHYO
Ondokuz Mayıs Üniversitesi
Lisansüstü Eğitim Enstitüsü
Makine Mühendisliği Bölümü
Doktora, Temmuz/2021
Danışman: Prof. Dr. Hakan ÖZCAN

Absorpsiyonlu soğutma sistemlerinin (ASS) ısıtma ve soğutma amacıyla çalıştırmasında yenilenebilir enerji kaynaklarının kullanılması, hem çevrenin korunması hem de enerji tasarrufu açısından avantajlıdır. Ancak bu sistemlerin klasik ısıtma/soğutma sistemlerine göre düşük performans katsayılarına sahip olmaları ve düşük sıcaklıktaki ısı kaynakları için yeterli ısıtma/soğutma yükü sağlayamamaları dezavantaj oluşturmaktadır. Bu çalışmada, DASS'ın özellikle düşük sıcaklıklı ısı kaynakları ile çalışabilen performans katsayılarının geliştirilmesi amaçlanmıştır. Literatürde, ikili çalışma çözümlerine dayalı olarak nanoferrofluidlerin test edilerek incelendiği detaylı bir çalışmaya rastlanmamıştır. Bu nedenle bu çalışma, yeni nanoferrofluidlerin araştırılması ve incelenmesi yönü ile özgündür. Öncelikle, soğutma solüsyonlarının karışımı için termofiziksel analizler yapılmış ve nanoferrofluidler (Fe_3O_4-aseton/$ZnBr_2$ ve Fe_3O_4-NH_3/H_2O) olarak verimlilik özellikleri incelenmiştir. DASS jeneratörünü etkileyen harici bir manyetik alanın varlığında, seçilen nanoferrofluidlerin kullanımının doğrulanması deneysel olarak araştırılmıştır. İnert gaz olarak helyum ile geçerli çözelti kullanılarak DARS performansında elde edilen iyileştirmenin deneysel bir çalışması sunulmuştur. Analizler, 300 ml amonyak/su baz sıvısı içinde % 0.05 (w/w) ve % 0.1 (w/w) Fe_3O_4 nanoparçacık konsantrasyonlarına sahip nanoferrofluidler üzerinde, % 1 (w/w) PVP yüzey aktif maddesinin eklenmesi ile gerçekleştirilmiştir. Dış manyetik alan konsantrasyonlarına ve varlığına/yokluğuna bağlı olarak analizler beş teste ayrılmıştır. Elde edilen analiz sonuçlarına göre, harici manyetik alan altında % 0,1 (w/w) nanoferroakışkan ile DASS, COP, ECOP, sırasıyla % 10.72, % 26.66 ve *f*'de % 2.70 azalma ile en iyi sistem özelliklerini göstermiştir.

Anahtar Kelimeler: difüzyon absorbsiyonlu soğutma sistemi; nanopartiküller; nanoakışkanlar; manyetik nanoakışkanlar.

ABSTRACT

INVESTIGATION OF PERFORMANCE IN THE DIFFUSION ABSORPTION REFRIGERATION SYSTEMS DRIVEN BY A LOW GENERATOR TEMPERATURE

Muhammed MEHYO
Ondokuz Mayis University
Institute of Graduate Studies
Department of Mechanical Engineering
Ph.D, July/2021
Supervisor: Prof. Dr. Hakan ÖZCAN

Using renewable energy sources to run the absorption refrigeration systems (ARSs) for heating and cooling purposes provides good environmental protection and energy-saving opportunity. However, the major disadvantages of these systems comparing to classical heating/cooling systems are their low-performance coefficients, and low-temperature heat sources cannot provide sufficient heating/cooling load. This research aims to develop Diffusion Absorption Refrigeration System (DARS)' performance coefficients that can work especially with low-temperature heat sources. No previous study has tested the nanoferrofluids based on the studied binary working solutions as it is performed in this research. So this work can be considered an investigation of new nanoferrofluids and a continuation of the previous studies. Thermophysical analyses were achieved for the mixture of refrigeration working solutions and examine its efficiency characteristics as nanoferrofluids (Fe_3O_4-acetone/$ZnBr_2$ and Fe_3O_4-NH_3/H_2O). Later, in presence of an external magnetic field that affects the DARS generator, the validation of using the chosen nanoferrofluids was experimentally investigated. Then an experimental study of obtained enhancement in DARS' performance was presented by using the valid solution with helium as an inert gas. The experiments were performed on nanoferrofluids of 0.05 wt.% and 0.1 wt.% Fe_3O_4 nanoparticles concentrations in 300 ml NH_3/H_2O base-fluid with addition 1 wt.% concentration of poly vinyl pyrrolidone (PVP) surfactant, which were equipped to DARS with and without an external magnetic field. Depending on the concentrations and presence or absence of the external magnetic field, the experiments divided into five tests. According to the obtained results of the analyses, DARS with 0.1 wt.% nanoferrofluid under the external magnetic field was the best system with enhancements in Coefficient of Performance (COP), Exergetic Coefficient of Performance (ECOP), reached 10.72%, 26.66%, respectively, and a decrease in Circulation Ratio (f) by 2.70%.

Keywords: diffusion absorption refrigeration system; nanoparticles; nanofluids; magnetic nanofluids.

ACKNOWLEDGEMENT

First of all, it is necessary to gratitude to my almighty Allah for his blessings on me to complete all steps regarding this Ph.D. program. Similarly, it is also impossible to close this research without showing my respect and love for our Hazrat Muhammad (PBUH). Moreover, I am dedicating this achievement to my beloved mother who saw me off to Turkey and continued praying for me every step. I would like to express my sincere gratitude to my advisor Prof. Dr. Hakan ÖZCAN, Department of Mechanical Engineering for the continuous support to my Ph.D. study and related research for his patience, motivation, and immense knowledge. Also. I would like to thanks my second supervisor Dr. Engin ÖZBAŞ for his efforts with me especially to achieve the last section of my research. I could not have imagined having better advisors and mentors for my Ph.D. study. Additionally, I also would like to special thanks to Assoc. Prof. Dr. Mustafa ÖZBEY, and Dr. İbrahim İNANÇ for giving their special attention and well wishes as well as courage during all the steps of this study. Therefore, the suggestions, pieces of advice given by all of them have been remarkable. As my teacher and mentor, they have taught me more than I could ever give them credit here. They have set outstanding examples, how a good scientist (and a person) should be. Their guidance has helped me all the time, during my research and while writing this thesis. I also thank the researchers Abdülvahap ÇAKMAK, and Fevzi ŞAHİN for helping me in my experiments and providing extensive and professional guidance. I have no word to express my feelings for my beloved as well as heartiest friends and brothers Mohamed GHELLAM and Hesham ALRAYESS for giving his extensive support as well as for encouraging me during each difficult step I faced in the last period; thanks, my dears. Similarly, I also would like to express my thanks to them for stimulating discussions, and for all the fun, we have had during the last five years. Nobody has been more important to me in the pursuit of this project than the members of my family. I also like to express my feelings to my father Haitham MEHYO, sisters Farah, Amar, Dounia, and my brother Abdulshafi MEHYO for their prayers and well wishes during my period of stay here. I would like to thank Ondokuz Mayis University for the financial support of the project (PYO.MUH.1904.19.011)

Muhammed MEHYO

TABLE OF CONTENTS

ABBREVIATION OF TERMS ..... **Vİİİ**
LIST OF FIGURES ..... **X**
LIST OF TABLES ..... **Xİİ**
1. INTRODUCTION **1**
1.1. Background and Justification 1
1.2. Research Objectives 4
1.3. Thesis Structure 5
2. LITERATURE REVIEW **8**
2.1. Theoretical Background 8
2.2. Refrigerating Process and Components 10
2.2.1. Absorption Refrigeration Systems (ARSs) 10
2.2.2. DARS Principle and Configuration 12
2.2.3. Optimization Methods of DARS 15
2.3. Main Binary Working Solutions 18
2.3.1. Conventional Working Solutions 19
2.3.2. Nanofluids 24
2.4. Modeling of DARS 28
3. MATERIALS AND METHODS **33**
3.1. Studied Working Solutions 33
3.1.1. Fe_3O_4 – acetone/$Znbr_2$ Nanoferrofluid 33
3.1.2. Preparation of Fe_3O_4 – acetone/$Znbr_2$ 35
3.1.3. Fe_3O_4 - NH_3/H_2O Nanoferrofluid 36
3.1.4. Preparation of Fe_3O_4 - NH_3/H_2O 39
3.1.5. Sources of the Materials 40
3.2. Diffusion Absorption Refrigeration Machines 40
3.2.1. Experimental Diffusion Absorption Refrigeration Device Setup 43
3.2.2. Uncertainty Analysis and Propagation 45
3.2.3. Thermodynamic Analysis 45
4. RESULTS AND DISCUSSION **52**
4.1. Fe_3O_4 – acaetone/$ZnBr_2$ Nanoferrofluid Analyses Results 52
4.1.1. Stability of Fe_3O_4 – acaetone/$ZnBr_2$ Nanoferrofluid 52
4.1.2. Thermophysical Properties 56
4.1.3. Thermal Conductivity 61
4.1.4. Vapor Pressure 63

4.2. Fe_3O_4 _ H_2O/NH_3 Nanoferrofluid Analyses Results 64
4.2.1. Stability of Fe_3O_4 _ H_2O/NH_3 Nanoferrofluid 64
4.2.2. Thermophysical Properties 69
4.2.3. Thermal Conductivity 72
4.3. Validation Investigation of Using acetone/$ZnBr_2$ as a Working Solution In DARS 74
4.4. The Valid Working Solution Characteristics 76
4.5. The Effect of Using Various Placements of Permanent Magnets Around the Generator-Bubble Pump Component on Heat Transfer 77
4.6. Mechanistic Explanation of Heat Transfer Enhancement 79
4.7. Various Nanoferroflid Concentrations Effects Under the Same Conditions of DARS Cycle 80
4.8. Thermodynamic Analysis Results 86
4.8.1. Energy Analysis Results 90
4.8.2. Exergy Analysis Results 93
4.9. Comparative Discussion of Exergy and Energy Efficiencies 95
5. CONCLUSION AND RECOMMENDATIONS **96**
5.1. Conclusion 96
5.2. Recommendations 100
REFERENCES **102**
CURRICULUM VITAE **116**
PUBLISHED STUDIES **116**

ABBREVIATION OF TERMS

SHE	Solution Heat Exchanger
GHX	Gas Heat Exchanger
RHE	Refrigerant Heat Exchanger
PHE	Plate Heat Exchanger
DARS	Diffusion Absorption Refrigeration System
ARS	Absorption Refrigeration System
CHP	Combined Heat And Power Generation
CFD	Computational Fluid Dynamics
g	Effectiveness Ratio
COP	Coefficient of Performance
ECOP	Exergetic Coefficient of Performance
f	Circulation Ratio
CNT	Carbon Nanotube

Symbols

$\dot{Q}$	Heat transfer rate (kJ s^{-1})
T	Temperature (^{o}C)
$\dot{m}$	Mass flow rate (kg s^{-1})
E	Specific exergy (kJ kg^{-1})
h	Specific enthalpy (kJ kg^{-1})
s	Specific entropy (kJ kg^{-1} K^{-1})

Subscripts

ig	Inert gas
ws	Weak working solution
rs	Rich working solution
gen	Generator
cond	Condenser
evap	Evaporator
rect	Rectifier
pip,r	pipelines and reservoir
dest	Destruction

co	Coolant
sol	Working solution
$ZnBr_2$	Zinc Bromide
H_2O	Water
NH_3	Ammonia

LIST OF FIGURES

Figure 1.1. Comparison of vapor compression systems, conventional ARSs, and DARS 2

Figure 1.2. The flow chart of the research..... 7

Figure 2.1. Principle of DARS.....14

Figure 2.2. A simple schematic of the bubble pump configuration..... 15

Figure 2.3. Flowchart for producing nanofluids, (Bhattad et al., 2018) 25

Figure 3.1. Experiments device: (a) Front and (b) Back.....43

Figure 3.2. Schematic diagram of the experiments set (DARS and the auxiliary equipment) with an external magnetic field: 1, main Helium storage tank; 2, pressure-control valve; 3, electromagnetic valve; 4, PID regulator; 5, Helium gas reservoir; 6–10, needle valves; 11, pressure signal device; 12, check valve; 13, DARS (test device); 14, magnetic field device; 15, vacuum pump; 16, working solution vessel; 17, Heater; 18, pressure sensor; 19, temperature sensor (an example of all temperature sensors); 20, data acquisition computer; T, temperature signal. P, pressure signal..... 44

Figure 3.3. Schematic diagram of the experimental DARS with measurement points 46

Figure 4.1. Color changes of acetone/$ZnBr_2$ solution samples with several concentrations by the time 52

Figure 4.2. Sedimentation and agglomeration of varies concentrations of Fe_3O_4 nanoparticles in acetone/$ZnBr_2$ base-fluid. 1–0.05 wt.%; 2–0.1 wt.%; 3–0.15 wt.%; 4–0.2 wt.% (with 2 h sonication). 5–0,1 wt.% (without sonication) 54

Figure 4.3. Effects of using different surfactants on the stability of nanoferrofluid (Fe_3O_4 - acetone/$ZnBr_2$) over time 55

Figure 4.4. Various SEM images of Fe_3O_4 nanoparticles suspension in the acetone/$ZnBr_2$ solution on a carbon film show randomly dispersed particles without any magnetic field 56

Figure 4.5. Changes of the nanoferrofluid density with different Fe_3O_4 nanoparticles mass fraction, experimentally and theoretically 58

Figure 4.6. Changes of the nanoferrofluid viscosity with different Fe_3O_4 nanoparticle mass fraction. 59

Figure 4.7. Changes of the nanoferrofluid specific heat capacity with different Fe_3O_4 mass fraction, experimentally and theoretically 61

Figure 4.8. Changes of the nanoferrofluid thermal conductivity with different Fe_3O_4 mass fraction, experimentally and theoretically 63

Figure 4.9. The plotted (*log p, T*) diagram of acetone/$ZnBr_2$ shows several concentrations of $ZnBr_2$ (wt.%) by Ajib and Karno, (2008) 64

Figure 4.10. Sedimentation and agglomeration of varies concentrations of Fe_3O_4 nanoparticles in NH_3/H_2O base-fluid. 1–0.1 *wt*.% (with 2 h sonication); 2–0.05 *wt*.%; 3–0.1 *wt*.%; 4–0.15 *wt*.%; 5–0.2 *wt*.% (with 2 h sonication). 5–0,1 *wt*.% (without sonication)..... 67

Figure 4.11. Effects of using different surfactants on the stability of nanoferrofluid (Fe_3O_4-NH_3/H_2O) over time 68

Figure 4.12. Various SEM images of Fe_3O_4 nanoparticles suspension in the NH_3/H_2O solution on a carbon film show randomly dispersed particles without any magnetic field 69

Figure 4.13. Changes of the nanoferrofluid density with different Fe_3O_4 nanoparticlesmass fraction, experimentally and theoretically 70

Figure 4.14. Changes of the nanoferrofluid viscosity with different Fe_3O_4 nanoparticle mass fraction 71

Figure 4.15. Changes of the nanoferrofluid specific heat capacity with different Fe_3O_4 mass fraction, experimentally and theoretically 72

Figure 4.16. Changes of the nanoferrofluid thermal conductivity with different Fe_3O_4 mass fraction, experimentally and theoretically (depending on Maxwell's equation) 74

Figure 4.17. Pressure-Temperature diagrams of pure acetone and pure ammonia, (Engineering ToolBox 2021) 76

Figure 4.18. Schematic diagram of DARS with three different placements of the permanent magnets around the generator-bubble pump component 78

Figure 4.19. Measured temperatures in the $DARS_{0.0\%,ref.}$ at the measuring points of the cycle over time 83

Figure 4.20. Measured temperatures in the $DARS_{0.05\%}$ at the measuring points of the cycle over time 83

Figure 4.21. Measured temperatures in the $DARS_{0.05\%.Ma.}$ at the measuring points of the cycle over time 84

Figure 4.22. Measured temperatures in the $DARS_{0.1\%}$ at the measuring points of the cycle over time 84

Figure 4.23. Measured temperatures in the $DARS_{0.1\%.Ma.}$ at the measuring points of the cycle over time 85

Figure 4.24. Measured internal temperature in the cooled areas of the $DARS_{0.0\%,ref.}$, $DARS_{0.05\%}$, $DARS_{0.05\%,Ma.}$, $DARS_{0.1\%}$, and $DARS_{0.1\%,Ma.}$ cycles over time 85

Figure 4.25. Measured pressure of the $DARS_{0.0\%,ref.}$, $DARS_{0.05\%}$, $DARS_{0.05\%,Ma.}$, $DARS_{0.1\%}$, and $DARS_{0.1\%,Ma.}$ cycles over time 86

Figure 4.26. Comparative heat transfer rates values of the different components for the studied system 91

Figure 4.27. Relative values of heat transfer rates of the different components for the studied systems 92

Figure 4.28. Relative values of exergy destruction of the different components for the studied systems. 94

Figure 4.29. Comparative exergy and energy efficiencies of the different components for the studied systems 95

LIST OF TABLES

Table 2.1. Examples of low-capacity commercial ARSs, (Orhan and Güngör, 2012) 11

Table 2.2. Summary of some previous studies that have investigated different kinds of refrigeration working solutions 21

Table 2.3. Summary of the used nanofluids in ARSs and DARSs 30

Table 4.1. The density of acetone/$ZnBr_2$ with various concentrations of acetone as measured experimentally in this study at 25 °C and in similar studies 57

Table 4.2. The density of the Fe_3O_4-acetone/$ZnBr_2$ (50 wt.% $ZnBr_2$) with various concentrations of Fe_3O_4 indicated experimentally and theoretically in this study at 25 °C 57

Table 4.3. The viscosity of the Fe_3O_4-acetone/$ZnBr_2$ (50 wt.% $ZnBr_2$) with various concentrations of Fe_3O_4 indicated experimentally in this study at 25 °C 58

Table 4.4. The specific heat capacity of the Fe_3O_4-acetone/$ZnBr_2$ (50 wt.% $ZnBr_2$) with various concentrations of Fe_3O_4 indicated experimentally and theoretically at 25 °C 60

Table 4.5. The thermal conductivity of the Fe_3O_4-acetone/$ZnBr_2$ (50 wt.% $ZnBr_2$) with various concentrations of Fe_3O_4 indicated experimentally and theoretically in this study at 25 °C 62

Table 4.6. The specific heat capacity of the Fe_3O_4-NH_3/H_2O (50 *wt.*% $ZnBr_2$) with various concentrations of Fe_3O_4 indicated experimentally and theoretically at 25 °C 72

Table 4.7. Thermal conductivity of the Fe_3O_4- NH_3/H_2O (25 % ammonia) with various concentrations of Fe_3O_4 indicated experimentally and theoretically in this study at 25 °C 73

Table 4.8. Measured parameters in the different tests at the measuring points of the cycle 87

Table 4.9. Calculated values of (x) in the different systems at the measuring points of the cycle 89

Table 4.10. Calculated values of mass flow rates (m) in the different systems at the measuring points of the cycle 89

Table 4.11. The results of the energy and exergy analyses and circulation ratio of the tested different systems 90

Table 4.12. The results of the exergy analyses of the tested systems 93

1. INTRODUCTION

1.1. Background and Justification

The increase in energy costs and especially in the countries that import large amounts of energy such as our country attach great importance to the efforts towards the energy supply security, efficient use of this energy, diversification of its resources, and maximum utilization of domestic resources. In our country, a significant part of the electrical energy is obtained from fossil fuels, that is meaning paying huge amounts of foreign currency. Therefore, encouraging the use of cooling systems that use heat energy (waste heat or solar energy) as primary energy instead of electrical energy can make an important economic contribution to Turkey. In addition, the achieved savings in the utilization of fossil fuel resources will bring advantages such as environmental protection. Recently, a huge need for refrigerating and air-conditioning accompanied with a large amount of low-quality energy from low-grade energy sources such as geothermal energy, solar heat, and waste heat from industrial processes, pushes the researchers to think seriously in investigating into utilizing these sources for cooling using heat-driven absorption systems. An attractive type of these absorption systems is DARS, due to its bubble pump which doesn't need any electricity to run. Von Platen and Munters (1920) invented the DARS in the 1920s. The DARS depends on the application of a limited amount of heat, and it is commonly used in domestic refrigerators, caravans, recreational vehicles, especially hotel rooms, camps, and promising use in war zones, (Sözen et al., 2015).

Figure 1.1. shows a brief explanation of the differences between the vapor compression system and a conventional ARS and DARS. It can be realized from it that the most crucial disadvantage of DRESs can be shown as their low COP values. Thus there is no sufficient heating/cooling load in the low-temperature heat resource. In the literature, many opinions have been presented about the utilization of a low-temperature heat resource to operate the absorption heating/cooling machine. In these studies, the effect of heat transfer rate, working solution, refrigerant, and the fluid temperature was used to improve the system. It was concluded that COP and ECOP values increase with the increase of generator and evaporator temperatures. Therefore, improving the properties of working solutions is necessary to improve the

efficiency of this kind of cycle when low-temperature heat sources are utilized. DARS technology seems to be interesting. Because it has advantages in small cooling capacities compared to conventional vapor compression. These advantages can be listed as the absence of no moving parts, noiseless operation, low cost, and ability to be run by alternative energy or waste heat resources. However, this technology approximately has 40% less efficient than conventional ARSs. From different studies that have been analyzed these kinds of systems, it can be concluded that the most important parameters affecting the energy efficiency of the system are the flux regime and activation temperature. Commercially, the most common working mixture is ammonia-water and hydrogen or helium as auxiliary gas. However, different mixtures should be studied to increase efficiency and find different input energy resources such as solar power. Therefore, It is important to spread this technology further in order to stimulate the research interest and the quest to improve system effectiveness. In this context, more research is needed to use new solution pairs to increase system effectiveness and to improve the performance of existing-working solution pairs.

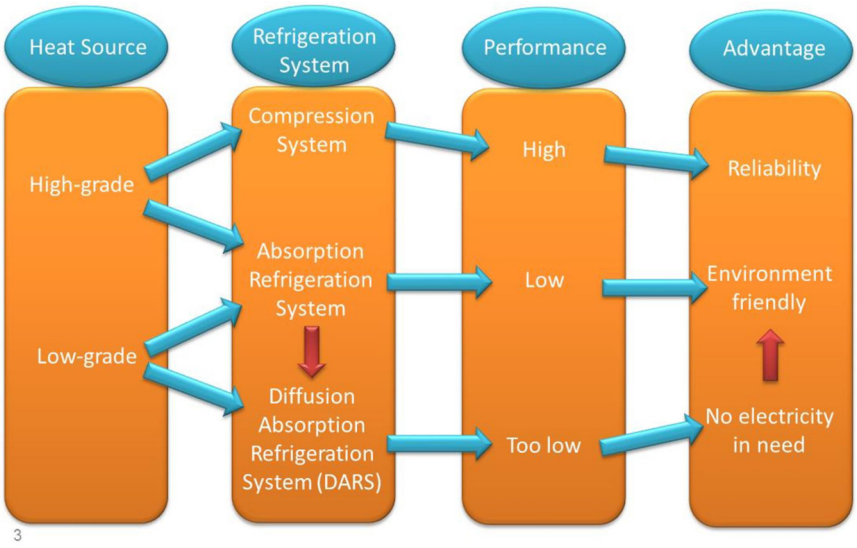

Figure 1.1. Comparison of vapor compression systems, conventional ARSs, and DARS

Newly, Refrigeration binary working solutions that have dispersed nanoparticles (called nanofluids) or hybrid nanofluids have acquired an interest in conventional ARS and DARS because of their excellent thermophysical properties which make it

used in these kinds of systems with many studies for performance improvement, (Lee et al., 2010; Yang et al., 2011; Wu et al., 2010; Cuenca et al., 2014; Sözen et al., 2015; Mohammed et al., 2020). The type, content, size of nanoparticles, temperature, and distribution stability are key parameters affecting the thermal conductivity of nanofluids. The working solution thermal performance increase significantly by increasing the stability of the nanofluids which in turn is affected by the type and size of the used nanoparticle the addition of surfactants. A unique type of nanofluids is nanoferrofluids. Comparing with the other nanofluids, the features and advantages of nanoferrofluid are fundamentally incarnated in the following aspects, (Kim et al., 2007):

1. Nanoferrofluids contain ferromagnetic nanoparticles that exhibit higher thermophysical properties, (Nourafkana et al., 2017; Hodenius et al., 2008).
2. Nanomagnetic fluids are novel functional fluid materials containing a solid/liquid mixture in which nanomagnetic particles (diameter <100 nm) are dispersed equally throughout a base-binary working solution to merge the magnetic features of solid magnetic materials and the flow properties of fluid materials, (Hodenius et al., 2008).
3. The literature has shown that a magnetic fluid in incorporation with an external magnetic field can be utilized as a new kind of heat transfer medium to considerably improve and handle the heat transfer operation, (Ranjan et al., 2004; Li et al., 2009; Yu et al., 2010).
4. There have been also different investigations searching for the ability of nanoferrofluids for enhancing mass transfer rates, thus increasing the circulation ratio in the refrigeration cycle, (Srinivas et al., 2007; Olle et al., 2006).

In the literature, researchers focus on how to improve the design and properties of the working fluid. The utilization of nanofluids improves the vapor absorption process and condensation heat transfer coefficients as well as boiling temperatures. This is helps to develop a system that is more compact, lighter, and consumes less thermal power, thus consuming less energy in general. It is necessary to investigate the utilization of nanoparticles with conventional working solutions, condensation, and boiling heat transfer phenomena based on many thermophysical properties due to the phase change process in the cooling system. Improving these properties leads us

to improve the overall cycle, and this study can be used to increase the effectiveness of the chosen system (DARS).

1.2. Research Objectives

Although DARSs have many advantages over mechanical vapor compression systems, the biggest disadvantages are low COP values and the inability to provide sufficient cooling load at low-temperature heat resources. The main aim of this study is to improve the performance of DARS (COP, ECOP, and f) by utilizing nanoferrofluids as low-temperature working solutions. In order to optimize the system performance, all aspects meant by this improvement, traceable success criteria are defined in the following sections of the study. Where the validation of using nanoferrofluids (Fe_3O_4-acetone/$ZnBr_2$ and Fe_3O_4-NH_3/H_2O) in DARS is investigated. Then an experimental and numerical investigation of obtained enhancement is presented in DARS' performance by using the valid solution with helium as an inert gas in accompanying with an external magnetic field. Also, the effect of performing this mechanism on the heat and mass transfer improvement in the system's generator-bubble pump component is examined. Thus, its effects on the performance of the DARS, in general, have investigated. Some mechanical modifications have been performed to install the magnate poles for creating the external field around the bubble pump which is necessary to provide significant stability of the valid nanoferrofluid.

No previous study has tested the nanoferrofluids based on the studied binary working solutions as it is performed in this work. So this work can be considered an investigation of new nanoferrofluids and a continuation of the previous studies. Consequently, a thermal study with the valid nanoferrofluid at the low generator temperature has not been investigated before to improve the performance of DARS.

To approach the above-mentioned main objective, more specific objectives were put forward as follows:

1. To review the absorption refrigeration technologies and working fluids with assurance on acetone/$ZnBr_2$ and NH_3/H_2O base-fluids. The main criteria for working fluids selection were also reviewed.
2. To achieve thermophysical analyses of working solutions of (Fe_3O_4-acetone/$ZnBr_2$ and Fe_3O_4-NH_3/H_2O) and examine its efficiency

characteristics as new nanoferrofluids. As a multi-factor experimental study is designed the experiments to see how the various concentrations of the nanoferrofluid mixture components affect their properties (thermal conductivity, density, dynamic viscosity, and specific heat capacity) then choose the optimal mixture for utilization in DARS driven by a low temperatures source.

3. To modify some mechanical parts around the bubble pump of DARS according to the necessity of creating the wanted external magnetic field.
4. To examine the validity of using the studied working solutions in DARS then investigate the performance of the system with the valid working solution firstly without the nanoparticles then with nanoparticles and under the magnetic field.
5. To determine the enhancement in COP, ECOP, and f of DARS because of the utilization of the new nanoferrofluid.
6. To establish the theoretical background to analyze the efficiency characteristics for chosen working solutions firstly without the nanoparticles then with nanoparticles in the laboratory-scale DARS that can operate at different low-temperature sources and confirm the numerical results with the experimental study ones.

1.3. Thesis Structure

In light of the flow chart which is shown in Figure 1.2. the works in this thesis can be divided into the following performed steps:

Step 1 is consecrated in explaining the background and justifications of this research that raise the prompting and objectives of this thesis.

Step 2 attended a literature review of the absorption refrigeration technologies which have been studied before especially those the closest to the main subject of the current research. In this chapter, the basic characterization of DARS was described in comparison with vapor compression refrigeration systems. Moreover, the operation precept of basic absorption systems, the working solutions usually utilized in ARS, and the prime needs of the working solutions were analyzed. The nanofluid mixtures and nanoferrofluid ones that are used for absorption refrigeration applications were also mentioned. Finally, a brief description of the COP evaluation and its

optimization methods (experimentally and numerically) which have studied untill performing this research, particularly those are depending on data for pre-selection and properties enhancement of working solutions were applied.

Step 3 thermophysical analyses were achieved for the mixture of working solution of (Fe_3O_4 – acetone/$ZnBr_2$) and examine its efficiency characteristics as a nanoferrofluid. Where it shows an investigation of (Fe_3O_4 - acetone/$ZnBr_2$) as a nanoferrofluid containing the preparation, stability, structure, and properties. As a multi-factor experimental study is designed the experiments to see how the various concentrations of the nanoferrofluid mixture components affect their properties (thermal conductivity, density, dynamic viscosity, and specific heat capacity).

Step 4 in this part of the research, the visual inspection of Fe_3O_4 nanoparticles stability, which are dispersed in the NH_3/H_2O base-fluid by using a mechanical method, is performed. Thermophysical analyses (density, specific heat capacity, dynamic viscosity, and thermal conductivity) were achieved to give a base for finding the optimal mixture of working solution of (Fe_3O_4-NH_3/H_2O) and examine its efficiency characteristics as a nanoferrofluid as a candidate binary solution for use in DARS driven by different low-temperatures sources.

Step 5 in this part of the research aimed for studying the validation of using nanoferrofluids (Fe_3O_4-acetone/$ZnBr_2$ and Fe_3O_4-NH_3/H_2O) in DARS, then presenting an experimental and theoretical investigation of obtained enhancement in DARS' performance by using the valid solution with helium as an inert gas in accompanying with an external magnetic field, hence illustrating the effect of performing this mechanism on the heat and mass transfer improvement in the system's generator. The energy and exergy analyses are completed for each component, including the gas heat exchanger, numerically, and experimentally. Where REFPROP 8.0 software was used for modeling the cycle and calculating the properties of the different studied points of the cycle.

Step 6 epitomized the main results in this thesis and awarded an overview of the future work required.

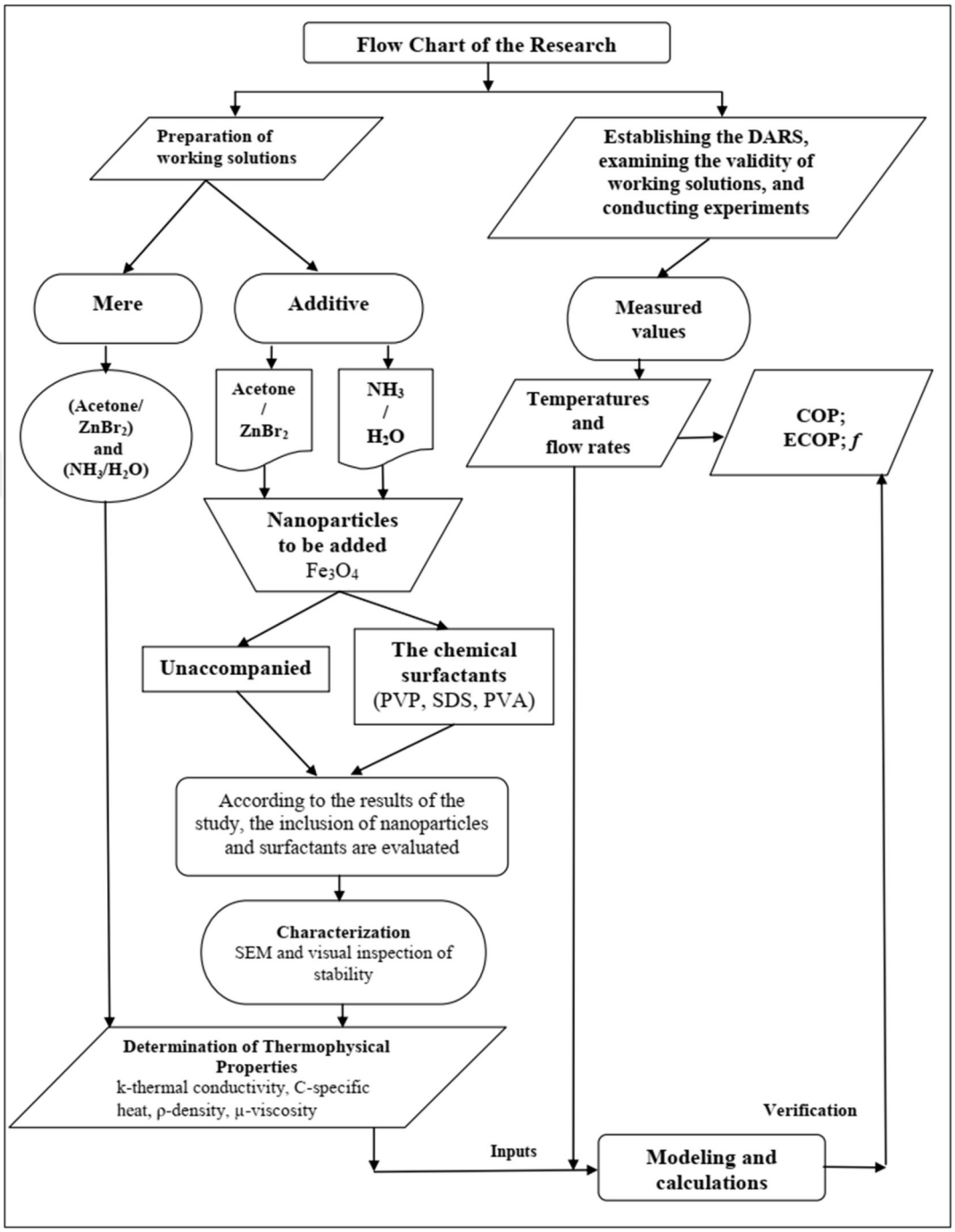

Figure 1.2. The flow chart of the research

2. LITERATURE REVIEW

2.1. Theoretical Background

Recently, scientists are working on issues such as increasing in the energy costs, depletion of fossil fuels and the environmental risks caused by the use of these fuels, researching and developing alternative energy sources, increasing the efficiency of the existing energy systems and energy-saving processes using renewable energy resources, such as solar energy and geothermal., and waste heat from industrial processes in order to run the absorption refrigeration systems for heating and cooling purposes, provide a good opportunity for both environmental protection and energy saving. The dependence of the absorption systems on electrical energy is between 2% and 9%, whereas the primary energy is heat energy (waste heat or solar energy, etc.). An attractive type of these absorption systems is DARS, due to its bubble pump which doesn't need any electricity to run. Von Platen and Munters, (1928) invented the DARS in the 1920s. The DARS based on the application of limited quantities of heat, and it is usually utilized in home refrigerators, caravans, recreational vehicles, especially residences rooms, camps, and promising utilize in war zones, (Sözen et al., 2015). However, the major disadvantages of these systems comparing to classical heating/cooling systems are their low-performance coefficients, and low-temperature heat sources cannot provide sufficient heating/cooling load. In the literature, condensation heat retrieval., absorption heat retrieval., condensation-absorption heat retrieval., multistage cycle applications, usage of different fluid pairs, and design changes are investigated in absorption systems to improve the cooling coefficients. These improvements may be obtained by enhancing the design of system components initially doing modifications on heat exchangers and then using new types of working fluids (nanofluids) with improved thermal properties. For the first methods, recently, many improved compact kinds of heat exchangers are utilized like a shell and tube kind heat exchangers, microchannel heat exchangers, plate form heat exchangers, etc.

Nanofluids are defined as a colloidal mixture of suspended particles of nanopowder (dimension of nanometer-scale) in a conventional refrigeration working solution as a base-fluid, (Bhattad et al., 2018). The base-fluid may be ethanol, water, water-based brine, glycol, coolant, lubricant, oil, etc. Nanoparticles may be different

metals or metal oxides, different types of carbon, metal carbides, and ceramics. Newly, the nanofluids with graphene nanoparticles have obtained special interest because of various excellent advantages of graphene depending on the low density, extraordinary high thermal conductivity, bigger specific surface region, and extraordinary anti-friction features, (Rasheed et al., 2016). Additionally to conventional nanofluids, newly hybrid nanofluids have obtained interest as a formidable enhancement of heat transfer features could be because of the synergistic influence occasion by crossbreeding, (Sarkar et al., 2015). Depending on suspended nanoparticle synthesis, the nanofluids may be generally presented in three sets:

a) Mono-nanofluids, consist of the same nanoparticles in base-fluid.
b) Hybrid nanofluids consist of dissimilar nanoparticles in base-fluid (solid or/and phase-variation materials).
c) Hybrid nanofluids consist of built-up nanoparticles in base-fluid (either solid materials or solid and phase-variation materials).

Heat transmit properties of refrigeration working mixtures utilizing nanoparticles are influenced through thermal conductivity enhancement and different mechanisms like Brownian motion, Brownian diffusion, dispersion, sedimentation, agglomeration, ballistic phonon transport, solid/liquid interface layer, and thermophoresis. The proportional motion among the nanoparticles and base-fluid is the major cause behind this enhancement, where occasioned by the circulation of the nanoparticles, moving the heat along an oblique solution consequencing extremely small convection created by the motion of the solution around the nanoparticles, (Pinto and Fiorelli, 2016). A unique type of nanofluids is nanoferrofluids. Nanoferrofluids content ferromagnetic nanoparticles that exhibit higher thermophysical properties, (Nourafkana et al., 2017; Hodenius et al., 2008).

This work presents a literature review of nanofluids in DARSs. Many investigations are discussed various kinds of refrigeration working mixtures as conventional solutions without added nanoparticles, then research on nanofluids and nanoferrofluids, and utilized various methods for improvement of absorption processes. Furthermore, a brief is achieved for an explanation of the cooling process and components, DARS and bubble pump configurations, and modeling studies of the DARS in literature. The literature summary is given in the following paragraphs in parallel with our subject areas, which are the basic work packages of it and mentioned above.

2.2. Refrigerating Process and Components

The most common refrigeration systems are mechanical vapor compression systems that are driven by electrical energy. Absorption chillers present an alternative approach, thus thermal energy is the operating energy. Thermal energy is commonly obtained from industrial waste heat, renewable energy resources, and other conventional thermal resources. Moreover, ARSs use natural working solutions, which have not harmful effects on the ozone layer, (Kaynakli and Kilic, 2007; Sozen, 2001; Saravanan and Maiya, 1998; Sun, 1998). Briefly, probability expectations related to the environmental benefits of thermally-driven ARSs are founded on, (Keppler, 2018):

- Essential energy savings are gained by utilizing directly thermal energy instated of electrical energy as running power, especially waste heat energy, the thermal energy that resulted from CHP, and from renewable energy resources.
- Ability to utilize available-heat capacities in summer times.
- Extremely sharing to reduce the peak loads in electricity networks in the summertime, where the major reason for this high required electricity loads are conventional vapor compression cooling systems.

2.2.1. Absorption Refrigeration Systems (ARSs)

Since 1970, many types of research have been carried out on absorption cooling machines for cooling and air-conditioning using solar energy and other low-temperature sources. Especially in recent years, as well as the development and installation of cooling machines powered by solar energy, their performance has also been evaluated. These developments are described and demonstrated in the open literature. The results of this study show that is an economical technology, ecologically, and technically promising in the near future. Ajib and Karno, (2008) examined a novel working solution to be utilized in solar heat ARSs. They examined the thermophysical properties of the novel refrigeration working mixture acetone/$ZnBr_2$ and tested it in ARS and the consequences assured the implementation of this novel working mixture. Ruiz et al.,. (2006) have investigated the effectiveness

of H_2O/LiBr absorption cooler running by the thermal energy which is obtained from PHEs. They calculated the heat transfer performance in desorber, condenser, and the solution heat recover using the equations provided in the literature for evaporation, condensation, and liquid-to-liquid heat transfer in PHEs. In the study, when the cooling capacity obtained is between 2 kW and 12 kW; COP values have been shown to vary between 0.5 and 0.8. Kaynakli and Kilic, (2007) presented an exhaustive thermodynamic analysis of H_2O/LiBr absorption cooling system. In this study, the effect of running temperature and heat exchanger effectiveness on thermal loads, COP and ECOP, and *g* of the parts were investigated. They presented that the ECOP and COP values increased with rising the generator and evaporation temperature but decreased with the increase of the condenser and absorber temperatures. In addition, it has been observed that the *g* rate changes as these temperatures change. Furthermore, The performance of the working mixture and cooler exchanger, the efficiency of the cycle, and its effect on mixture temperatures were compared. Results showed that SHE has a greater influence on the tested parameters than RHE. While SHE raises the COP value to a maximum of 44%, RHE has only 2.8%. Table 2.1. shows some examples of low-capacity commercial absorption systems and water absorption coolers using water as a refrigerant. According to this table, the COP values obtained with these working solution pairs vary between 0.56-0.7.

Table 2.1. Examples of low-capacity commercial ARSs, (Orhan and Güngör, 2012)

Cycle	**Absorber**	**Refrigerant**	**Cooling power (kW)**	**Heat source temperature (^oC)**	**Design conditions and nominal COP**
Absorption	Silica gel	Water	70	55-90	T_g=75 ^oC; T_c=29 ^oC; T_e=9 ^oC; COP=0.60
Absorption	Silica gel	Water	67	55-95	T_g=90 ^oC; T_c=29 ^oC;

Absorption	Silica gel	Water	15	55-90	T_e=7 °C; COP=0.65
Absorption	Silica gel	Water	7.5	55-90	T_g=75 °C; T_c=27 °C; T_e=18 °C; COP=0.56
Absorption	Lithium Bromide	Water	35	80-100	T_g=75 °C; T_c=27 °C; T_e=18 °C; COP=0.56
Absorption	Lithium Bromide	Water	15	75-95	T_g=87 °C; T_c=30 °C; T_e=9 °C; COP=0.70
Absorption	Ammoniac	Water	100	> 90	T_g=85 °C; T_c=30 °C; T_e=12 °C; COP=0.70
					T_c=32 °C; T_e<2 °C; COP=0.64

2.2.2. DARS Principle and Configuration

As is mentioned before, Von Platen and Munters, (1928) invented DARS in 1920s. DARS is widely utilized in household refrigeration, caravans, camps, recreational vehicles, especially residences rooms and offices, as it allows the use of limited heat and silent running. The most important disadvantage of this type of system is its low efficiency. Refrigerators traditionally founded on this technology and offering a refrigerating capacity of 200 to 400 W have COP values between 0.2 and 0.25. Therefore, over the years, studies have been conducted to achieve a considerable enhancement in energy effectiveness for household appliances (Narayankhekar et al., 1985; Gutiérrez 1998; Smirnov et al., 1996). However, the highest COP has detected is 0.3. Bubble pump is the most investigated part of DARSs due to its positive effects on the energy effectiveness of the cycle. Other

investigations have shown that geometrical parameters and the features of the heat influx system are factors affecting the system effectiveness, (Shelton et al., (2002); Benhmidene et al., 2011a, 2011b); Dammak et al., 2010; Abu-Mulaweh et al., 2011; Abduwadood et al., 2012). Pfaff et al., (1998) suggested that the LiBr/H_2O solution may be utilized as the working mixture for DARS. In order to operate the bubble pump, an inlet temperature between 66 ^oC and 78 ^oC is required in the generator, which makes this mixture attractive for solar cooling systems. Acuna et al., (2013) combined the $NH_3/LiNO_3$ mixture and their consequences confirmed that this mixture lowers the activation temperatures. In addition, the effectiveness of $NH_3/LiNO_3$ mixture is almost 50% better than conventional NH_3/H_2O mixtures and 27% better than NH_3/NaSCN under the same process conditions. Infante Ferreira, (1984) developed relations to describe the thermophysical properties of $NH_3/LiNO_3$ and NH_3/NaSCN. Koyfman et al., (2003) performed an experimental investigation utilizing R22/DMF as a refrigeration working mixture. In the generator, it was achieved running temperatures between 50 ^oC and 90 ^oC and evaporation temperatures below 0 ^oC and a COP value reached 0.35. Zohar et al., (2009) included R32, R124, R125, and R134 coolants in their test utilizing DMF as an absorber for each case. The study presented that these mixtures could be operated at low temperatures (150 ^oC), this situation resulted in a low COP, higher condensation, and higher evaporation temperatures compared to the NH_3/H_2O mixture. Ezzine et al., (2010) showed that R124/DMAC is a valid binary working solution as a result of their study. Because of lower vapor pressure and activation temperature between 80 ^oC and 180 ^oC, that has been achieved with DMF. This makes them ideal as it can be run by solar energy, geothermal., waste heat, and others. Singh et al., (2019) have studied thermodynamic modeling and analysis of DARS runs by solar energy with NH_3/H_2O and helium as a pressure-equalizing inert gas. The results showed the decrease in COP is 2.8% higher than the refrigerating capacity reduction at low running temperature while there is no minor decrease at a higher temperature.

2.2.2.1. Cooling Process and Components

DARS consists of the next major components: a generator (includes bubble pump), condenser, evaporator, SHE, GHX, tank, and absorber. These kinds of

systems usually are divided into three main operation circuits as followed: refrigeration circuit, gas circuit, and dissolution circuit. The circuits run under Dalton's law precept founded on fractional pressures and the pressure in every main part of the system is preserved steady utilizing an auxiliary gas. DARS runs at two various pressure values while in process, identical to conventional cooling devices in this aspect, (Rodríguez-Muñoz and Belman-Flores, 2014).

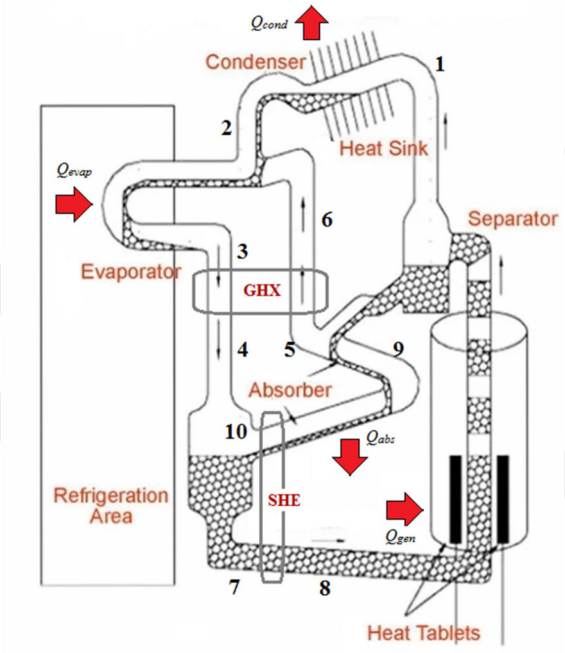

Figure 2.1. Principle of DARS

As is shown in Figure 2.1., Q_{gen} is supplied by heat tablets to the mixture which has a high level of coolant and passes from the reservoir (8). Heating creates vapor bubbles that go up through the tube carried a little amount of fluid finally these bubbles are detached. The weak mixture (9) fluxes across SHE where it gives up thermal energy to the rich mixture in the coolant (7) and is then forwarded to the absorber (10). The rich coolant (1) goes on to the condenser, thus it is condensed by extracting Q_{cond} from it then passing to the evaporator (2). Because the evaporator is full gas (6) the fluid's partial pressure drops quickly and as a consequence, the liquid starts evaporating, the cooling effect is obtained and Q_{evap} is absorbed. The moment that out of the evaporator, (3), the heat exchanges between the rich mixture and coolant and GHX, whose purpose is to minimize the temperature of the gas (4) to send it to the reservoir. In the absorber, the coolant is absorbed by the salt of the

mixture, and thermal energy Q_{abs} is released either by the cooling cycle or by the ambient effect; while the gas has a lower density than the coolant, it is detached (5) and passed back to the GHX to go on the cycle and the cooling effect.

2.2.2.2. Bubble Pump Configuration

Basically, there are two kinds of the thermosiphon precept, the single-phase and the two-phase precept. Both of them are founded on variations in solution density. In the following, just the two-phase thermosiphon precept is debated which is the operation precept of bubble pumps. Partly evaporation of the solution causes form vapor bubbles that lift the liquid. The main precept of a bubble pump is illustrated schematically in Figure 2.2. a vertical tube and a separator reservoir at its end with a horizontal connection form the bubble pump configuration, (Bierling et al., 2019).

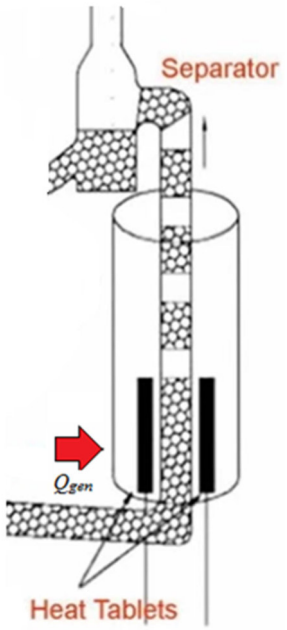

Figure 2.2. A simple schematic of the bubble pump configuration

2.2.3. Optimization Methods of DARS

Absorption systems have low COP and ECOP values (especially DARS). Furthermore, ARSs are more expensive than compression ones, also need

thermodynamic and economic optimization, (Misra et al., 2006). For this reason, the literature has included several ways in order to improve the effectiveness of this kind of cycle. In these studies, the effect of heat transfer rate, working solution, refrigerant, and the fluid temperature was used to enhance the system. It was concluded that COP and ECOP values increase with the increase of generator and evaporator temperatures. Generally, these methods are divided into three main portions in this work as follows:

2.2.3.1. Enhancement of Heat Transfer

Recently, many improved compact kinds of heat exchangers are utilized like shell and tube kind heat exchangers, microchannel heat exchangers, plate type heat exchangers, etc. But the most important enhancement methods deepened on improving the heat flux process in the bubble pump or in the generator. Many researchers have worked on absorption systems in the fields of modeling into heat and mass transfer analyses, heat transfer additives, and heat and mass transfer experiments for absorption systems, (Gessner et al., 2006; Kim et al., 2006; Killion et al., 2001; Vemuri et al., 2006). Bierling et al., (2019) have performed an experimental study of the effect of different heating kinds on the pumping efficiency of a bubble pump. The measurement results presented a large effect of the heating kind on the pumping effectiveness. The lower the proportional length of the heating, the higher is the pumping rate. Kim et al., (2020) have studied R1234ze(E) and R600a as natural refrigerants in the DARSs with dimethylacetamide (DMAC) and isooctane as the absorbents, respectively. The highest COP of DARS was reached utilizing R600a/isooctane and it was estimated as 0.157 with abubble pump tube diameter of 3.17 mm and that of R1234ze(E)/DMAC DARS was evaluated as 0.134 with the tube diameter of 4.76 mm.

2.2.3.2. Optimization of the Bubble Pump

Many extensive investigations have been carried out to improve the design of different bubble pump configurations, (Zohar et al., 2008; Benhmidene et al., 2010; Benhmidene et al., 2011). The thermally heated bubble pump was studied in previous investigations utilizing burned gas as a heating resource for domestic diffusion

absorption refrigerators as enhanced systems, (Wang and Herold 1992; Herold and Chen 1993; Kim et al., 1994; Herold 1996). (Stierlin and Ferguson 1990; Stierlin et al., 1994) have advanced a burned gas heated diffusion-absorption heat pump with a running heat capacity between 3.0 and 3.5 kW at generator temperatures of 150 °C and cooling effect temperatures from -15 °C up to +5 °C. COPs between 1.4 and 1.5 were achieved. Chen et al., (1996) have advanced a new ARS generator configuration that enhanced the COP of the system by 50%. The old design collects the generator and the bubble pump into one composition. The generator contains a bubble pump, a heating resourse, and a coaxial heat exchanger. This configuration fulfills a decrease in heat waste consequently enhancing the effectiveness of the heating operation thus enhancement in COP. Later, several studies that worked on the performance of bubble pumps of DARS were numerically presented that the bubble pump effectiveness was considerably influenced by the motive head, (Shelton and White Stewart, 2002). The small motive head was useful to huge refrigerant flux rate but drove to a small mixture flux rate, (Koyfman et al., 2003; Pfaff et al., 1998). Moreover, supplied heat flow could also be enhanced to obtain a maximum fluid flux rate and pumping ratio, (Benhmidene et al., 2011; Benhmidene et al., 2016). Han et al., (2015) experimentally have investigated the pumping performance of the bubble pump with various mixture concentrations and various lifting tube diameters. Augustin et al. (2013) have proposed in the numerical study that the flow rate of pumped fluid may be enhanced with more elasticity either by reducing the tube diameter or by rising the position of the heating resource. Also, various makeups of lifting tubes, for example, Zhang et al., (2006) have illustrated lifting tubes with the lunate channel, An et al., (2017) have studied variable cross-section lifting tubes, (Lin et al., 2016; Gurevich et al., 2015) have represented multiple tubes, and Bierling et al., (2019) have experimentally investigated different heating types to enhance the performance of bubble pumps.

2.2.3.3. Adding Nanoparticles to Working Solutions

Last years, nanotechnology has been used in the absorption field to improve heat and mass transfer performance, (Kang et al., 2006). Changwei et al., (2012) have used silver (Ag) as a nanoparticle to prepare binary nanofluids (NH_3/H_2O binary mixture with Ag nanoparticles) for applying in the bubble absorber. The

measurement uncertainty in the repeatability of absorption average was treated as 2.80%. NH_3/H_2O bubble absorption experiments were executed in two steps, with and without refrigerant (H_2O). The results presented that the mass transfer in nanofluids increased compared to that without refrigerant. The highest achievable increase in absorption rate with this refrigerant was observed as 55% with 0.02 wt.% Ag nanoparticles. Kim et al. (2007) have tested nanofluid, which is a binary working solution with nanoparticles, to apply it to ARS. Cu, CuO, and Al_2O_3 nanoparticles were added to the NH_3/H_2O solution to make nanofluids and 2-ethyl-1- as a surfactant (hexanol, n-octanol, and 2-octanol were used). The results showed that the addition of surfactants and nanoparticles increased absorption performance 5.32 times. Sözen et al., (2015) investigated the effects of the passive heat transfer enhancement method combining NH_3/H_2O with Al_2O_3 nanoparticles on DARS heat performance. The experimental results illustrated that the nanofluid system provides better absorption of heat in the generator, also the refrigerant in the nanofluid evaporated faster than the refrigerant of the working solution without the nanoparticles. Adding Al_2O_3 nanoparticles for DARS increases COP and ECOP values by 55.56% and 22.8%, respectively, and reduces *f* by 51.72%. Wang et al., (2019) have suggested and structured a new diffusion absorption heat transformer. The temperature lift effectiveness of this cycle was experimentally investigated with the diffusion gas provided by an electrical gas pump or a thermally driven pump, and the total temperature lift was recognized as high as 17.6 C and 11.8 C, respectively. The higher concentration of HCOOK in H_2O/HCOOK mixture, the lower flow rate of H_2O/HCOOK mixture, and the bigger flow rate of coolant were all useful to higher temperature lift. Schmid et al. (2019) have investigated a diffusion absorption chiller straightly run by solar energy with improved efficiency. The generator, working as the bubble pump of DARS, is incorporated into a double-glazed flat plate collector. The results showed that the percentage of the insolation incident on the solar flat plate transformed into refrigeration capacity was 11.4 %. Thus, efficiency is bigger than in similar literature.

2.3. Main Binary Working Solutions

A refrigeration working mixture for an ARS, in general., is a binary solution blend of a coolant and an absorbent. Both components should have the

characterizations that the coolant ought to be excellently absorbed in cooling cycle temperatures for absorbing process in absorber between 20–40 ^{o}C and vaporizable of the coolant out of the mixture again at desorption temperatures more than 50 ^{o}C. Moreover, the refrigeration working mixture should achieve most or all the following aspects:

- Well stability in its thermophysical properties and chemical characterizations
- Non-explosive and non-toxicity.
- Low viscosity.
- High heat of evaporation.
- Weakly specific heat capacity.
- Low prices.

Basically, the salt of the binary solution (absorbent) should have a high absorption capacity for the coolant with a low freezing degree and a higher boiling degree comparing with the coolant so that the salt absorbs the coolant easily and significantly, (Ajib and Karno, 2008).

2.3.1. Conventional Working Solutions

There has been considerable technology employment and huge investigation interest in the single-stage DARS using NH_3/H_2O (The coolant is pure water) as the working mixture. This is because of the chemical stability of the mixture within a major average of running pressures and temperatures. Ammonia has good thermal properties represented by a high potential vaporization heat and a low icing point (77 ^{o}C) showing it as eligible to utilize in other purposes driven by low evaporation temperatures. A rectifier is utilized to separate the water that vaporized with the ammonia because of NH_3/H_2O volatilization, which increases the amount of heat waste and decreases general effectiveness. In addition, NH_3/H_2O has the feature of non-influencing the environment and its prices are 10–20% lower than synthetic coolants, (McLinden et al., 1998). The thermophysical properties of NH_3/H_2O can be acquired from various resources, (Ziegler and Trepp 1984; El-Sayed and Tribus, 1985; Herold et al., 1988; Park et al., 1990). Disadvantages of utilizing NH_3/H_2O as a working mixture are its altitude running pressure, poisoning, and corrosive act on copper or copper alloys, chaining its utility to materials like carbon steel.

In DARSs, utilized inert gas usually is hydrogen for equiponderate the pressure in the cycle. This gas should have the following characterizations in order to be valid for use in these kinds of systems: weak density and viscosity, low specific heat capacity and thermal conductivity, non-solvability, and non-adhesion to construction substances, (Narayankhekar et al., 1985). Though, its high burn ability problems border the potential of utilizing this gas with more than a refrigerating capacity of 400 W. For eliminating these disadvantages and for enhancing refrigeration capabilities, helium is suggested as an ideal replacement for hydrogen, (Narayankhekar et al., 1985; Kouremenos et al., 1988; Kouremenos et al., 1994; Herold et al., 1994; Zohar et al., 2005). In addition, other ideal gases like neon and argon have also been investigated as a potential replacement intend of hydrogen in these types of cycles, fulfilling in very identical effectiveness to those represented when using the $NH_3/H_2O/H_2$ working solution, (Zohar et al., 2005). Other fluids that consist of ammonia and some salts have also been investigated to define which synthesis is the most suitable to decrease running temperature and enhance COP, (Bourseau et al., 1986). Results illustrated that the NH_3/NaSCN has better efficiency than the NH_3/H_2O. Acuña et al., (2013) have studied $NH_3/LiNO_3$ and emphasized that these solutions have a good effect side to decrease running temperatures. Moreover, the $NH_3/LiNO_3$ solutions have efficiency with a percentage almost equal to 50% better than the efficiency of NH_3/H_2O, and almost 27% better than the efficiency of NH_3/NaSCN at the same running conditions. Thermophysical properties of $NH_3/LiNO_3$ and NH_3/NaSCN are achieved from the equations explained by Infante Ferreira, (1984).

The next most common refrigeration working mixture for ARSs is H_2O/LiBr with H_2O as coolant and LiBr as absorbent salt, (Rodríguez-Muñoz and Belman-Flores, 2014). There has been a considerable technology investment and huge investigation interest on the single-stage DARS using H_2O/LiBr as a refrigeration working solution. Safarik, (2008) illustrated and studied some enhancements on some solar systems thermally driven absorption H_2O/LiBr chiller. The results presented that these systems are an encouraging one from an economically, ecologically, and technically in the near term. To understand the air conditioning process driven by low-temperature heat from solar resources several plants were installed and studied with H_2O/LiBr, (Schweigler et al., 2002; Safarik, 2008). These plants were examined relying on the cooling water temperatures with a heating water

temperature between 75-95 ^{o}C. The results presented that the cooling effect temperature was between 12 and 16 ^{o}C and the achieved COP was between 0.60 and 0.75. Kaynakli and Yamankaradeniz, (2007) investigated the first and second law thermodynamic test of a single-stage ARS with H_2O/LiBr as a refrigeration working solution. Analyzes were achieved for 10 kW cooling capacity and the taken resulted values were a generator temperature 90 °C, ε_{RHE} = 0.50 (ε is effectiveness) and η_P = 0.90. It is established that with a reduction in the condenser–absorber temperatures, and a rise in the generator–evaporator temperatures, the effectiveness of the system enhances.

Recently, many propositions were made to find new refrigeration working mixtures whose coolant starts to evaporate at low-drive temperatures (about 55 ^{o}C) in the generator. Ajib and Karno, (2008) have presented the acetone/$ZnBr_2$ as a novel refrigeration working mixture for ARS, and all thermophysical properties (vapor pressure, density, viscosity, specific heat capacity, specific electrical resistance, and specific enthalpy of the mixture) of this solution was tested at several concentrations and temperatures. The case diagrams (log p, T, and h, T) for the mixture and the log P, h diagram for pure acetone were calculated, performed, and debated. The calculated results illustrated good agreement with the measured results. The advantages of utilizing this mixture are founded on the usability of the low run temperature of the heat resource. The disadvantages are founded on the low heat flux efficiency from and to acetone, thus on the low COP.

In order to have a more wide mention for many working fluids else utilized in ARSs, a summary of investigation refrigeration working mixtures are shown in Table 2.2.

Table 2.2. Summary of some previous studies that have investigated different kinds of refrigeration working solutions

Author, Year	**Working mixture (coolant + absorbent)**	**Operating Conditions**	**Observations**
Kaushik et al., (1985)	NH_3/$LiNO_3$	ARS, Two stage, with NH_3/$LiNO_3$ run driven by low-temperature	Resulting in higher COP than NH_3/H_2O

Cai et al., (2016)	$NH_3/LiNO_3$ and NH_3/NaSCN	The experimental device runs steadily under various working conditions.	Cycle utilizing NH_3/NaSCN had better performance
Patel et al., (2017)	$LiCl/H_2O$	Performance comparison among $LiCl/H_2O$ and LiBr-H_2O absorption systems is estimated under the same running conditions.	$LiCl/H_2O$ executes thermodynamically better compared to $LiBr/H_2O$ in ARSs
Zhu and Gu, (2009)	NH_3/NaSCN	A mathematical model is created to test the system features and performance	COP is about 10 percent higher than the ones for the NH_3/H_2O at identical conditions.
Won and Lee, (1991)	H_2O/LiCl	Double-effect ARSs utilized for computer simulation	COP is higher for the H_2O/LiCl than for the H_2O/LiBr
Won et al., (1991)	H_2O/LiBr-LiScN	A computer simulation that is founded on mass, material., and heat balance correlations for each part of ARS	Higher COP and lower *f* for H_2O/LiBr-LiSCN mixture than for the H2O/LiBr or for the H_2O/LiCl
Lee et al., (2000)	H_2O/LiBr-$LiNO_3$–LiI–LiCl	Different running conditions [2≤Te≤14 °C, 30≤Ta≤50 °C, 30≤Tc≤50 °C, (crystallization limit)] by a computer simulation	The suggested working mixture was established to be viable to the cycle operation of an air-refrigerated absorption chiller with no crystallization issue at a higher absorber temperature
Cai et al., (2015)	NH_3/NaSCN, $NH_3/LiNO_3$	Thermodynamically analyses of a double effect ARS is driven by a high-temperature heat resource	Higher performance with NH_3/NaSCN than $NH_3/LiNO_3$
Iyoki and	H_2O/LiBr–	A theoretical analyses	The quaternary working

Uemura, (1990)	$ZnCl_2$–$CaBr_2$	of a single-stage ARS utilizing the enthalpies at different temperatures, pressures, and absorbent concentrations	solution produced a bigger performance than H_2O/LiBr
Sun, (1998)	NH_3/H_2O, $NH_3/LiNO_3$, NH_3/NaSCN	A theoretical and experimental study performed for single effect ARS	ARS performance with NH_3/NaSCN is better than that with $NH_3/LiNO_3$
Bourouis et al., (2005)	H_2O/LiBr–LiI-$LiNO_3$–LiCl	Investigated for air-cooled absorption air-conditioning systems	Minimal corrosivity, lower requested generator temperature, bespoke for systems driven by low-temperature heat resources
Steiu et al., (2009)	NH_3/H_2O-NaOH	Single effect laboratory-device stainless steel (316SS) inverse osmosis cell SEPA CF fitted to withstand pressures of up to 69 bar, Max. temperature (°C) 177, Flooding volume (ml) 70, Membrane effective domain (m^2) 155	Enhancing the coolant separation in the generator, minimize generation temperature, COP increased by 20% compared to NH_3/H_2O
Arivazhagan et al., (2005)	R134a/DMAC	Simulation investigations performed on a half effect ARS	Performance enhanced with the R134a/DMAC contrasted to NH_3/ H_2O
Ajib and Karno, (2008)	acetone /$ZnBr_2$	low operating temperatures (47–60 °C) utilizing the flat plate solar collectors	The mixture is suitable to operate ARS at low temperatures (more than 50 °C)
Donate et al., (2006)	LiBr/NaK	Single effect conventional ARS, the	The efficiency enhanced slightly; lower running

		experimental device was prepared out to gain equilibrium data with accuracy	temperature needed
Arshi Banu and Sudharsan, (2017)	H_2O/LiBr–LiI-$LiNO_3$–LiCl	Single-effect ARS of one-ton capacity for air-cooled applications	H_2O/LiBr-LiI-$LiNO_3$-LiCl will execute better at all the running temperatures and the running temperature average is higher than the H2O/LiBr system
Bai et al., (2021)	[Na(TX-7)]SCN/NH_3	Different devices in laboratory condtiins were used to test the thermophysical properties then the simulation model was performed.	Improving the thermal effectiveness of the ionic fluid systems and resolves the crystallization issue of NaSCN/NH_3 and LiBr/H_2O systems
Zhou et al., (2021)	R290/POE-oil	Boiling temperature 55.3, 58.7, 62.5 ^oC, Boiling pressure 1.2, 1.3, 1.4 (MPa), Inlet solution concentration 11.1%, Mass flux of solution 166, 221, 276, 332, 387 (kg m^{-2} s^{-1}), Heat flux 1.00–30.74 (kW m^{-2}), Exit vapor quality 0.032–0.071, Heating water volume flow rate 0.029–0.084 (m^3 h^{-1})	Well to the application of R290/POE-oil refrigeration fluid and the design and enhancement of the finned-tube generators in ARSs

2.3.2. Nanofluids

Nanofluid is an advanced type of fluid, which contains nanometer-sized particles that are named nanoparticles. Nanoparticles improve the features of the conventional

working solutions. Recently, nanorefrigerant has become participation in many experimental and theoretical studies of refrigeration systems because of a reduction in energy resources and environmental considerations, (Singh et al., 2015). It is known that nanorefrigerant obtained from metal oxides which are added into coolant/absorber base-fluid in a definite measure and size could absorb heat better, and it could back up the better separation of the coolant from absorber in the generator. Thus, the required generator temperature is achieved rapidly by using minimal energy from low-temperature thermal resources, and the system fetches more energy saving, (Mahbubal et al., 2013).

2.3.2.1. Preparation and Characterization

The preparation process of the nanofluids is the main and most substantial aspect which influences the stability and features of them. this process needs specific ways for fulfilling regular and stable mixtures with minimal agglomeration and sedimentation troubles. Nanofluids are obtained by dispersing metal oxides, metal., or non-metals of nanoparticles in the base-fluid like water and brine. Preparing of nanofluids with water and brine as base-fluids have been briefed by many researchers for example (Saidur et al., 2011; Fan et al., 2011; Philip et al., 2012; Tiwari et al., 2012; Kumar et al., 2014; Lin et al., 2015; Sridhara et al., 2015; Nourafkana et al., 2017).

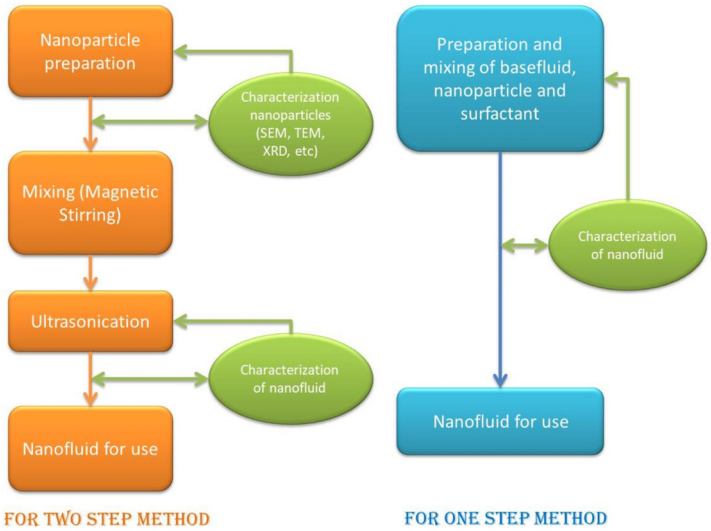

Figure 2.3. Flowchart for producing nanofluids (Bhattad et al., 2018)

As is shown in Figure 2.3., the single-step method and the two-step one are fundamentally the two methods for preparing nanofluids, chemically or mechanically. Nanoparticles are obtained and dispersed in a mixture jointly in the single-step method. While, for the two-step method, nanoparticles are obtained and thereafter dispersed afterward preserving the stability of nanofluids, (Bhattad et al., 2018).

2.3.2.2. Thermal Conductivity of Nanofluids

The first and the most influential step on the heat transfer process effectiveness for improving DARSs is enhancing thermal conductivity which in its turn depends on many parameters such as volumetric distribution, temperature, particle size, particle shape, pH value, additive and preparation method (Fan et al., 2011; Philip et al., 2012; Tiwari et al., 2012; Sridhara et al., 2015; Solangi et al., 2015; Angayarkanni et al., 2015; Azmi et al., 2016). Lee et al. (2010) found that the absorption rate and the heat transfer rate of Ammonium-Water nanofluid with 0.002% Al_2O_3 nanoparticles were 29% and 18% higher, respectively than Ammonium-Water without nanoparticles, and the NH_3/H_2O nanofluid with 0.002% Al_2O_3 nanoparticles was the most suitable candidate for improving water absorption performance. Yang et al., (2011) conducted comparative experiments with NH_3/H_2O and NH_3/H_2O solutions containing various nanoparticles. They presented that the effective absorption rate can be increased by 70% and 50%, respectively, with Fe_2O_3 and $ZnFe_2O_4$ nanofluids, while the initial mass fraction of NH_3 is 15%. Enhancing the heat transfer properties of a single-type of liquid by adding nanoparticles has been studied by many researchers. Choi, (1995) reported that the thermal conductivity of the basic fluid increased by 40% using low concentrations of nanoparticles and nanotubes. Keblinski et al., (2002) proposed potential mechanisms for increasing thermal conductivity, such as Brownian motion, fluid layers, and nanoparticle aggregation, to explain Choi's experimental results. Furthermore, You et al., (2003) notified that the critical heat stream in pool boiling of Al_2O_3 nanofluids increased hugely (approximately 200%) compared with the pure water state. Kim et al., (2004) studied the convective instability caused by the buoyancy and heat transfer features of nanofluids. Xuehu et al., (2007) used CNT- NH_3 nanofluids

(binary nanofluids). The thermal conductivity of binary nanofluids and the improvement of the bubble absorption process have been experimentally studied. The results showed that the thermal conductivity of the CNT/NH_3 nanofluid was 16% higher than that of the NH_3/H_2O solution. In addition, CNT/NH_3 greatly increased the absorption of NH_3/H_2O of the nanofluid. Yang et al., (2012) prepared various types of nanofluids by mix up polyacrylic acid (PAA) and Al_2O_3 nanoparticles with polyethylene glycol (PEG 1000), also, TiN, and SiC, with PEG 10000 to the hydroxyapatite NH_3/H_2O solution, respectively. Results showed that thermal conductivity enhanced by increasing the nanoparticle content and the temperature and by decreasing the nanoparticle volume. For the given nanoparticle materials and the base-fluids, the thermal conductivity ratio of the nanofluid increased as the content nanoparticle and temperature of the NH_3/H_2O fluid increased and decreased as the increase in the nanoparticle's size. Also, the thermal conductivity rate increases as enhancing the stability of nanoparticles in the base-fluid, by adding surfactants, or by choosing the ammonia content appropriate to the fluid. Cuenca et al., (2014) experimentally studied the enhancement of thermal conductivity by adding CNT in the working pairs ($NH_3/LiNO_3$). This study showed that a stable dispersion of CNTs in the elementary fluid can be achieved by surface modification of CNTs through oxidation. The highest thermal conductivity value was obtained by combining 0.01wt.% of CNTs in 40 wt.% of NH_3 base-fluid. The maximum measured increase here was 7.5% higher than the $NH_3/LiNO_3$ solution. Mohammed et al., (2019) examined experimentally graphene/acetone/$ZnBr_2$ nanofluid in a rectangular duct. The results show that as increasing the nanoparticle concentration from 0 to 05 vol.%, heat flow and heat transfer coefficient on the heated surface of the rectangular duct increase from 8638 W m^{-2} and 106 W m^{-2} K to 13164 W m^{-2} and 167 W m^{-2} K, respectively. Mohammed et al., (2020) studied else experimentally the thermal conductivity property of ZnO-acetone/$ZnBr_2$ nanofluid. The thermal conductivity enhancement reached 10.53% at utilization 1.2 vol.% of ZnO nanoparticles concentration in acetone/$ZnBr_2$ base-fluid. Niu et al., (2007), experimentally, proved that the absorption of ammonia-based falling-film absorption fluids is weakened in the magnetic field aligned in the same direction as the vertical film, while the increase in the magnetic field accelerated in the opposite direction to the vertical film. Elsafty and Al-Dain, (2002) investigated, experimentally, the influence of a magnetic field on the vapor absorption process with lithium bromide

working solution containing surfactants. The results showed that the absorption rate increased by approximately 22% using the magnetic field at the initial 61% aqueous lithium bromide concentration. In addition, the researchers explained the instability of the Marangoni convection in the system because of "salting-out effect" and the "spreading effect". Nourafkan et al., (2019) have investigated the photo-thermal conversion features of a long-term and the stability against the agglomeration and sedimentation of a stable nanofluid (nanosize particles in 50 wt.% lithium bromide of water-lithium bromide base-fluid). Experimental results represented that the utilize of nanofluid could considerably enhance the light-trapping efficiency and, therefore, the bulk temperature, which in turn could enhance the evaporation average because of surface centralized heat generation.

Nourafkana et al., (2017) developed a method (Microemulsion mediated method) for the synthesis and dispersion of Fe_3O_4 nanoparticles in a high-ionic medium of water-lithium bromide as a base-fluid. Nanoparticle samples analysis in the presence of lithium bromide (TEM, observation, and LUMiSizer) showed stability over a long period (> 6 months). Steric repulsion is defined as the main mechanism of stability of nanoparticles, verified by the DLVO theory. Wu et al., (2013) examined the addition of Fe_3O_4- NH_3/H_2O nanoferrofluid with the application of an external magnetic field as a new method to increase the absorption in a bubble-type absorber and conducted a detailed experimental study of its effects on bubble absorption. The results showed that the combination of an external magnetic field and nanoferrofluids significantly enhancement in NH_3/H_2O bubble absorption and the reached enhancement in co-use under the same conditions was better than using each separately. The optimal concentration of nanoferrofluid was determined in the investigated range to achieve better improvement and found that the absorption was further improved by increasing the magnetic field intensity at constant nanoferrofluid concentration. Initially, the effective absorption rate at 20 wt.% of NH_3, 0.10 wt.% of Fe_3O_4 nanoparticles, and 280 mT external magnetic field intensity reached 1.0812 ± 0.0001 under adiabatic conditions. Finally, the researchers debated the absorption enhancement technique and the external magnetic field with nanoferrofluids in such a system.

2.4. Modeling of DARS

The bubble pump of DARS is briefly a tube immersed in the generator, different configurations of the bubble pump have been studied in the literature experimentally and through CFD for DARS, (Demir et al., 2016; Zohar et al., 2008). Bubble pump of DARS had been run with H_2O/LiBr as a binary working solution, (Pfaff et al., 1998). They developed a mathematical model using the manometer principle to predict the performance of the bubble pump. The pumping action increases as the heat supply increases and decreases as the tube diameter increases. Benhmidene et al., (2010) checked the bubble pumps for heating. Initially, the first versions of such pumps were represented as a single lifting tube providing heat for the reservoir at the bottom, into which the end of the pipe was immersed. Later, other configurations of lift tubes emerged but were combined with solar collectors, waste heat exchangers, or other types of heat generators. Zohar et al., (2008) achieved a thermal investigation of the effects of three different generator and bubble pump combinations on the efficiency of DARS and found that the system which combines the generator and bubble pump was the best. Soo et al., (2013) conducted a multi-axis CFD study of a saturated flow boiling heat flow in DARS's bubble pump. The geometric configuration of the pump is a vertical tube and heat is regularly supplied from the boundary surfaces along with the pump. The results showed that it is more realistic in terms of performance than one-dimensional numerical studies. It is possible to treat nanoferrofluid as a single-phase flow with an acceptable error due to the nanosize of Fe_3O_4 particles, (Xuan et al., 2000). CFD is a theoretical method of scientific and engineering research. It deals with heat and mass transfer problems as well as fluid dynamics, (Sharma et al., 2015). Mohammed et al., (2018) examined the flow of ZnO nanoparticles and acetone/$ZnBr_2$ solution in a flat tube using CFD. The simulation results showed a promising improvement in the overall performance of the heat transfer of ARS with nanoparticles. Where the improvement of up to 180% of the base-fluid was achieved only with a 1.5 vol.% of particles. The concentration of the salt in the base-fluid together with the nanoparticle concentration has an important influence on the heat transfer improvement. On the other hand, Niu et al., (2007) investigated the effects of an external magnetic field on absorption properties of nanoferrofluids with NH_3/H_2O base-fluid by numerical simulation through theoretical macro modeling, momentum analysis, heat and mass transfer characteristics in ammonia vertical film process under the influence of the magnetic field. The results had positive effects by the magnetic field on ammonia falling-film

absorption. Jemaa et al., (2018) have presented an experimental investigation on DARS and improve a theoretical simulation model of the system utilizing the flow-sheeting software HYSYS. The calculated results presented good approval with the experimental data showed that the model represents completely well the machine. Aman et al., (2018) have performed a dimensional analysis of a bubble pump, and a mathematical model has been advanced to illustrate the bubble pump effectiveness with terms of non-dimensional numbers, which is able to utilize in all bubble pump-driven DARS. the results showed that the operating occurs at a Reynolds number of more than 104. The efficiency of the bubble pump (79%) is carried out at a high fluid Froude number. Harraz et al., (2019) have developed a SAFT-γ Mie group-contribution equation of case that has been utilized to estimate the thermodynamic properties of the refrigeration working solution performed within a thermodynamic model of DARS. For heat supply from 150 to 500 W, the COP extended between 0.15 and 0.24 with the highest COP at a generator heat-supply of 250 W. Lee et al., (2020) have investigated an R600a/n-octane as a new refrigerant/absorbent binary working solution for DARS through numerical analysis. The results showed that R600a/n-octane has considerable potential for DARS application, as the highest COP of 0.162 is reached at a running temperature of 100 °C, making it more suitable than other low-GWP refrigerant working solutions and usable for solar cooling.

Table 2.3. summarizes the preparation of the last investigations of nanorefrigerants in ARSs and DARSs.

Table 2.3. Summary of the used nanofluids in ARSs and DARSs

Author, Year	**Nanorefrigerant**	**Operating Conditions**	**Observations**
Cuenca et al., (2014)	CNT-NH_3/$LiNO_3$	Φ_{NH3}= 30, 40 & 50 *wt.*%; Φ_{CNT}= 0.02, 0.04, 0.08 & 0.8 *vol.*%. D_o= 20–30 *nm*, D_i= 5–10 *nm*, L= 10–30 *μm*, T= 303.15–353.15 *K*	The best improvement in the thermal conductivity of 7.5% with 0.01 wt% of CNTs in the base-fluid of 40 wt.% NH_3
Lee et al., (2010)	Al_2O_3 & CNT-NH_3/H_2O	Φ_{NH3}=20%; Φ_{CNT}=0-0.08 vol.%; Φ_{Al2O3}=0-0.06 *vol.*%	The heat transfer average and absorption average with 0.02 *vol.*% Al_2O_3 nanoparticles

			were obtained to be 29% and 18% better than those without nanoparticles, respectively
Sözen et al., (2015)	Al_2O_3-NH_3/H_2O	Φ_{NH3}=20%; Φ_{Al2O3}= 2% of 170 *ml*; D= 14 μm.	Enhancement in COP and ECOP by 55.56% and 22.8%, respectively, and decrease f by 51.72%.
Kim et al., (2007)	Al_2O_3, Cu & CuO-NH_3/H_2O	The concentration of NH_3 and surfactants are the key parameters.	The results illustrate that the addition of surfactants and nanoparticles enhances the absorption effectiveness up to 5.32 times.
YANG et al., (2012)	Al_2O_3 & PAA-NH_3/H_2O, TiO_2 & PEG 1000 -NH_3/H_2O, TiN, SiC, hydroxyapatite & PEG 1000-NH_3 /H_2O, respectively,	Mass fraction of NH_2-H_2O, Al_2O_3, TiO_2 and PEG 10000 are 0-25 %, 0.3 %, 0.25% and 0.5 % respectively, T=20 ^oC	Results showed that thermal conductivity enhances by increasing the nanoparticle content and the temperature and by decreasing the nanoparticle volume
Changwei et al. (2012)	Mono silver Ag-NH_3/H_2O	Φ_{Ag} =0.02 wt.%	The highest absorption average improvement is spotted to be 55%
Xuehu et al. (2007)	CNTs- NH_3/H_2O	Φ_{NH3}= 12.5 & 25 %, Φ_{CNTs}=0.05 %, T=10 – 40 ^oC	The thermal conductivity of the CNTs- NH_3 nanofluid is better by 16% than that of NH_3/H_2O solution.
Wu et al. (2013)	Fe_3O_4-NH_3/H_2O	Φ_{NH3}=20 %, Φ_{Fe3O4}=0.10%, An external magnetic field intensity of 280 mT	The joint influence of the nanoferrofluid and the external magnetic field considerably improved NH_3/H_2O bubble absorption, and the improvement of the combined factors was bigger than that by either factor alone in the same

			conditions.
Nourafkana et al. (2017)	Fe_3O_4 - H_2O/LiBr	Φ_{LiBr} = 20 to 50 *wt*.%	The created nanoparticles illustrated the best stability against agglomeration
Mohammed et al. (2018)	ZnO-acetone/$ZnBr_2$	Φ_{ZnBr2} =50 *wt*.% , Φ_{ZnO}=1.5 *wt.%*	The CFD simulation results showed that The overall performance of the solution with the nanoparticles shows an enhancement of up to 180% of base fluid can be achieved with only 1.5% volume fraction of particles.
Jiang et al. (2019)	TiO_2-NH_3/H_2O	Φ_{TiO2} = 0.1 *wt.*% - 0.3 *wt.*%, & 0.5 *wt.*%. Φ_{TiO2}=0.5 *wt.*% & Φ_{SDBS}=0.02 *wt.*%	COP enhanced by 27% by adding TiO_2 particles to the base-fluid
Mohammed et al. (2019)	Graphene-acetone/$ZnBr_2$	50 *wt*.% $ZnBr_2$, $\Phi_{graphene}$ =0 to 05 *vol.*%,	By increasing the nanoparticle concentration from 0 to 05 vol%, heat flow and heat transfer coefficient on the heated surface of the rectangular duct increase from 8638 W/m^2 and 106 W/m^2.K to 13164 W/m^2 and 167 W/m^2.K, respectively
Mohammed et al. (2020)	ZnO-acetone/$ZnBr_2$	Φ_{ZnBr2} = 40 *wt.*% - 65 *wt.*%, Φ_{ZnO}= 0-1.2 *vol.*%	The thermal conductivity enhancement reached 10.53% at utilization 1.2 vol.% of ZnO nanoparticles concentration in acetone/$ZnBr_2$ base-fluid.

3. MATERIALS AND METHODS

3.1. Studied Working Solutions

3.1.1. Fe_3O_4 – acetone/$Znbr_2$ Nanoferrofluid

A unique type of nanofluids is nanoferrofluid. Nanoferrofluids content ferromagnetic nanoparticles that exhibit higher thermophysical properties, (Nourafkana et al., 2017; Hodenius et al., 2008). The problem with magnetic particles is that the long-range magnetic forces always will overcome any charge ('electrostatic') stabilization attempts, and Van der Waals forces are always attractive. If it is wanted to prevent agglomeration, we have to modify the surface of magnetite nanoparticles. Unless it is attached to any ligand to the particles, they will tend to agglomerate eventually. One route to stabilization is steric and a polymer such as PEG or PEI on the nanoparticles, (Markhulia, 2016). Farhanian et al., (2018) had studied a new methodology that drives to an active covering with a thickness of 1.4–10 nm, assured by HRTEM and TGA. XPS and TOF-SIMS description confirms that the covering has consisted of both aliphatic and polymerized carbon chains, with combined organometallic bands and oxygen-containing moieties. There are other studied routes to stabilization by applying magnetic vortex or sonication (which both methods will be performed in this project). The magnetic vortex method to stabilization had investigated by Wu et al., (2013), the addition of a Fe_3O_4 nanoferrofluid in incorporation with the applying of an external magnetic field as a novel method for improving the absorption in an ammonia-water bubble pump absorber and carried out an exhaustive experimental investigation of its influence on the bubble absorption process. The results represented that the incorporation influence of the nanoferrofluid and the external magnetic field considerably improved ammonia-water bubble absorption. Furthermore, results refer to that thermal forces can deactivate agglomerates when the rate of thermal energy to dipole-dipole contact energy turns into more than unity, (Chuncheng et al., 2014).

From the other side, Problems with acetone include high volatility, flammability, low density, low viscosity, difficulty in adding ionic components (insolubility), no concept of pH and difficulty manipulating the external continuous phase, hardening of many plastics used in beakers and tubing. But a sufficient dispersivity of acetone or of any medium has acetone as a component in it (such as

the used solution in this study) for many oxides has been documented in the literature, (Abe and Narita, 1997). Where the magnetite particles are scattered in acetone and detached by filtrate easily, (Koikea and Abeb, 2004). In Ajib and Karno's study (2008), the dissolubility experiments of acetone/$ZnBr_2$ working solution have shown that with a concentration of 30% of $ZnBr_2$ almost all of the acetone has been vaporized at experimental conditions 50 ^oC and a 750 mbar. Other samples have been investigated with different experiment conditions, it had satisfying results too. Therefore, this working solution is attractive for being a cooling mixture fluid in DARSs driven by different low temperatures sources.

The main objective of this step of the research is to perform the visual inspection of nanoparticle stability ad thermophysical analyses for the mixture of working solutions of (Fe_3O_4 – acetone/$ZnBr_2$) and examine its efficiency characteristics as a nanoferrofluid for use in DARS. Where before using any binary fluid in DARS, it is very necessary to investigate its thermophysical properties and its chemical steadiness. These properties have a major effect on the COP efficiency of the DARS and on the wanted running temperatures, (Al-Najjar, 2002). Only one experimental investigation has been performed to determine the thermophysical properties of the suggested acetone/$ZnBr_2$ solution, (Ajib and Karno, 2008). And just one more researcher studied the thermophysical properties of the suggested working solutions as nanofluids by using ZnO and Graphene in two separated investigations as suspension nanoparticles, (Mohammed et al., 2019; Mohammed et al., 2020). At the same time, No previous study has tested the nanoferrofluid based acetone/$ZnBr_2$ as it is performed in this work. So this work can be considered a investigation of a new nanoferrofluid and a continuation of the two previous works. Thermophysical analyses (density, specific heat capacity, dynamic viscosity, and thermal conductivity) were achieved to give us a base for using it to find the optimal mixture of working solution of (Fe_3O_4–acetone/$ZnBr_2$) and examine its efficiency characteristics as a nanoferrofluid for a laboratory DARS driven by different low temperatures sources. It shows also an investigation of (Fe_3O_4-acetone/$ZnBr_2$) as a nanoferrofluid including the preparation, stability, structure, and properties. The thermophysical properties are tested at a liquid saturated case at the atmospheric pressure or vapor pressure. The uncertainties for the experiments were relying on the tested properties and on the used devices.

3.1.2. Preparation of Fe_3O_4 – acetone/$Znbr_2$

The most critical step during the investigation of the nanofluid is its preparation process as it influences the stability and properties of nanofluid. The elaboration of nanofluid needs some distinctive ways for less agglomeration and sedimentation problems. Basically, nanofluid is created by dispersing metal., metal oxides, non-metals in base-fluids such as water and brine. Water and brine-based nanofluids elaboration have been described in the literature such as (Saidur et al., 2011; Kumar et al., 2014; Lin et al., 2015; Fan et al., 2011; Philip et al., 2012; Tiwari et al., 2012; Sridhara et al., 2015; Nourafkana et al., 2017). Fundamentally, the preparation of nanofluid is summarized in two processes: single-step process and a two-step process. These can be performed by utilizing the chemical method or mechanical one. In the single-step, process nanoparticles are synthesized and dispersed in the liquid simultaneously. In the two-step, process nanoparticles are synthesized separately then dispersed in a base-fluid and maintaining its stability. the one-step process is better in terms of nanoparticle agglomeration. But for the two-step process is easier for obtaining, especially when the researchers who work on this project have no enough experience in the chemistry field.

The nanoferrofluid (Fe_3O_4-acetone/$ZnBr_2$) is prepared with different fraction mass concentrations (40 wt.% - 65 wt.% of $ZnBr_2$, 0,05 wt.% - 0.2 wt.% of Fe_3O_4) using the two-step process. The experiments are designed to see how effects of various concentrations of the nanoferrofluid mixture and to obtain the optimal concentration of the nanoferrofluid components which will be used in DARS depending on its physical-properties. The most effective approache for enhancing nanoparticle suspension is prepared as follows; The nanoferrofluid samples are left in an ultrasonic device (bath type, 40 kHz, 160 W, model HY- 6 Lt D) produced by HI TEKNOLOJI LTD for 2 hours, (Hyteknoloji Limited, 2020).

The mixture is cooled down in certain time periods during mixing because the heating of metal particles would lead to the evaporation of refrigerant in the mixture. dispersion behavior. During preparing the based-fluid working solution heat is emitted from the mixture because of the dissolve reaction, may reach 65°C depending on added $ZnBr_2$ concentration to the acetone. (Mohammed et al., 2020). In order to understand the dispersion characteristics of the Fe_3O_4 nanoparticles in the solutions for the experiments (without a magnetic field before using the solution in

the DARS with an external magnetic field) a Scanning Electron Microscope (SEM) analysis of the nanoferrofluid samples is carried out. The nanoferrofluid was also compared after the sonication process in a visible way using sedimentation by gravitation over time between several samples with different concentrations of Fe_3O_4 and with a non-sonicated sample. Then testing the density, heat capacity, thermal conductivity, and viscosity which their results are compared with those were found in the previous literature (Ajib and Karno, 2008; Mohammed et al., 2020) for the same acetone/$ZnBr_2$ base-fluid.

3.1.3. Fe_3O_4 - NH_3/H_2O Nanoferrofluid

Through the years, there has been considerable technology employment and huge investigation interest in the single-stage DARS using NH_3/H_2O (The coolant is pure water) as the working mixture. This is because of the chemical stability of the mixture within a major average of running pressures and temperatures. Also, it has the ability to be used under altitude running pressure (15 bar in the diffusion absorption cycle) driven by low-temperature heat resources. This availability does not exist in most conventional working solutions whose absorbent is a salt, thus they are not suitable for use as working solutions in this kind of cycle. Ammonia has good thermal properties represented by a high potential vaporization heat and a low icing point (77 ^oC) showing it as eligible to utilize in other purposes driven by low evaporation temperatures. A rectifier is utilized to separate the water that vaporized with the ammonia because of NH_3/H_2O volatilization, which increases the amount of heat waste and decreases general effectiveness. In addition, NH_3/H_2O has the feature of non-influencing the environment and its prices are 10–20% lower than synthetic coolants, (McLinden et al., 1998). The thermophysical and thermodynamic properties of NH_3/H_2O can be acquired from various resources, (King et al., 1930; Ziegler and Trepp, 1984; El-Sayed and Tribus, 1985; Herold et al., 1988; Park et al., 1990; Conde-Petit, 2004; Mohd Razif et al., 2015). Disadvantages of utilizing NH_3/H_2O as a working mixture are poisoning, and corrosive act on copper or copper alloys, chaining its utility to materials like carbon steel. Newly, Refrigeration binary fluids that have dispersed nanoparticles (called nanofluids) or hybrid nanofluids have acquired an interest in refrigeration and air conditioning fields due to their excellent thermophysical properties which make it used in these kinds of systems with many

studies for performance improvement, (Lee et al., 2010; Yang et al., 2011; Wu et al., 2010; Cuenca et al., 2014; Sözen et al., 2015). Yang et al., (2012) prepared various types of nanofluids by mix up polyacrylic acid (PAA) and Al_2O_3 nanoparticles with polyethylene glycol (PEG 1000), also, TiN, and SiC, with PEG 10000 to the hydroxyapatite NH_3/H_2O solution, respectively. Results showed that thermal conductivity enhanced by increasing the nanoparticle content and the temperature and by decreasing the nanoparticle volume. For the given nanoparticle materials and the base-fluids, the thermal conductivity ratio of the nanofluid increased as the content nanoparticle and temperature of the NH_3/H_2O fluid increased and decreased as the increase in the nanoparticle's size. Also, the thermal conductivity rate increases as enhancing the stability of nanoparticles in the base-fluid, by adding surfactants, or by choosing the ammonia content appropriate to the fluid. Changwei et al., (2012) used silver (Ag) as a nanoparticle to prepare binary nanofluids (NH_3/H_2O binary mixture with Ag nanoparticles) for applying in the bubble absorber. The measurement uncertainty in the repeatability of absorption average was treated as 2.80%. NH_3/H_2O bubble absorption experiments were executed in two steps, with and without refrigerant. The results presented that the mass transfer in nanofluids increased compared to that without refrigerant.

A unique type of nanofluids is nanoferrofluids. Nanoferrofluids content ferromagnetic nanoparticles that exhibit higher thermophysical properties, (Nourafkana et al., 2017; Hodenius et al., 2008). Aghayari et al., (2015) have investigated the synthesis and thermophysical properties inclusive thermal conductivity and viscosity of Fe_3O_4 nanoferrofluid (water is base-fluid). Testing different properties of nanoferrofluids results show that the thermal conductivity, electrical conductivity, and viscosity of nanoferrofluids increase with increasing the nanoparticle volume concentration.

The problem with magnetic particles is that the long-range magnetic forces always will overcome any charge ('electrostatic') stabilization attempts, and van der Waals forces are always attractive. If it is wanted to prevent agglomeration, we have to modify the surface of magnetite nanoparticles. Unless it is attached to any ligand to the particles, they will tend to agglomerate eventually. One route to stabilization is steric and a polymer such as PEG or PEI on the nanoparticles, (Markhulia, 2016). Farhanian et al., (2018) had studied a new methodology that drives to an active covering with a thickness of 1.4–10 nm, assured by HRTEM and TGA. XPS and

TOF-SIMS description confirms that the covering has consisted of both aliphatic and polymerized carbon chains, with combined organometallic bands and oxygen-containing moieties. There are other studied routes to stabilization by applying magnetic vortex or sonication. The magnetic vortex method to stabilization had investigated by Wu et al., (2013). The addition of a Fe_3O_4 nanoferrofluid in incorporation with the applying of an external magnetic field as a novel method for improving the absorption in an ammonia-water bubble pump absorber and carried out an exhaustive experimental investigation of its influence on the bubble absorption process. The results represented that the incorporation influence of the nanoferrofluid and the external magnetic field considerably improved ammonia-water bubble absorption. Furthermore, results refer to that thermal forces can deactivate agglomerates when the rate of thermal energy to dipole-dipole contact energy turns into more than unity, (Chuncheng et al., 2014).

The main objective of this step of the research is to perform the visual inspection of nanoparticle stability, which are dispersed in the base-fluid by using a mechanical method, and thermophysical analysis for the mixture of working solutions of (Fe_3O_4 - NH_3/H_2O) and examine its efficiency characteristics as a nanoferrofluid for use in DARS. To our knowledge, no thermal conductivity data, and also no experimental viscosity data of nanoferrofluid based ammonia-water refrigeration working solution are available in the literature. Before using any binary fluid in DARS, it is very necessary to investigate its thermophysical properties and its chemical steadiness. These properties have a significant effect on the COP efficiency of the DARS and on the wanted running temperatures, (Al-Najjar, 2002). Thermophysical analyses (density, specific heat capacity, dynamic viscosity, and thermal conductivity) were achieved to give a base for finding the optimal mixture of working solution of (Fe_3O_4-NH_3/H_2O) and examine its efficiency characteristics as a nanoferrofluid as a candidate binary solution for use in DARS driven by different low-temperatures sources. It shows also an investigation of (Fe_3O_4-NH_3/H_2O) as a nanoferrofluid including the preparation, stability, structure, and properties. The thermophysical properties are tested at a liquid saturated case at the atmospheric pressure or vapor pressure. The uncertainties for the experiments were relying on the tested properties and on the used devices.

3.1.4. Preparation of Fe_3O_4 - NH_3/H_2O

The most critical step during the investigation of the nanofluid is its preparation process as it influences the stability and properties of nanofluid. The elaboration of nanofluid needs some distinctive ways for less agglomeration and sedimentation problems. Basically, nanofluid is created by dispersing metal., metal oxides, non-metals in base-fluids such as water and brine. Water and brine-based nanofluids elaboration have been described in the literature such as (Saidur et al., 2011; Kumar et al., 2014; Lin et al., 2015; Fan et al., 2011; Philip et al., 2012; Tiwari et al., 2012; Sridhara et al., 2015; Nourafkana et al., 2017). Fundamentally, the preparation of nanofluid is summarized in two processes: a single-step process and a two-step process. These can be performed by utilizing the chemical method or mechanical one. In the single-step, process nanoparticles are synthesized and dispersed in the liquid simultaneously. In the two-step, process nanoparticles are synthesized separately then dispersed in a base-fluid and maintaining its stability. the one-step process is better in terms of nanoparticle agglomeration. But for the two-step process is easier for obtaining, especially when the researchers who work on this project have no enough experience in the chemistry field.

The nanoferrofluid (Fe_3O_4-NH_3/H_2O) is prepared with different fraction mass concentrations (25% of ammonia and 75% of distilled water, 0.05, 0.1, 0,15, and 0.2 *wt.*% of Fe_3O_4) using the two-step process. The experiments are designed to see how effects of various concentrations of the nanoferrofluid mixture and to obtain the optimal concentration of the nanoferrofluid components which will be candidate for using in DARS depending on its physical properties. The most effective approach for enhancing nanoparticle suspension is prepared as follows; The nanoferrofluid samples are left in an ultrasonic device (bath type, 40 kHz, 160 W, model HY- 6 Lt D) produced by HI TEKNOLOJI LTD for 2 hours and one sample for 3 hours, (Hyteknoloji Limited, 2020).

The mixture is cooled down in certain time periods during mixing because the heating of metal particles would lead to the evaporation of refrigerant in the mixture. dispersion behavior. During preparing the based-fluid working solution heat is emitted from the mixture because of the dissolve reaction, may reach 65°C. In order to understand the dispersion characteristics of the Fe_3O_4 nanoparticles in the solutions for the experiments SEM analysis of the nanoferrofluid samples is carried

out. The tested nanoferrofluid samples with different concentrations after the two hours sonication process in a visible way using sedimentation by gravitation over time were also compared with the three hours sonicated sample and with non-sonicated sample. Then testing the density, heat capacity, thermal conductivity, and viscosity of different concentrations of the nanoferrofluid.

3.1.5. Sources of the Materials

Acetone, $ZnBr_2$, NH_3/H_2O (containing 25% of ammonia and 75% of distilled water), and pure nanoparticles Fe_3O_4 99% (50-100 nm particle size (SEM), 97% trace metals basis) were ordered from RASAL KIMYA Company Ltd.

3.2. Diffusion Absorption Refrigeration Machines

Diffusion absorption refrigeration machines have advantages such as silent running where there are no mobile components. No moving parts which meaning low maintenance cost, extended toughness, and may be operated by different kinds of heat resources such as waste heat or solar energy. The most important disadvantage of this type of system is its low efficiency. Refrigerators traditionally founded on this technology and offering a refrigerating capacity of 200 to 400 W have COP values between 0.2 and 0.25. Therefore, over the years, studies have been conducted to achieve a considerable enhancement in energy effectiveness for household appliances, (Narayankhekar et al., 1985; Gutiérrez, 1998; Smirnov et al., 1996). However, the highest COP has detected is 0.3. Bubble pump is the most investigated part of DARSs due to its positive effects on the energy effectiveness of the cycle. Other investigations have shown that geometrical parameters, the features of the heat influx system, and the properties of used working solution are factors affecting the system effectiveness, (Shelton et al., 2002; Benhmidene et al., 2011a, 2011b; Dammak et al., 2010; Abu-Mulaweh et al., 2011; Abduwadood et al., 2012). Thus, using an exclusive type of nanofluids as working solutions, which is called nanoferrofluids, is a new method for improving the overall DARS' performance.

Comparing nanoferrofluids with the other kinds of nanofluids, the features and advantages of nanoferrofluid are fundamentally incarnated in many aspects, Kim et al. (2007). Such as nanoferrofluids contain ferromagnetic nanoparticles that exhibit

higher thermophysical properties, (Hodenius et al. 2008; Nourafkana et al., 2017). Also, Nanomagnetic fluids are novel functional fluid materials containing a solid/liquid mixture in which nanomagnetic particles (diameter <100 nm) are dispersed equally throughout a base-binary working solution to merge the magnetic features of solid magnetic materials and the flow properties of fluid materials, (Hodenius et al., 2008). Furthermore, literature has shown that a magnetic fluid in incorporation with an external magnetic field can be utilized as a new kind of heat transfer medium to considerably improve and handle the heat transfer operation, (Ranjan et al., 2004; Li et al., 2009Yu et al., 2010). On the other hand, there have been also different investigations searching for the ability of nanoferrofluids for enhancing mass transfer rates, (Olle et al, 2006; Srinivas et al., 2007). Takahashi et al., (1993), Bashtovoi et al., (1993), Kamiyama and Ishimoto, (1995), and Liu et al., (2004) carried out experimental investigations to describe the boiling heat flux utilizing magnetic fluids (water is the base-fluid), which presented that the boiling heat transfer characteristics of the magnetic fluids are robustly affected by the magnetic field. Generally, It is observed that the previous studies of the heat transfer procedure of magnetic fluid are more limited in the numerical models and fewer in experimental studies. For example, Niu et al., (2007) investigated the effects of an external magnetic field on absorption properties of nanoferrofluid with NH_3/H_2O base-fluid by numerical simulation through theoretical macro modeling, momentum analysis, heat and mass transfer characteristics in NH_3 vertical film process under the influence of the magnetic field. The results had positive effects by the magnetic field on NH_3 falling-film absorption. Wu et al., (2013) examined the addition of Fe_3O_4-NH_3/H_2O nanoferrofluid with the application of an external magnetic field as a new method to increase the absorption in a bubble-type absorber and conducted a detailed experimental study of its effects on bubble absorption. The results showed that the combination of an external magnetic field and nanoferrofluids significantly enhancement in NH_3/H_2O bubble absorption and the reached enhancement in co-use under the same conditions was better than using each separately. The optimal concentration of nanoferrofluid was determined in the investigated range to achieve better improvement and found that the absorption was further improved by increasing the magnetic field intensity at constant nanoferrofluid concentration. Initially, the effective absorption rate at 20 wt.% of NH_3, 0.10 wt.% of Fe_3O_4

nanoparticles, and 280 mT external magnetic field intensity reached 1.0812 ± 0.0001 under adiabatic conditions.

In DARSs, utilized inert gas usually is hydrogen for equiponderate the pressure in the cycle. This gas should have the following characterizations in order to be valid for use in these kinds of systems: weak density and viscosity, low specific heat capacity and thermal conductivity, non-solvability, and non-adhesion to construction substances, (Narayankhekar et al., 1985). Though, its high burn ability problems border the potential of utilizing this gas with more than a refrigerating capacity of 400 W. For eliminating these disadvantages and for enhancing refrigeration capabilities, helium, which is used in this study, is suggested as an ideal replacement for hydrogen, (Narayankhekar et al., 1985; Kouremenos et al., 1988; Kouremenos et al., 1994; Herold et al., 1994; Zohar et al., 2005). In addition, other ideal gases like neon and argon have also been investigated as a potential replacement intend of hydrogen in these types of cycles, fulfilling in very identical effectiveness to those represented when using the $NH_3/H_2O/H_2$ working solution, (Zohar et al., 2005).

The main objective in this step of the research is studying the validation of using nanoferrofluids (Fe_3O_4-acetone/$ZnBr_2$ and Fe_3O_4-NH_3/H_2O) in DARS, then presenting an experimental and numerical investigation of obtained enhancement in DARS' performance by using the valid solution with helium as an inert gas in accompanying with an external magnetic field, hence illustrating the effect of performing this mechanism on the heat and mass transfer improvement in the system's generator. No previous study has tested the validation of using acetone/$ZnBr_2$ as a working solution in DARS. Also, no previous study investigated the enhancement of COP and ECOP to be obtained by using the nanoferrofluids as working solutions in DARS under influence of an external magnetic field. The energy and exergy analyses are completed for each component, including the gas heat exchanger, experimentally and numerically. Where REFPROP 8.0 software was used for modeling the different studied cycles of DARS and calculating the properties of the measuring points of every cycle. The results showed that this study is an important step on the way of improving the low effectiveness of DARS and give a good base for more future improvements for this kind of systems by using nanoferrofluids, thus widely commercially utilization of DARSs in some fields such as domestic applications or with special usefulness of using them in some areas which are poor of electricity like war zones. On the other hand, the performed

theoretical study presents a good mathematical model for more future investigations depending on different operation conditions in DARS running with the suggested working solutions.

3.2.1. Experimental Diffusion Absorption Refrigeration Device Setup

The experimental device that is utilized in this study composed of a commercial refrigerator cycle, model mini-fridge, with a test refrigeration area of 10-liter capacity as is shown in Figure 3.1.

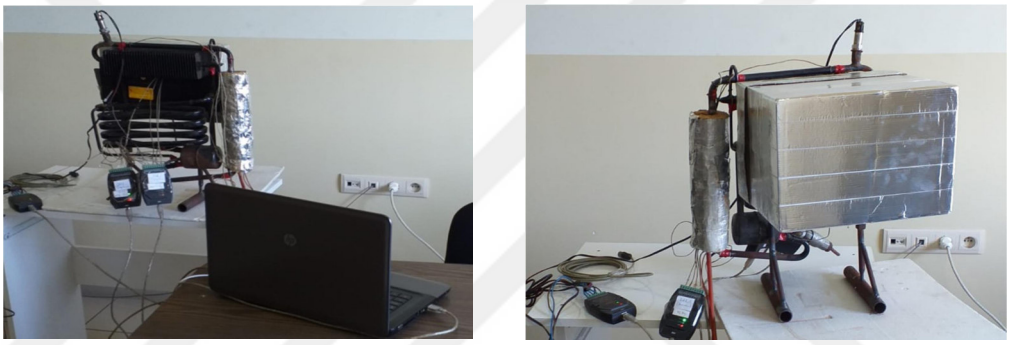

(a) (b)

Figure 3.1. Experiments device: (a) Front and (b) Back

Within the scope of this study, it is planned to establish an experimental setup whose schematic representation is given in Figure 3.2. The establishment of this experimental setup is aimed to start the experiments and to investigate the validation of using the studied nanoferrofliuds in DARS, then determine the parameters of valid solution which are listed in Table 5.2. The test procedure to be applied in this framework is defined as follows. The tested working solutions in the system are the conventional acetone/$ZnBr_2$ binary solution and its nanoferrofluid (Fe_3O_4-acetone/$ZnBr_2$), and conventional NH_3/H_2O mixture and its nanoferrofluid (Fe_3O_4-NH_3/H_2O). The applied working solutions in DARS for each mixture have the same amount at the same ambient conditions. The amount of provided energy for each application and the amount of heat it absorbs both times are equal and constant. The system has a 75 W electrical heater. The supplied power to the generator was measured by a wattmeter (Fluke-43b analyser), (Fluke Corporation, 2021). After every test, acetone was utilized to flush the cycle in case some precipitations or

nanoparticles attached to the pipes or joints. All necessary changes to be made to the experimental DARS machine will be made depending on the experimental conditions including the addition of the external magnetic field. The external magnetic field intensity is adapted by varying the number of permanent magnet pieces around the bottom part of the generator-bubble pump component at a constant diameter.

A K-type thermocouple was used for temperature measurement and a Keller PA-21Y pressure transmitter was used for system pressure measurement. All temperature and pressure data of the system given in the experiment setup Figure 3.4. were recorded on the computer with ORDEL UDL 100 Universal Data Logger.

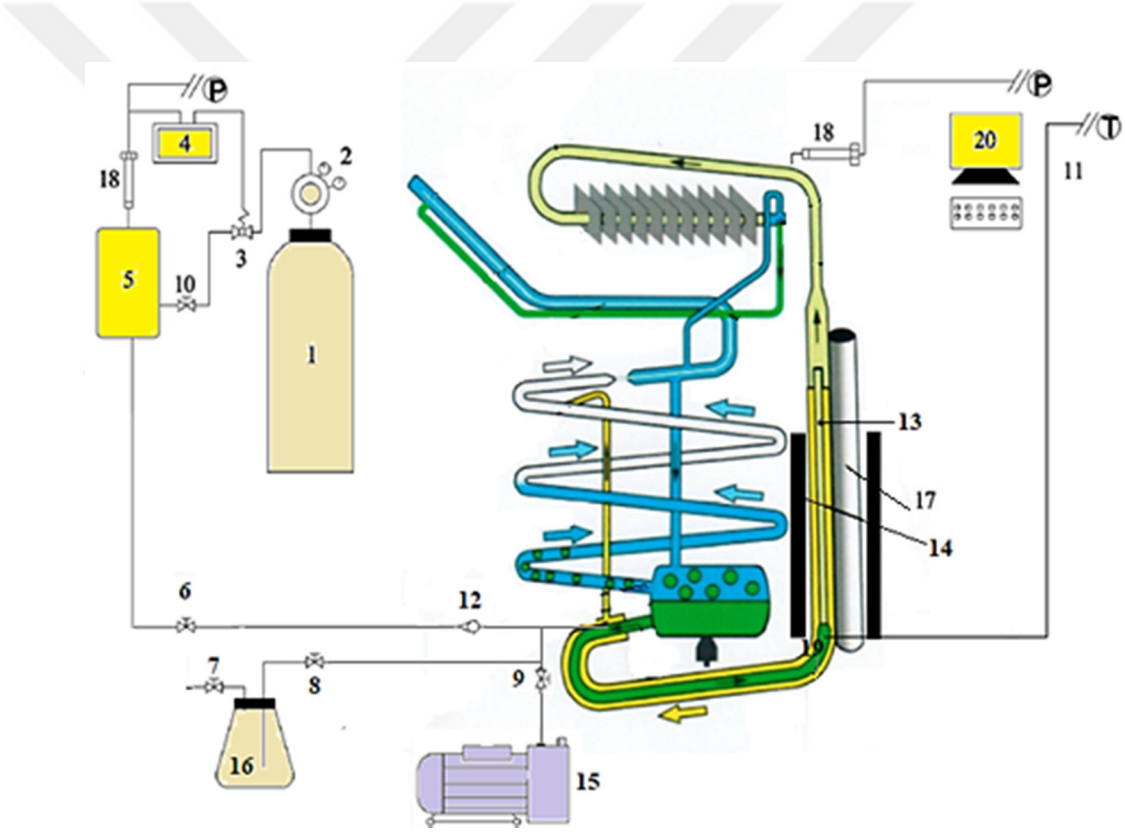

Figure 3.2. Schematic diagram of the experiments set (DARS and the auxiliary equipment) with an external magnetic field: 1, main Helium storage tank; 2, pressure-control valve; 3, electromagnetic valve; 4, PID regulator; 5, Helium gas reservoir; 6–10, needle valves; 11, pressure signal device; 12, check valve; 13, DARS (test device); 14, magnetic field device; 15, vacuum pump; 16, working solution vessel; 17, Heater; 18, pressure sensor; 19, temperature sensor (an example of all temperature sensors); 20, data acquisition computer; T, temperature signal. P, pressure signal

3.2.2. Uncertainty Analysis and Propagation

Depending on the aberration of measured parameters the error analysis and propagation of the experimental results were specified. Since the measurements of the temperature of the specified points were not performed near the fluid, and to prevent the solution leaks from the cycle, the values were obtained from the external wall of the tubes and wrapped with a thermal insulation plaster. The average of the measured temperatures by K-type thermocouples was obtained after repeating each test three times. The nominal power of the used electrical heater in the generator-bubble pump component equals 75 W. For the overall thermal conductivity in the experiment, the correlation equation of the uncertainty can be presented as, (Sözen et al., 2015):

$$U_m = \sqrt{\frac{\Delta T}{T} + \frac{\Delta Q}{Q}} \tag{3.1}$$

The thermocouples accuracy was indicated ±0.1°C and the wattmeter accuracy was ±0.5 W. Also the cycle running pressure data were recorded every 5 min during a 2 h period by analog manometer which its accuracy was ±0.2 bar. Depending on Equation (5.1) the uncertainty of the performed experiments have a rate of ±3.3%.

3.2.3. Thermodynamic Analysis

Initially, in order to simplify the thermodynamic calculations of DARS the following necessary assumptions are suggested, (Pitatowsky et al., 2001; Sözen et al., 2015):

1. The operation occurs by assuming no pressure decline through the pipes where the pressure in every ingredient is equivalent to the working fluid vapor pressure. The condenser pressure and the generator pressure, are the same, also the absorber pressure and the evaporator pressure are the same during the operation.
2. The heat wastage from the generator to the environment is negligible because of the isolation.
3. The weak solution and the vapor bubbles leave the generator is at the same temperature as in the generator.

4. The pure coolant which quits the condenser is a saturated fluid and its temperature equal to the condensation temperature T_{cond} ,
5. The pure coolant quits the evaporator is saturated vapor and its temperature equal to the evaporation temperature T_{evap}.
6. The rich solution leaving the reservoir is a completely saturated fluid at the temperature and concentration that exists in the absorber.
7. Accepting that the mixture of the coolant and auxiliary gas at the entrance of the evaporator is adiabatic.
8. h_0 , s_0 , and T_0 are the enthalpy and entropy of the fluid at ambient temperature.
9. The specific heat capacity is steady for every phase of the working solution.
10. Exergy destruction for some components such as pipelines and reservoir is negligible.

The energy and exergy analysis of the refrigeration system is performed by using the concept of mass and energy conservation and the second law of thermodynamics. The used correlations in the calculations of the cycle are presented as follows for each component and for the overall cycle according to Figure 3.3., (Yıldız and Ersöz, 2013).

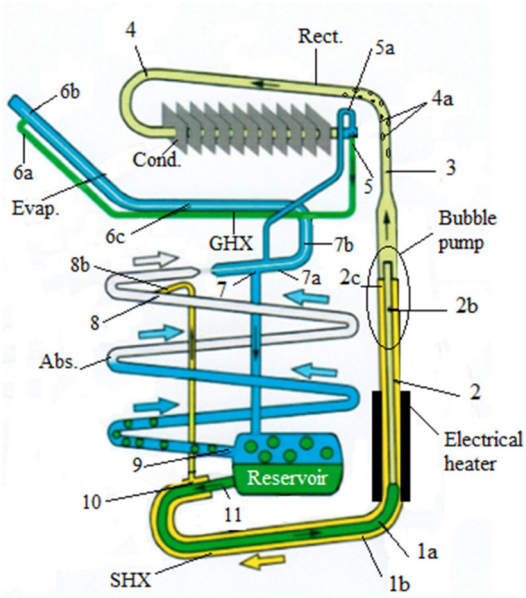

Figure 3.3. Schematic diagram of the experimental DARS with measurement points

3.2.3.1. Energy Analysis

a) Generator and bubble pump

The required energy Q_{gen} for running the cooling operation and starting vaporization and separating the coolant from the rich working solution in the bubble pump is provided by an external electric resistance which is around the bottom part annular pipe of the generator-bubble pump component. The mass and energy balance correlations of this component are written as follows:

$$\dot{m}_{1a} - \dot{m}_3 - \dot{m}_{2c} = 0 \quad \textbf{(3.2)}$$

$$\dot{m}_{1a} x_{1a} - \dot{m}_3 x_3 - \dot{m}_{2c} x_{2c} = 0 \quad \textbf{(3.3)}$$

$$\dot{Q}_{gen} = \dot{m}_3 h_3 + \dot{m}_{2c} h_{2c} - \dot{m}_{1a} h_{1a} \quad \textbf{(3.4)}$$

b) Rectifier

The evaporated fluid which leaving the bubble pump has small drops of absorbent. In the rectifier, the vapor releases the attached drops back to the generator again by a partial condensation process, thus, almost pure refrigerant vapor is gained. The mass flow of the refrigerant vapor and the waste heat to the environment can be defined from the mass and energy balance correlations of the rectifier component as follows:

$$\dot{m}_3 - \dot{m}_4 - \dot{m}_{4a} = 0 \quad \textbf{(3.5)}$$

$$\dot{m}_3 x_3 - \dot{m}_4 x_4 - \dot{m}_{4a} x_{4a} = 0 \quad \textbf{(3.6)}$$

$$\dot{Q}_{rect} = \dot{m}_3 h_3 - \dot{m}_{4a} h_{4a} - \dot{m}_4 h_4 \quad \textbf{(3.7)}$$

c) SHX (Solution heat exchanger)

The heat exchanging process happens between the weak working solution exiting from the generator which has a relatively high temperature and the rich working solution leaving the absorber which has a low temperature. The mass and

energy balance and heat flux process correlations of the SHX component are written as follows:

$$\dot{m}_{11} = \dot{m}_{1a} = \dot{m}_{rs} \quad \textbf{(3.8)}$$

$$\dot{m}_{1b} = \dot{m}_{10} = \dot{m}_{ws} \quad \textbf{(3.9)}$$

$$\dot{m}_{1b} - \dot{m}_{2c} - \dot{m}_{4a} = 0 \quad \textbf{(3.10)}$$

$$\dot{m}_{1b} x_{1b} - \dot{m}_{2c} x_{2c} - \dot{m}_{4a} x_{4a} = 0 \quad \textbf{(3.11)}$$

$$\dot{m}_{1b} h_{1b} - \dot{m}_{2c} h_{2c} - \dot{m}_{4a} h_{4a} = 0 \quad \textbf{(3.12)}$$

$$\dot{Q}_{SHX} = \dot{m}_{1b} h_{1b} + \dot{m}_{11} h_{11} - \dot{m}_{10} h_{10} - \dot{m}_{1a} h_{1a} \quad \textbf{(3.13)}$$

d) Condenser

The coolant exits the rectifier and enters the condenser where condenses to a liquid under high pressure which is equal to the operating pressure of the system. The mass and energy balance correlations of the condenser component are presented as follows:

$$\dot{m}_4 - \dot{m}_5 = 0 \quad \textbf{(3.14)}$$

$$\dot{Q}_{cond} = \dot{m}_4 h_4 - \dot{m}_5 h_5 \quad \textbf{(3.15)}$$

e) Evaporator

Because the evaporator is full of inert gas the partial pressure of the coolant liquid, which exits from the condenser at the operating pressure, drops quickly and as a consequence, the liquid starts evaporating, the cooling effect is obtained and heat is absorbed from the cooled area. The mass and energy balance correlations of the evaporator component are presented as follows:

$$\dot{m}_{6a} + \dot{m}_{ig} - \dot{m}_{7a} = 0 \quad \textbf{(3.16)}$$

$$\dot{Q}_{evap} = \dot{m}_{7a} h_{7a} - \dot{m}_{6a} h_{6a} - \dot{m}_{ig} h_{ig} \quad \textbf{(3.17)}$$

f) Absorber

In this component the coolant vapor that comes from the evaporator mixes and is absorbed from the weak working solution (absorbent) which comes from the generator. the resulted rich working solution drops to the reservoir. Helium and the small drops of acetone flow toward the evaporator again. The balance correlations of mass, energy, and the waste heat to the surrounding of the absorber are presented as follows:

$$\dot{m}_9 + \dot{m}_{ig} - \dot{m}_{7a} - \dot{m}_{8b} = 0 \quad \textbf{(3.18)}$$

$$\dot{Q}_{abs} = \dot{m}_{7a} h_{7a} + \dot{m}_{8b} h_{8b} - \dot{m}_9 h_9 - \dot{m}_{ig} h_{ig} \quad \textbf{(3.19)}$$

g) COP (Coefficient of energy performance)

COP represents the effectiveness of the overall system which is defined as the gained heat from the cooling area (cooling effect) to the supplied energy to the generator. COP correlation equation is written as follows:

$$COP = \frac{\dot{Q}_{evap}}{\dot{Q}_{gen}} \quad \textbf{(3.20)}$$

3.2.3.2. Exergy Analysis

Exergy is defined as the beneficial work potential of any system at a certain state. Also, the exergy analysis is an essential part of the overall thermodynamic analysis of the cycle. Where it completes and presents the unclear aspects of the first law of thermodynamics. Whereas the main principle of exergy is relying on the first and second laws of thermodynamics. The energy which is decay in every component of the cycle may be calculated by the exergy analysis, thus more understanding of the ables to improve the overall system. Exergy analysis determines the destruction and losses of exergy in various components and hence the exergetic coefficient of performance (ECOP) of the overall system, (Mehyo et al., 2018).

The general exergy destruction correlation can be written as follows:

$$\sum(1-\frac{T_o}{T_p})\,\dot{Q}_p - \dot{W} + \sum \dot{m}_{in} E_{in} - \sum \dot{m}_{out} E_{out} = \dot{E}_{dest} \quad \textbf{(3.21)}$$

The general exergy rate equation is expressed as follows:

$$\dot{E} = \dot{m}_1 E = \dot{m}_1 (h - h_0 - T_0 (s - s_0)) \quad \textbf{(3.22)}$$

Considering that the positive direction of heat transfer is to be to the system, the general generation entropy correlation can be written as follows:

$$\dot{s}_{generation} = \sum \dot{m}_{out} s_{out} - \sum \dot{m}_{in} s_{in} - \sum \frac{\dot{Q}_p}{T_p} \quad \textbf{(3.23)}$$

Form equations (3.23), the exergy destruction can be expressed in the following form:

$$\dot{E}_{dest} = T_o \dot{s}_{generation} \quad \textbf{(3.24)}$$

The exergy destruction of the different components, the total exergy destruction, and ECOP equations of the studied DARS are presented in Table 3.1.:

Table 3.1. The exergy destruction equations of the different components, the total exergy destruction, and ECOP

Component	**Equation**	
Generator and bubble pump	$\dot{E}_{dest,gen} = T_0 \left(\dot{m}_3 s_3 + \dot{m}_{2c} s_{2c} - \frac{\dot{Q}_{gen}}{T_{gen}} - \dot{m}_{1a} s_{1a} \right)$	**(3.25)**
Rectifier	$\dot{E}_{dest,rect} = T_0 \left(\dot{m}_4 s_4 + \dot{m}_{4a} s_{4a} + \frac{\dot{Q}_{rect}}{T_{rect}} - \dot{m}_3 s_3 \right)$	**(3.26)**
SHX	$\dot{E}_{dest,SHX} = T_0 \left(\dot{m}_{rs} (s_{1a} - s_{11}) + \dot{m}_{ws} (s_{10} - s_{1b}) - \frac{\dot{Q}_{SHX}}{T_{SHX}} \right)$	**(3.27)**

Condenser	$\dot{E}_{dest,cond} = T_0\left(\dot{m}_5 s_5 - \frac{\dot{Q}_{cond}}{T_{cond}} - \dot{m}_4 s_4\right)$	**(3.28)**
Evaporator	$\dot{E}_{dest,evap} = T_0\left(\dot{m}_{7a} s_{7a} - \dot{m}_{6a} s_{6a} - \dot{m}_{ig} s_{ig} - \frac{\dot{Q}_{evap}}{T_{evap}}\right)$	**(3.29)**
Absorber	$\dot{E}_{dest,abs} = T_0\left(\dot{m}_9 s_9 + \dot{m}_{ig} s_{ig} + \frac{\dot{Q}_{abs}}{T_{abs}} - \dot{m}_{7a} s_{7a} - \dot{m}_{8b} s_{8b}\right)$	**(3.30)**
Total exergy destruction	$\dot{E}_{dest,tot} = \dot{E}_{dest,gen} + \dot{E}_{dest,rect} + \dot{E}_{dest,SHX} + \dot{E}_{dest,cond} + \dot{E}_{dest,evap} + \dot{E}_{dest,abs}$	**(3.31)**
ECOP	$ECOP = \frac{\dot{E}_{out}}{\dot{E}_{in}} = 1 - \frac{\dot{E}_{dest,tot}}{\dot{E}_{gen}}$	**(3.32)**
	or,	
	$ECOP = \frac{\dot{Q}_{evap}\left(1 - \frac{T_0}{T_{evap}}\right)}{\dot{Q}_{gen}\left(1 - \frac{T_0}{T_{gen}}\right)}$	**(3.33)**

Finally, The circulation ratio of the DARS is defined as follows:

$$f = \frac{\dot{m}_{11}}{\dot{m}_4} \ (\mathrm{kg}_{sol}\ \mathrm{kg}_{co}^{-1}) \qquad \textbf{(3.34)}$$

4. RESULTS AND DISCUSSION

4.1. Fe_3O_4 _ acaetone/$ZnBr_2$ Nanoferrofluid Analyses Results

4.1.1. Stability of Fe_3O_4 _ acaetone/$ZnBr_2$ Nanoferrofluid

4.1.1.1. Visual Inspection of acetone/$ZnBr_2$ Base-fluid

Mohammed et al., (2020) had found that the heat (55 °C) or light (or both of them) has an effect on changing the color of acetone/$ZnBr_2$ and becomes brown over time. However, in the current study, it is found that even in a dark medium (dimming by using aluminum paper) with in-room temperature (25 °C), the color of the solution changes to brown over time as is shown in Figure 4.1. This is due to the degradation of $ZnBr_2$ forming bromine.

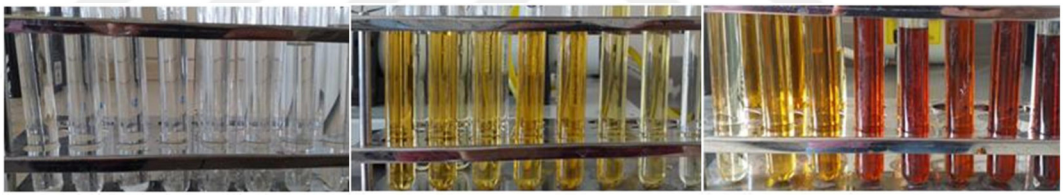

(After mixing directly) (After 4 days) (After 16 days)

Figure 4.1. Color changes of acetone/$ZnBr_2$ solution samples with several concentrations by the time

4.1.1.2. Dispersion Characteristics of Fe_3O_4 Nanoparticles In the Base-fluid

As is mentioned before, the problem with magnetic particles is that the long-range magnetic forces always will overcome any charge ('electrostatic') stabilization attempts, and van der Waals forces are always attractive, thus more agglomeration and sedimentation. For overcoming these forces a sonication process is performed experimentally on the nanoferrofluid (acetone – $ZnBr_2$/ Fe_3O_4, 50% $ZnBr_2$ of base-fluid) samples with Fe_3O_4 nanoparticle concentrations of 0.05, 0.1, 0,15, and 0.2 wt.%.The nanoferrofluid samples are left in an ultrasonic device (bath type, 40 kHz, 160 W, model HY- 6 Lt D) produced by HI TEKNOLOJI LTD for 2 hours,

(Hyteknoloji Limited, 2020). After several pre-experiments performed on different samples that had different concentrations of nanoparticles in the used ultrasonic device with various sonication process periods, it can be inferred the sonication process time on the nanoferrofluid has no significant influence on the suspension stability.

4.1.1.3. Visual Inspection of Stability

Figure 4.2. illustrates nanoferrofluid suspensions with several concentrations of Fe_3O_4. Tube number 5 was prepared without sonication and with 0.1 wt.% of Fe_3O_4 concentration. It can be seen from Figure 4.2. (a) that the sonication process has an obvious influence on the samples comparing with tube 5 (non-sonicated sample). Sonicated samples have less agglomeration and the upper section of tube 5 is, somewhat, more net than the same section of others over time. On the other hand, from Figure 4.2. (b, c, d), it can be realized that although there is an increasing trend to produce bigger agglomerations in samples that have a greater concentration of nanoparticles, there is no obvious difference in sedimentation in each solution under natural gravity. These results elucidate that the Fe_3O_4 nanoferrofluid of acetone/$ZnBr_2$ base-fluid has good dispersion and weak stability characteristics. That pushes us to use an additional method by applying a magnetic vortex to get good stability when this nanoferrofluid is applied in the DARS.

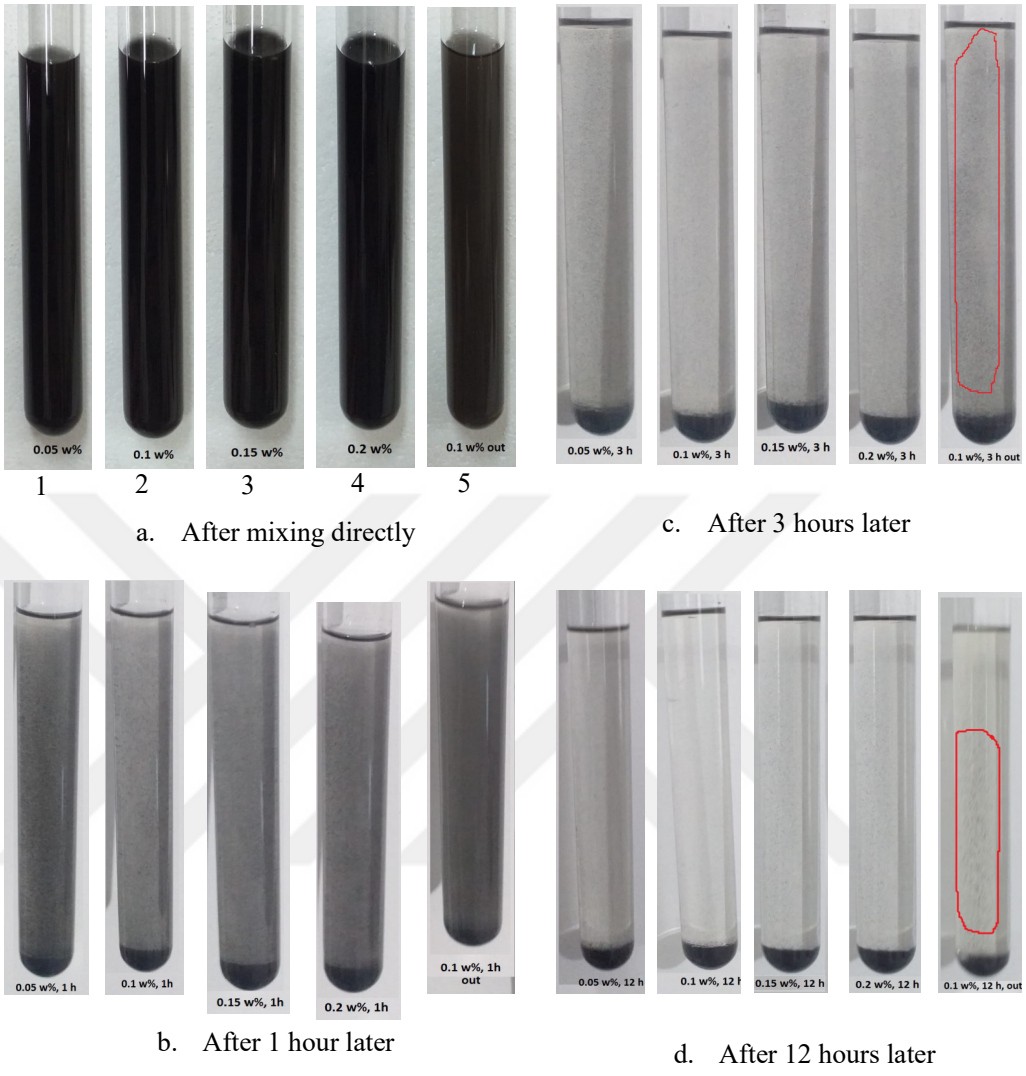

Figure 4.2. Sedimentation and agglomeration of varies concentrations of Fe_3O_4 nanoparticles in acetone/$ZnBr_2$ base-fluid. 1–0.05 wt.%; 2–0.1 wt.%; 3–0.15 wt.%; 4–0.2 wt.% (with 2 h sonication). 5–0,1 wt.% (without sonication)

4.1.1.4. Examination of the Chemical Surfactant Factors Effects

Three chemical surfactant factors (poly vinyl pyrrolidone (PVP), sodium dodecyl sulfate (SDS), and polyvinyl alcohol (PVA)) were examined in a try to enhance the sonicated nanoferrofluid stability. The sample used in this test was a solution with a 0.1 wt.% concentration of nanoparticles that were prepared with the same by adding 1 wt.% of the three surfactants separately. Figure 4.3. shows that these types of surfactants have no useful effect on the dispertion of the nanoparticles over time. Where directly after the sonication process particles start agglomerating.

Also, the surfactants cannot dissolve and start to collect on the top of the solution. Over time these effects become clearer.

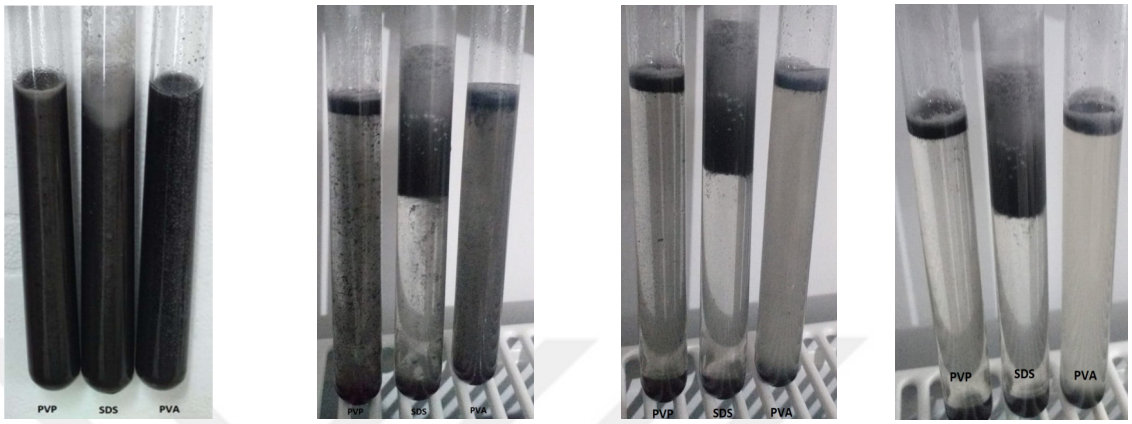

a. After sonication directly b. 1 hour later c. 3 hours later d. 12 hours later

Figure 4.3. Effects of using different surfactants on the stability of nanoferrofluid (Fe_3O_4 - acetone/$ZnBr_2$) over time

4.1.1.5. Scanning Electron Microscope (SEM) Analysis

The surface morphology and particle sizes of the samples were carried out using a high-resolution SEM (JEOL-JSM-7001F) type which exists in Black Sea Advanced Technology Research and Application Center Laboratories (KITAM) operating at 15 kV. Figure 4.4. shows SEM images of Fe_3O_4 nanoparticles of 0.1% mass concentration nanoferrofluid. The images display no clear agglomeration, which shows the Fe_3O_4 nanoparticles have almost a typical and random distribution situation, without a magnetic field, in the liquid. And this distribution occurred after sonication because of just the nanoparticles' thermal motion.

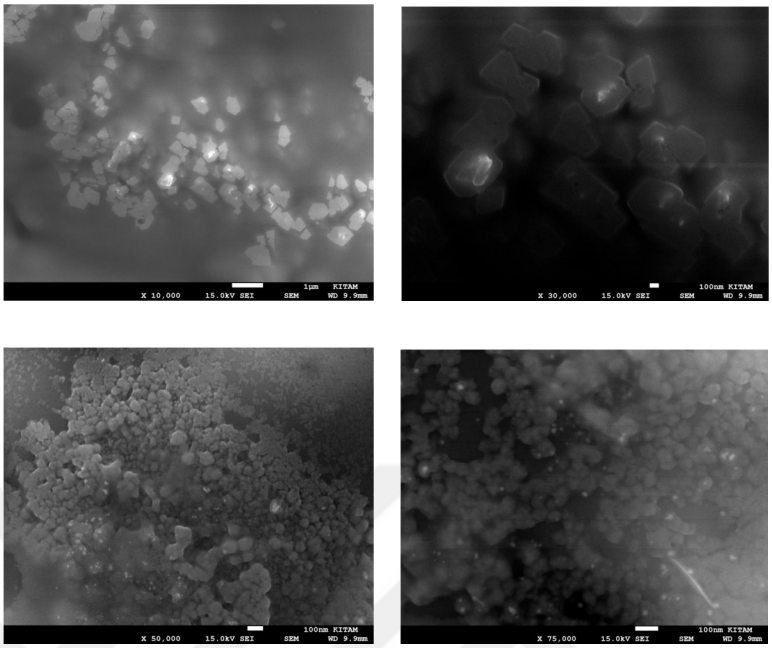

Figure 4.4. Various SEM images of Fe_3O_4 nanoparticles suspension in the acetone/$ZnBr_2$ solution on a carbon film show randomly dispersed particles without any magnetic field

4.1.2. Thermophysical Properties

4.1.2.1. Density

The measured density of several acetone/$ZnBr_2$ concentrations at 25°C in this study was significantly similar to those investigated by Mohammed et al., (2020) and dissimilar to which was investigated by Ajib and Karno, (2008). Because of the increase of the solution volume when the salt ($ZnBr_2$) is added and dissolved in the solvent (acetone) which was not taken into account in Ajib and Karno study (2008). During the experiment by taking the volumetric flask error (0.5 to 1%) into consideration and depending on the volumes used (10 ml sample), Table 4.1. represents the variation among the measured densities of several acetone/$ZnBr_2$ concentrations as found experimentally in this study and the literature. There is no previous study about the density of nanoferrofluid in the literature with acetone/$ZnBr_2$ as a base-fluid. Table 4.2. shows increasing in The density of the nanoferrofluid from 1.366 to 1.606 (g cm^{-3}) with an increasing concentration of the weight fraction from 0.0 to 0.2 wt.% of the added nanoparticles. And also, Figure

4.5. shows almost identical values of the theoretical density (which set by Equation 1) with experimental ones, (Mohammed et al., 2020).

$$\rho_{tot} = \frac{1}{\frac{X_s}{\rho_s} + \frac{X_p}{\rho_p}} \quad \textbf{(4.1)}$$

Where the subscripts tot, s, and p indicate nanoferrofluid, base-fluid and nanoparticles respectively, ρ and X indicate the density and mass fraction respectively. ρ_p=5 (g cm^{-3}), (Merck KgaA, 2020).

Table 4.1. The density of acetone/$ZnBr_2$ with various concentrations of acetone as measured experimentally in this study at 25 °C and in similar studies

$ZnBr_2$ Concentration	**Reported density in (Ajib and Karno, 2008) (g cm^{-3})**	**Reported density in (Mohammed et al., 2020) (g cm^{-3})**	**Measured density of this study (g cm^{-3})**
40 %	1.291	1.164	1.161
45 %	1.420	1.228	1.230
50 %	1.581	1.360	1.366
55 %	1.778	1.426	1.431
60 %	2.013	1.550	1.553
65 %	2.292	1.662	1.663

Table 4.2. The density of the Fe_3O_4-acetone/$ZnBr_2$ (50 wt.% $ZnBr_2$) with various concentrations of Fe_3O_4 indicated experimentally and theoretically in this study at 25 °C

Fe_3O_4 nanoparticles Concentration (wt.%)	**Calculated density (theoretically) (g cm^{-3})**	**Measured density of this study (g cm^{-3})**
0.00	1.366	1.366
0.05	1.417	1.406
0.1	1.473	1.470
0.15	1.533	1.545
0.2	1.598	1.606

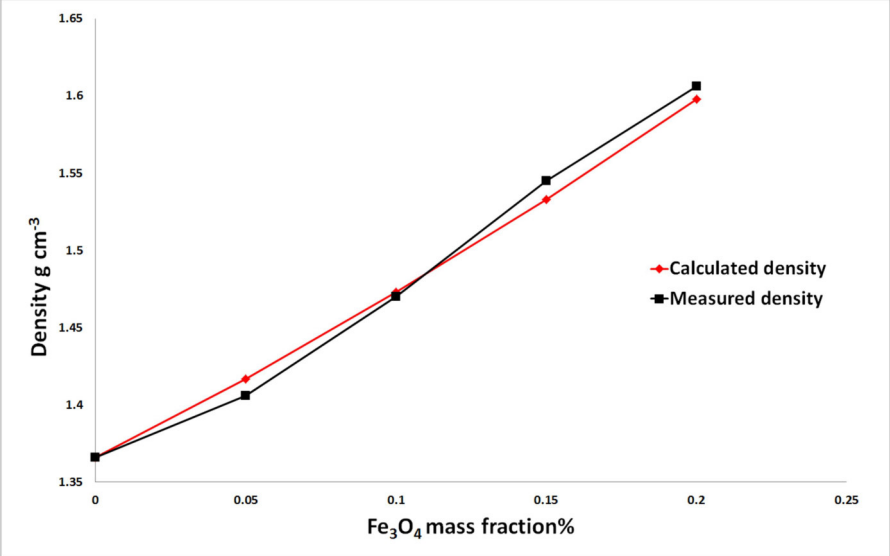

Figure 4.5. Changes of the nanoferrofluid density with different Fe_3O_4 nanoparticles mass fraction, experimentally and theoretically

4.1.2.2. Viscosity

The viscosities of several concentrations of acetone/$ZnBr_2$ were measured at 25°C, using Thermo Scientific™ HAAKE™ MARS™ 40 Rheometer, (Thermo Fisher Scientific Inc, 2020). The results of this test have no substantial difference with those measured in literature (Ajib and Karno, 2008; Mohammed et al., 2020) as shown in Table 4.3. On the other hand, it can be realized from Figure 4.6. that a major increase in viscosity happened from 3.384 to 9.206 mPa.s with an increasing concentration of Fe_3O_4 from 0 to 0.2 wt.%. Hence, the nanoferrofluid has a high viscosity comparing with its base fluid. And also has a high viscosity comparing with another kind of nanofluid with the same base-fluid, (Mohammed et al., 2020). The viscosity measurements were repeated at least 3 times. The measurement error at the given temperature was less than 1%. It is assumed that nanoferrofluid has a single-phase liquid.

Table 4.3. The viscosity of the Fe_3O_4-acetone/$ZnBr_2$ (50 wt.% $ZnBr_2$) with various concentrations of Fe_3O_4 indicated experimentally in this study at 25 °C

Fe_3O_4 nanoparticles Concentration (wt.%)	**Measured viscosity mPa.s**
0.00	3.384
0.05	4.384

0.1	5.724
0.15	8.058
0.2	9.206

Finally, we should mention that the presence of a magnetic field causes starting the figuration of string aggregates which drives to increase of viscosity in parallel with increasing magnetic field intensity, (Chuncheng et al., 2014).

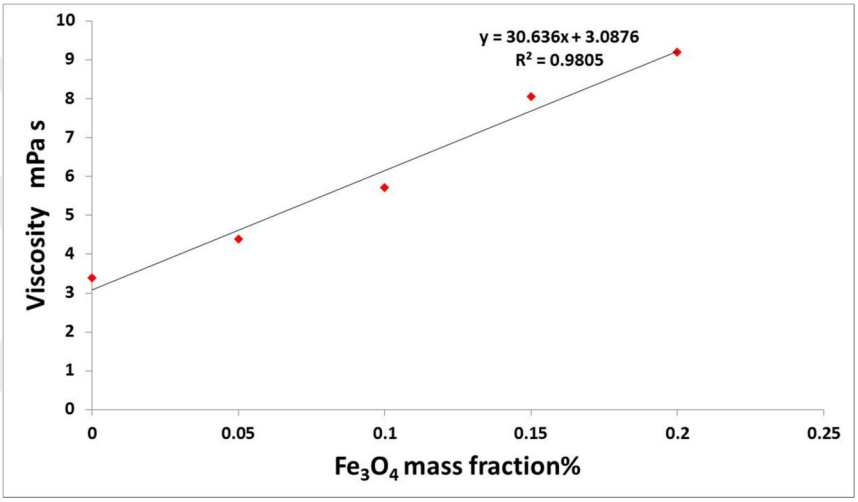

Figure 4.6. Changes of the nanoferrofluid viscosity with different Fe_3O_4 nanoparticle mass fraction

4.1.2.3. Specific Heat Capacity at Constant Pressure

The specific heat capacity of several concentrations of acetone/$ZnBr_2$ base-fluid was measured using KD2 Pro Thermal Properties Analyzer, Decagon Devices, Inc. (Decagon Devices, 2020). The results of this analysis have no substantial difference with those measured in literature (Ajib and Karno, 2008; Mohammed et al., 2020). But no previous study has tested the specific heat capacity of a nanoferrofluid with acetone/$ZnBr_2$ as a base-fluid, which is studied in this work. Table 4.4. illustrates the specific heat capacity of the Fe_3O_4-acetone/$ZnBr_2$ (50 wt.% $ZnBr_2$) with various concentrations of Fe_3O_4 indicated experimentally and theoretically at 25 °C. It can be realized from Figure 4.7. that the specific heat capacity decrease with increasing the particles (Fe_3O_4) concentration. It is a logical consequence because of the low heat capacity value of the nanoparticles (0.653 J g^{-1} K^{-1}) compared with the specific heat

capacity of acetone/$ZnBr_2$ (1.140 J g^{-1} K^{-1}) and the higher concentration, the higher agglomerations. More agglomeration causes bigger particles in the nanoferrofluid which drops the total heat capacity and that is also what was mentioned in the literature with other kinds of nanofluids, (Zhou and Ni, 2008; Sekhar and Sharma, 2015; Mohammed et al., 2020). But while we have an excellent suspension of nanoparticles in this work, there is no major decline in tested values to the computational values of the heat capacities comparing with other kinds of nanoparticles which have studied before in the literature.

While there are several methods for assessing the heat capacities of pure liquids, very few set correlations have been proposed for mixtures. Furthermore, since there is no model obtainable to calculate the specific heat capacity of nanofluids, a simple method (Equation 4.2) depended on the corresponding state principle is proposed for the calculation of the heat capacities of liquid mixtures, (Teja, 1983; Sohel Murshed, 2011).

$$c_{p_{tot}} = X_s c_{p_s} + X_p c_{p_p} \quad \textbf{(4.2)}$$

Where c_p is the specific heat capacity

Table 4.4. The specific heat capacity of the Fe_3O_4-acetone/$ZnBr_2$ (50 wt.% $ZnBr_2$) with various concentrations of Fe_3O_4 indicated experimentally and theoretically at 25 °C

Fe_3O_4 nanoparticles Concentration (wt.%)	**Calculated specific heat capacity (J g^{-1} K^{-1})**	**Measured specific heat capacity of this study (J g^{-1} K^{-1})**
0.00	1.140	1.140
0.05	1.115	1.112
0.1	1.091	1.085
0.15	1.066	1.055
0.2	1.042	1.019

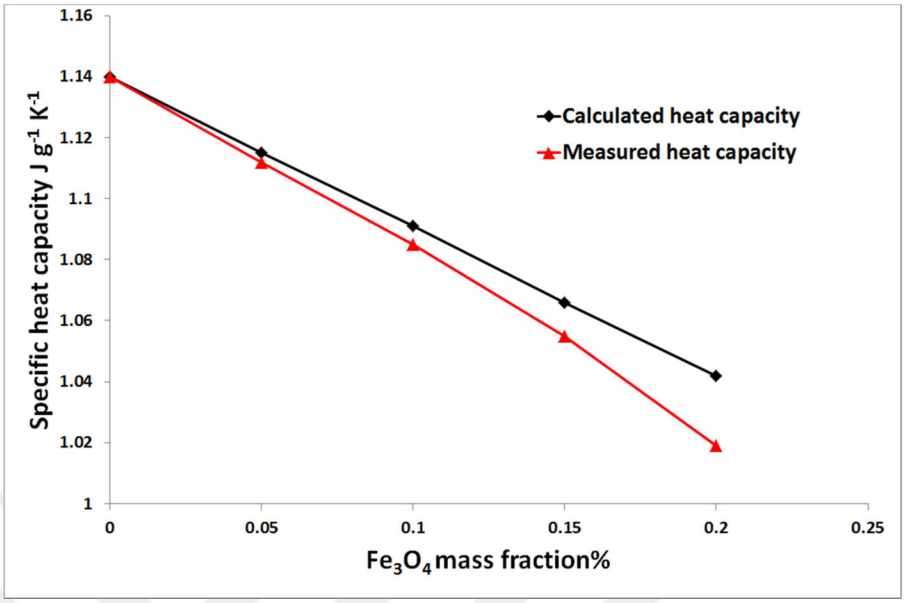

Figure 4.7. Changes of the nanoferrofluid specific heat capacity with different Fe_3O_4 mass fraction, experimentally and theoretically

4.1.3. Thermal Conductivity

The thermal conductivity is a very important property in our study. Because it can be used to illustrate the enhancement of heat transfer in the bubble pump of DARS by using the nanoferrofluid instead of the conventional working solution, which is the main aim of this work. Ajib and Karno, (2008) have not studied this property in their research. Thermal conductivity of acetone/$ZnBr_2$ with several concentrations of $ZnBr_2$ in the solution (40–65 wt.%) were tested using KD2 Pro Thermal Properties Analyzer, Decagon Devices, Inc. (Decagon Devices, 2020). The results of the thermal conductivity measurements of acetone/$ZnBr_2$ which were obtained in this study are significantly similar to those were by Mohammed et al., (2020). After performing 2 h sonication process, the nanoferrofluid samples (The base-fluid is acetone/$ZnBr_2$ with 50 wt.% of salt) with different concentrations of nanoparticles (0.05, 0.1, 0.15, and 0.2 wt.% of Fe_3O_4) experimentally and theoretically were studied.

As is shown in Table 4.5, the thermal conductivity increases from 0.150 to 0.167 (W m^{-1} K^{-1}) when the concentration of the Fe_3O_4 nanoparticles increases from 0 to 0.2 (wt.%), also the enhancement of thermal conductivity reaches to 10.179 % at 0.2 (wt.%).

Table 4.5. The thermal conductivity of the Fe_3O_4-acetone/$ZnBr_2$ (50 wt.% $ZnBr_2$) with various concentrations of Fe_3O_4 indicated experimentally and theoretically in this study at 25 °C

Fe_3O_4 nanoparticles Concentration (wt.%)	**Calculated thermal conductivity $k_{Maxwell}$ (W m^{-1} K^{-1})**	**Measured thermal conductivity (W m^{-1} K^{-1})**	**Enhancement %**
0.00	0.15000	0.150	-
0.05	0.15022	0.157	4.458
0.1	0.15045	0.161	6.832
0.15	0.15068	0.164	8.536
0.2	0.15091	0.167	10.179

The maximum values of the uncertainty had a considerable amount during the preparation experiments (due to the used analyzer). Later, we overcame this by performing the measurements for 3 same samples from every studied concentration and more than 15 times for every sample of them at the same ambient conditions. Finally, the measurement error at a given temperature was less than 1.5 %.
The effective thermal conductivity can be calculated by

$$k_{\text{Maxwell}} = \left[\frac{2k_s + k_p + 2\varphi(k_p - k_s)}{2k_s + k_p - \varphi(k_p - k_s)} \right] k_s \qquad \textbf{(4.3)}$$

Where φ refer to the volume fraction. k_p=0.61 W m^{-1} K^{-1} at 25 °C, (Sundar et al., 2013).

It is known as the classical Maxwell's equation, (Maxwell, 1904). Later, a lot of researchers tried to improve this model by correlating it to their experimental studies. Thus, they proposed predictive models for thermal conductivity, (Prasher and Phelan, 2006; Xu et al., 2006; Jang and Choi, 2007; Vajjha and Das, 2009; Rizvi et al., 2013; Hong et al., 2005). However, their model is complex and there are different experimental parameters, including the fractal dimension and the ratio of the minimum to a maximum diameter of nanoparticles. Also, they do not have satisfying results in such the current study.

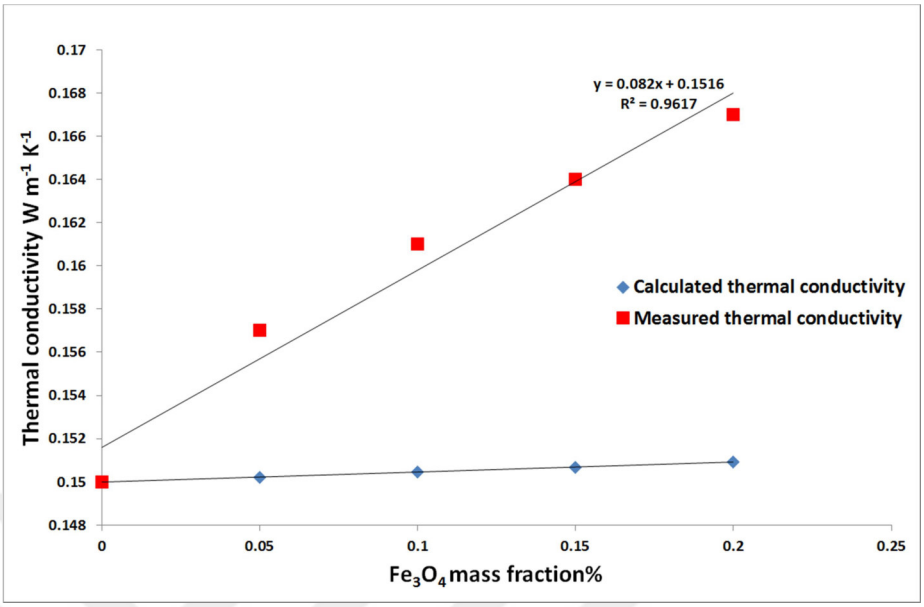

Figure 4.8. Changes of the nanoferrofluid thermal conductivity with different Fe_3O_4 mass fraction, experimentally and theoretically

Figure 4.8. shows the difference in thermal conductivity between the theoretical (depending on the Maxwell model) and experimental values which are related to the concentration of Fe_3O_4 nanoparticles. Where it can be realized that although the high viscosity value comparing with base-fluid the Fe_3O_4-acetone/$ZnBr_2$ which weakens the Brownian motion of suspended nanoparticles, the Maxwell equation does not give a significant prediction on the thermal conductivity of nanoferrofluid without Brownian motion of suspended nanoparticles, and the conduction part of the prediction model cannot be obtained from Maxwell prediction, (Hong et al., 2005).

4.1.4. Vapor Pressure

The (log p, T) diagram of acetone/$ZnBr_2$ as a working solution is used to determine the base-fluid concentration domain of the running process of the DARS. Relying on this domain, we can be able to study the cooling cycle (determining the temperatures of main points in the cycle and especially the needful heat resource temperature to run the machine in light of the ambient conditions).

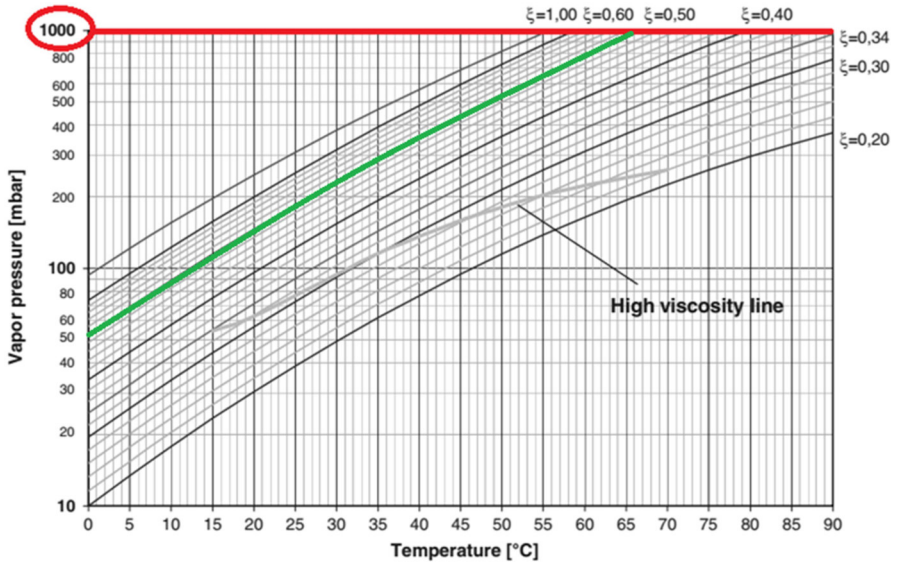

Figure 4.9. The plotted (*log p, T*) diagram of acetone/$ZnBr_2$ shows several concentrations of $ZnBr_2$ (wt.%) by Ajib and Karno, (2008)

Figure 4.9., carried out by Ajib and Karno, (2008), shows a *log p, T* diagram of acetone/$ZnBr_2$ working solution up to 1 bar. The green line illustrates the 50 wt.% $ZnBr_2$ which is the used concentration of the studied base-fluid with different Fe_3O_4 nanoparticles concentrations in this investigation.

4.2. Fe_3O_4 _ H_2O/NH_3 Nanoferrofluid Analyses Results

4.2.1. Stability of Fe_3O_4 _ H_2O/NH_3 Nanoferrofluid

4.2.1.1. Dispersion Characteristics of Fe_3O_4 Nanoparticles In the Base-fluid

As is mentioned before, the problem with magnetic particles is that the long-range magnetic forces always will overcome any charge ('electrostatic') stabilization attempts, and van der Waals forces are always attractive, thus more agglomeration and sedimentation. Furthermore, with the non-attendance of any surface coating substance, the Fe_3O_4 nanoparticle has hydrophobic surfaces with a huge surface area to volume ratio, thus nanoparticles start to agglomerate and shape bigger particles. Over time and because of the bigger particles, vigorous magnetic dipole-dipole

attractions between them start to be obvious and, consequently, ferromagnetic behavior is shown. The coating process with high-density materials is one of the used methods for more stabilizing iron oxide nanoparticles in the base fluid. So, to curb the aggregation incident of the nanoparticles, a stabilizer (a surfactant or a polymer) is commonly utilized at the time of preparation. The used polymers cohere to surfaces in a substrate-specific way. There are several kinds of synthetic or natural polymeric coating substances, for example of synthetic ones: polyethylene glycol, poly (vinyl alcohol), poly (lactic-co-glycolic acid), poly (vinyl-pyrrolidone), poly(ethylene-co-vinyl acetate), etc. Also, for enhancing the dispersibility in an aqueous medium, different surfactants, like sodium oleate, dodecylamine, and sodium carboxymethyl cellulose are commonly utilized, (Ali et al, 2016).

For overcoming these forces a sonication process is performed experimentally on the nanoferrofluid samples with Fe_3O_4 nanoparticle concentrations of 0.05, 0.1, 0,15, and 0.2 *wt.*%. The nanoferrofluid samples are left in an ultrasonic device (bath type, 40 kHz, 160 W, model HY- 6 Lt D) produced by HI TEKNOLOJI LTD for 2 hours except one sample where left for 3 hours in order to compare the effect of sonication process period on the nanoparticles suspension stability, (Hyteknoloji Limited, 2020). Then three chemical surfactant substances (sodium dodecyl sulfate, poly vinyl pyrrolidone, and polyvinyl alcohol) were examined in a try to enhance the sonicated nanoferrofluid stability.

4.2.1.2. Visual Inspection of Stability

Figure 4.10. illustrates nanoferrofluid suspensions with several concentrations of Fe_3O_4. Tube number 1 was prepared with 3 hours of sonication and with 0.1 wt.% of Fe_3O_4 concentration in order to present the effect of sonication process time on the stability of suspension nanoparticles in the nanoferrofluid. Tube number 5 was prepared without sonication and with 0.1 wt.% of Fe_3O_4 concentration. It can be seen from Figure 4.10.a that the sonication process has an obvious influence on the samples comparing with tube 6 (non-sonicated sample). Sonicated samples have less agglomeration and the upper section of tube 6 is, somewhat, more net than the same section of others over time. On the other hand, from Figures. 4.10.b, 4.10.c, and 4.10.d, it can be realized that although there is an increasing trend to produce bigger agglomerations in samples that have a greater concentration of nanoparticles, there

is no obvious difference in sedimentation in each solution under natural gravity. These results elucidate that the nanoferrofluid has good dispersion and weak stability characteristics. That pushes us to use an additional method by applying a magnetic field to get good stability when this nanoferrofluid is applied in DARS.

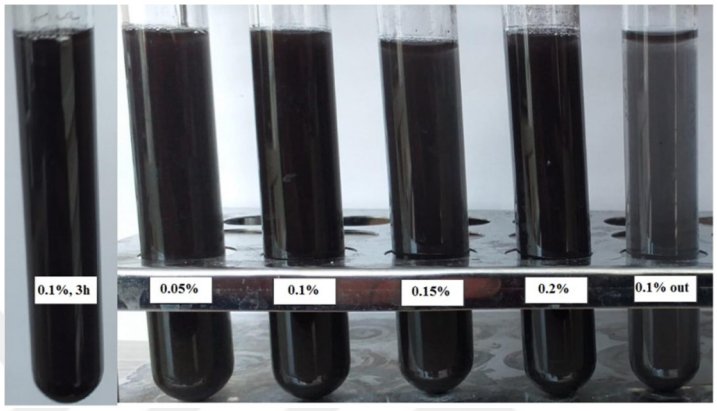

1 2 3 4 5 6

(After sonication directly) (a)

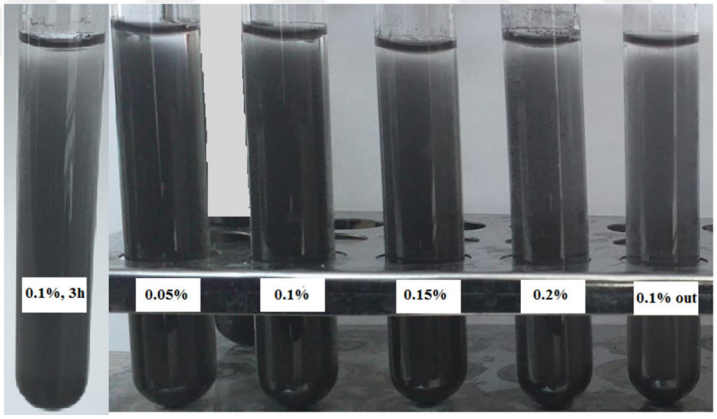

(15 minutes later) (b)

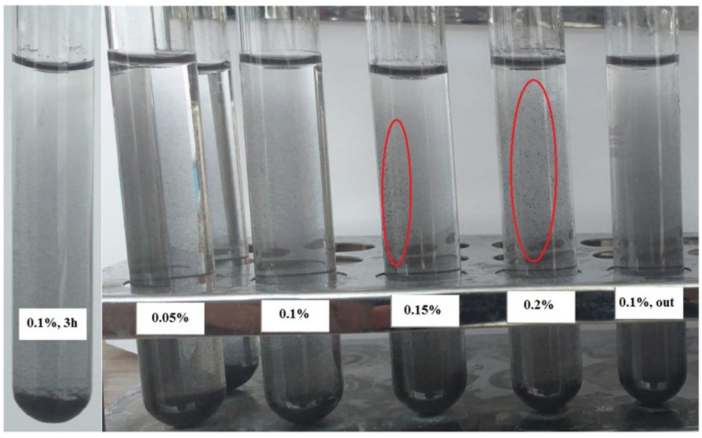

(1 hours later) (c)

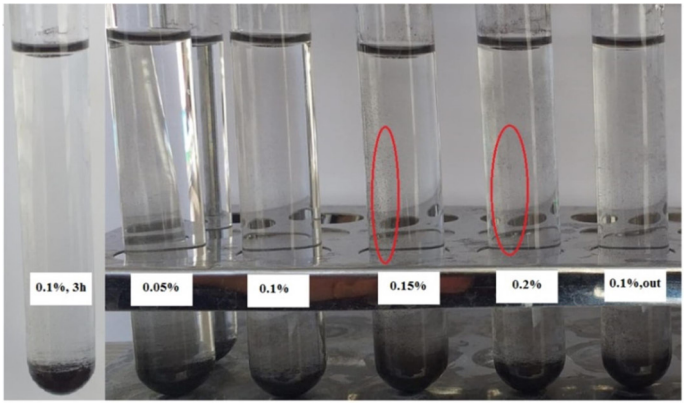

(3 hours later) (d)

Figure 4.10. Sedimentation and agglomeration of varies concentrations of Fe_3O_4 nanoparticles in NH_3/H_2O base-fluid. 1–0.1 *wt.*% (with 2 h sonication); 2–0.05 *wt.*%; 3–0.1 *wt.*%; 4–0.15 *wt.*%; 5–0.2 *wt.*% (with 2 h sonication). 5–0,1 *wt.*% (without sonication)

After several pre-experiments performed on different samples that had different concentrations of nanoparticles in the used ultrasonic device with various sonication process periods, and from comparing sample 1 with the other samples, it can be inferred the sonication process time on the nanoferrofluid has no significant influence on the suspension stability.

4.2.1.3. Examination of the Chemical Surfactant Factors Effects

Three chemical surfactant factors (poly vinyl pyrrolidone (PVP), sodium dodecyl sulfate (SDS), and polyvinyl alcohol (PVA)) were examined in a try to enhance the sonicated nanoferrofluid stability. The sample used in this test was a solution with a 0.1 *wt.*% concentration of nanoparticles that were prepared with the same by adding 1 *wt.*% of the three surfactants separately. Figure 4.11. shows that PVP surfactant dissolved well in the solution and has a useful effect on the dispersion of the nanoparticles over time. Where after the sonication process particles start a late agglomeration comparing with other samples that have other surfactants, even comparing with the same concentration sample without surfactant. SDS has a good dissolving but no useful effect on the dispersion of the nanoparticles, even has a foam that obstructs us to use it in such as diffusion absorption cycle. PVA has a less useful effect on the dispersion than PVP effect, also cannot dissolve well

and start to collect on the bottom of the sample tube. Over time these effects become clearer.

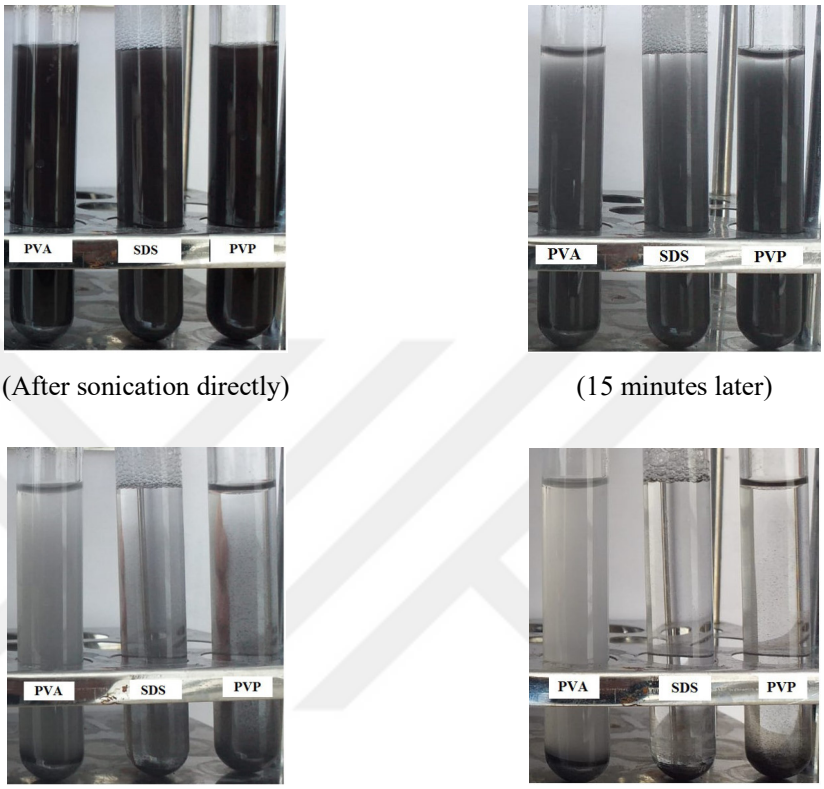

(After sonication directly) (15 minutes later)

(1 hours later) (3 hours later)

Figure 4.11. Effects of using different surfactants on the stability of nanoferrofluid (Fe_3O_4-NH_3/H_2O) over time

4.2.1.4. Scanning Electron Microscope (SEM) Analysis

The surface morphology and particle sizes of the samples were carried out using a high-resolution SEM (JEOL-JSM-7001F) type which exists in Black Sea Advanced Technology Research and Application Center Laboratories (KITAM) operating at 15 kV. Figure 4.12. shows SEM images of Fe_3O_4 nanoparticles of 0.05 *wt.*% mass concentration nanoferrofluid. The images display no clear agglomeration, which shows the Fe_3O_4 nanoparticles have almost a typical and random distribution situation, without a magnetic field, in the liquid. And this distribution occurred after sonication because of just the nanoparticles' thermal motion.

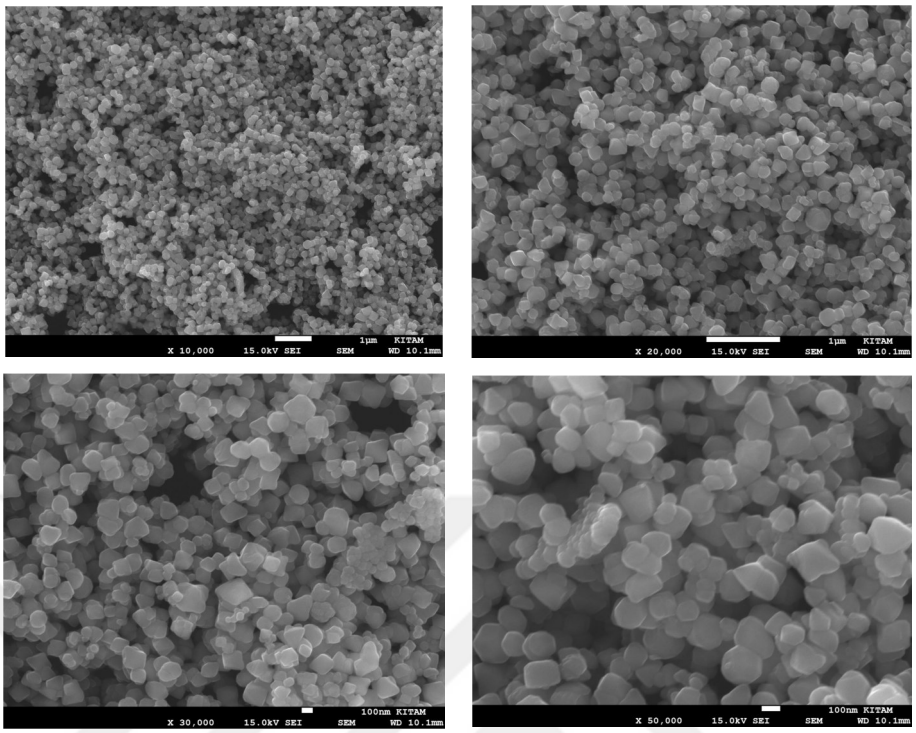

Figure 4.12. Various SEM images of Fe_3O_4 nanoparticles suspension in the NH_3/H_2O solution on a carbon film show randomly dispersed particles without any magnetic field

4.2.2. Thermophysical Properties

4.2.2.1. Density

The measured density of base-fluid (containing 25% of ammonia and 75% of distilled water) at 25°C in this study was significantly similar to those investigated in the literature, (Conde-Petit, 2004; Mohd Razif et al., 2015). During the experiment by taking the volumetric flask error (0.5 to 1%) into consideration and depending on the volumes used (10 ml sample). Figure 4.13. shows an increase in the density of the nanoferrofluid from 0.9150 to 0,9165 g cm^{-3} with an increasing concentration of the mass fraction from 0.0 to 0.2 *wt.*% of the added nanoparticles. And also, almost identical values of the theoretical density (which set by compensation ρ_s*=0,915* g cm^{-3}, ρ_p*=5* g cm^{-3}, (Merck KgaA, 2020), in Equation 4.1) with experimental ones, (Mohammed et al., 2020).

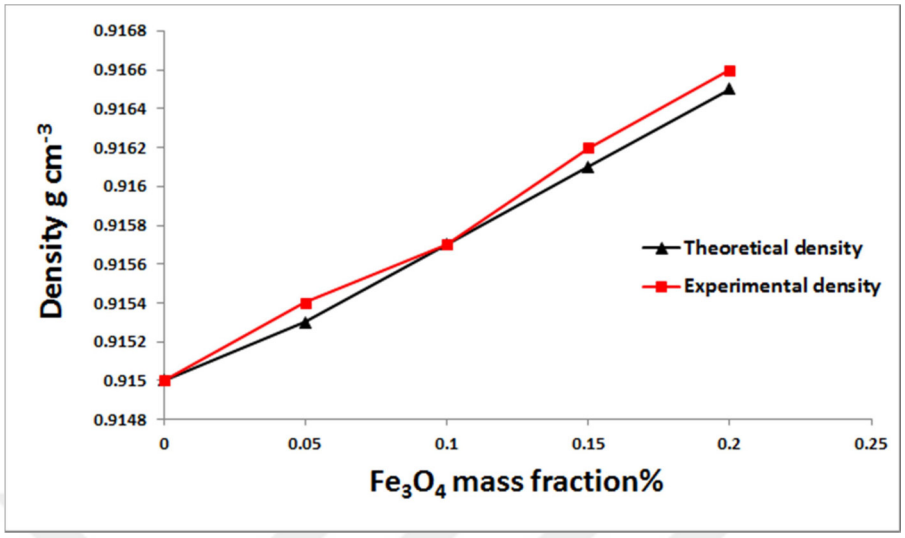

Figure 4.13. Changes of the nanoferrofluid density with different Fe_3O_4 nanoparticlesmass fraction, experimentally and theoretically

4.2.2.2. Viscosity

The viscosity of base-fluid (containing 25% of ammonia and 75% of distilled water) was measured at 25°C, using Thermo Scientific™ HAAKE™ MDARS™ 40 Rheometer, (Thermo Fisher Scientific Inc, 2020). The measured viscosity was significantly similar to those investigated in the literature, (Conde-Petit, 2004; Mohd Razif et al., 2015). On the other hand, it can be realized from Figure 4.14. that a major increase in viscosity of mixture happened from 1.815 to 7.637 mPa s with increasing concentration of Fe_3O_4 from 0 to 0.2 wt.%. Consequently, the nanoferrofluid has a high viscosity comparing with its base fluid. And also has a high viscosity comparing with another kind of nanofluid with the same base-fluid. The viscosity measurements were repeated at least 3 times. The measurement error at the given temperature was less than 1%. It is assumed that nanoferrofluid has a single-phase liquid.

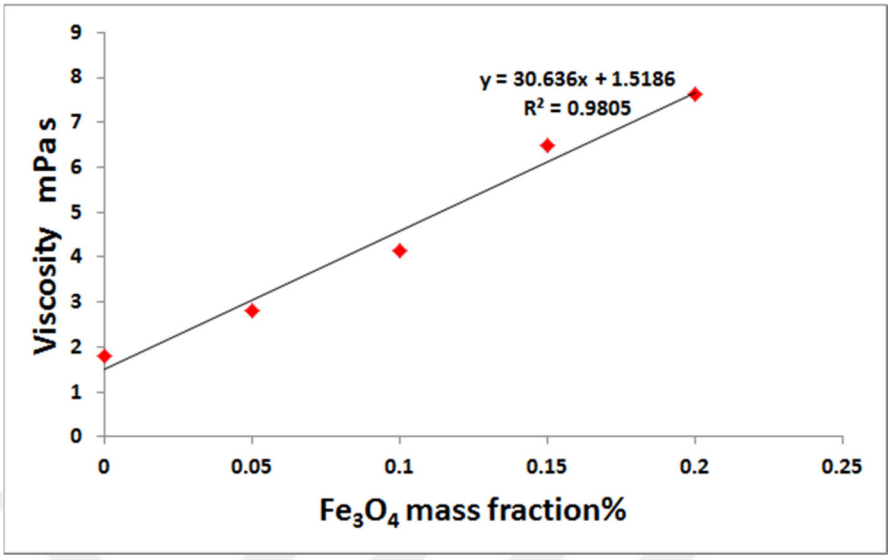

Figure 4.14. Changes of the nanoferrofluid viscosity with different Fe_3O_4 nanoparticle mass fraction

4.2.2.3. Specific Heat Capacity at Constant Pressure

The viscosity of base-fluid (containing 25% of ammonia and 75% of distilled water) at 25 °C was measured using KD2 Pro Thermal Properties Analyzer, Decagon Devices, Inc., (Decagon Devices, 2020). The result of this analysis has no substantial difference with those measured in literature, (Conde-Petit, 2004; Mohd Razif et al., 2015). But there is no previous study that has tested the specific heat capacity of a nanoferrofluid with NH_3/H_2O as a base-fluid, which is studied in this work. Table 4.6. illustrates the specific heat capacity of the Fe_3O_4- NH_3/H_2O (25 wt.% ammonia) with various concentrations of Fe_3O_4 indicated experimentally and theoretically at 25 °C and pressure equal to 1 bar.

While there are several methods for assessing the heat capacities of pure liquids, very few set correlations have been proposed for mixtures. Furthermore, since there is no model obtainable to calculate the specific heat capacity of nanofluids, a simple method (which set by Equation 4.2) depended on the corresponding state principle is proposed for the calculation of the heat capacities of liquid mixtures, , (Teja, 1983; Sohel Murshed, 2011).

It can be realized from Figure 4.15. that the specific heat capacity decrease with increasing the particles (Fe_3O_4) concentration. It is a logical consequence because of the low heat capacity value of the nanoparticles (0.653 J g^{-1} K^{-1}) compared with the

specific heat capacity of NH_3/H_2O (4134.15 J g^{-1} K^{-1}). The higher concentration, the higher agglomerations. Thus, more agglomeration causes bigger particles in the nanoferrofluid which drops the total heat capacity and that is also what was mentioned in the literature with other kinds of nanofluids, (Zhou and Ni, 2008; Sekhar and Sharma, 2015; Mohammed et al., 2020).

Table 4.6. The specific heat capacity of the Fe_3O_4-NH_3/H_2O (50 *wt.*% $ZnBr_2$) with various concentrations of Fe_3O_4 indicated experimentally and theoretically at 25 °C

Fe_3O_4 nanoparticles Concentration (*wt.*%)	**Calculated specific heat capacity ($J\ g^{-1}\ K^{-1}$)**	**Measured specific heat capacity of this study ($J\ g^{-1}\ K^{-1}$)**
0.00	4134.15	4134.15
0.05	4132.08	4131.05
0.1	4130.02	4128.10
0.15	4128.06	4125.01
0.2	4125.88	4120.51

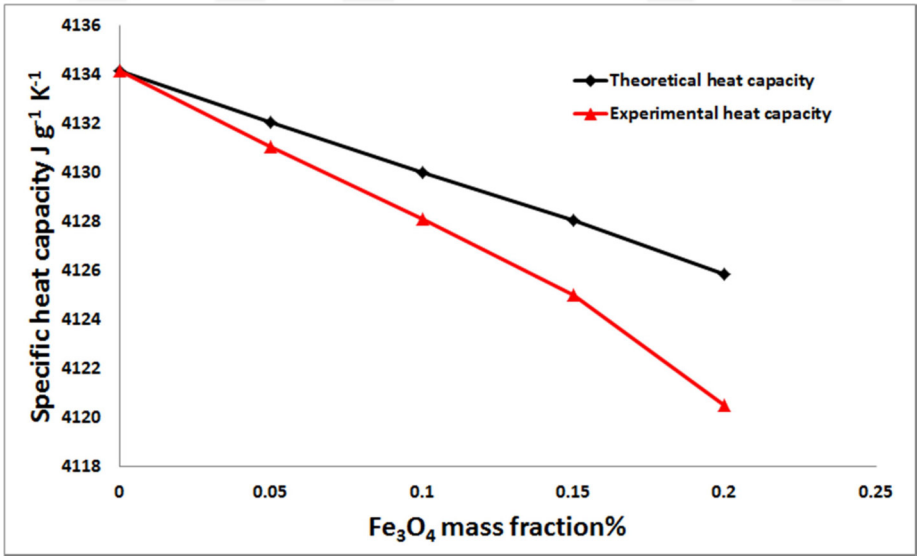

Figure 4.15. Changes of the nanoferrofluid specific heat capacity with different Fe_3O_4 mass fraction, experimentally and theoretically

4.2.3. Thermal Conductivity

Thermal conductivity is a very important property in our study. Because it can be used to illustrate the enhancement of heat transfer in the generator of DARS by

using the nanoferrofluid instead of the conventional working solution. Thermal conductivity of NH_3/H_2O (containing 25% of ammonia and 75% of distilled water) at 25 ℃ was tested using KD2 Pro Thermal Properties Analyzer, Decagon Devices, Inc., (Decagon Devices, 2020). The result of the thermal conductivity measurement of NH_3/H_2O which was obtained in this study is significantly similar to those were by (Conde-Petit, 2004; Mohd Razif et al., 2015). After performing 2 hours sonication process, the nanoferrofluid samples with different concentrations of nanoparticles (0.05, 0.1, 0,15, and 0.2 *wt.*% of Fe_3O_4) experimentally were studied and also obtained theoretically by compensation the k_p=0.61 W m^{-1} K^{-1} at 25 °*C* in Maxwell's equation 4.3 (Sundar et al., 2013).

As is shown in Table 4.7., the thermal conductivity increases from 0.550 to 0.570 W m^{-1} K^{-1}, when the concentration of the Fe_3O_4 nanoparticles increases from 0 to 0.2 *wt.*%. The enhancement in thermal conductivity reaches 3.508 % at 0.2 *wt.*%.

Table 4.7. Thermal conductivity of the Fe_3O_4- NH_3/H_2O (25 % ammonia) with various concentrations of Fe_3O_4 indicated experimentally and theoretically in this study at 25 °C

Fe_3O_4 nanoparticles Concentration (*wt.*%)	**Calculated thermal conductivity $k_{Maxwell}$ (W m^{-1} K^{-1})**	**Measured thermal conductivity (W m^{-1} K^{-1})**	**Enhancement %**
0.00	0.55000	0.550	-
0.05	0.55001	0.557	1.256
0.1	0.55002	0.561	1.960
0.15	0.55003	0.566	2.826
0.2	0.55004	0.570	3.508

The maximum values of the uncertainty had a considerable amount during the preparation experiments (due to the used analyzer). Later, we overcame this by performing the measurements for 3 same samples from every studied concentration and more than 15 times for every sample of them at the same ambient conditions. Finally, the measurement error at a given temperature was less than 1.5 %.

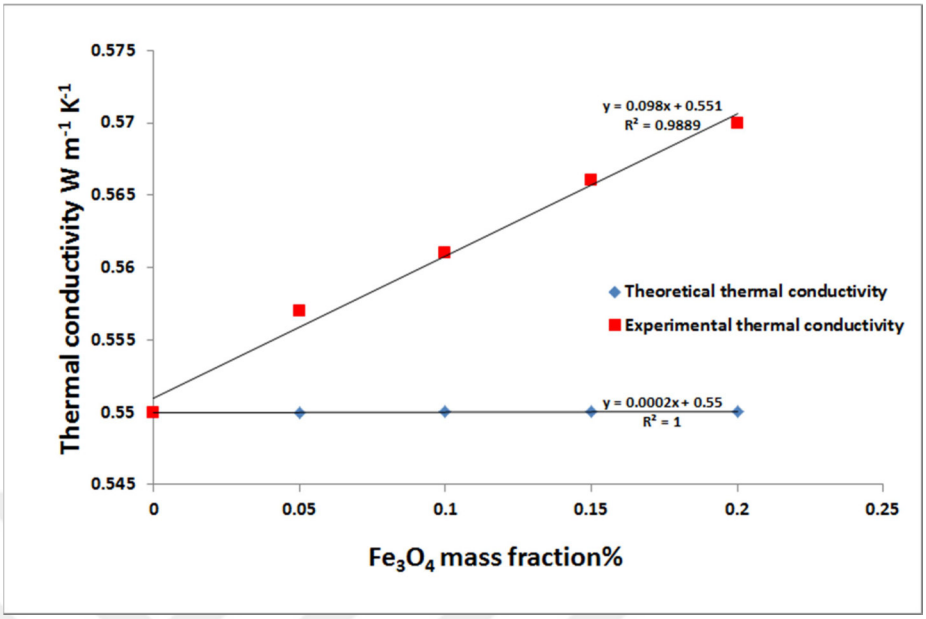

Figure 4.16. Changes of the nanoferrofluid thermal conductivity with different Fe_3O_4 mass fraction, experimentally and theoretically (depending on Maxwell's equation)

Figure 4.16. shows the difference in thermal conductivity between the theoretical (depending on the Maxwell model) and experimental values which are related to the concentration of Fe_3O_4 nanoparticles. Where it can be realized that although the high viscosity value comparing with base-fluid the Fe_3O_4-NH_3/H_2O which weakens the Brownian motion of suspended nanoparticles, the Maxwell equation does not give a significant prediction on the thermal conductivity of nanoferrofluid without Brownian motion of suspended nanoparticles, and the conduction part of the prediction model cannot be obtained from Maxwell prediction, (Hong et al., 2005).

4.3. Validation Investigation of Using acetone/$ZnBr_2$ as a Working Solution In DARS

Since acetone/$ZnBr_2$ is a new binary solution and it has not been used in DARS as a refrigeration working solution before, it had to be studied the validation for utilizing it in this kind of cycle. The acetone/$ZnBr_2$ refrigeration working solution with 50 wt.% concentration of $ZnBr_2$ was prepared. The measured main parameters of this solution at 25 ^{o}C are presented as follows: density of 1.366 (kg m^{-3}), viscosity 3.384 (mPa s), specific heat capacity 1.14 (J g^{-1} K^{-1}), and thermal conductivity 0.150

($W\ m^{-1}\ K^{-1}$). In order to examine the validation of utilizing this conventional working solution (without nanoparticles), DARS was charged with 300 ml of working solution and a sufficient amount of helium gas. The experiment was performed two times under the same surrounding conditions, firstly under operation pressure equal to 15 bar which is the working standard pressure of DARSs. Then the experiment was repeated with less operation pressure (5 bar). The supplied power to the system for every experiment was the same (by a 75 W electrical heater). The experiment for every time continued for 1 hour.

Theoretically, the system can be started running with the chosen operation conditions under cycle pressure less than 10 bar as is shown in the acetone phase diagram (Figure 4.17.). Whereas the results presented that acetone/$ZnBr_2$ binary solution is not valid for use in DARS due to the following reasons:

1. In literature, acetone/$ZnBr_2$ has used mainly with refrigeration applications that run under low operating pressure. Ajib and Karno, (2008) examined the working solution and found that is suitable to operate ARS at low temperatures (more than 50 °C) and 750 mbar operation pressure in the cycle. Mohammed et al., (2019) extended the *log p, T* diagram of the solution up to 1.39 bar because its experiment reached the operating pressure almost equal to this value. Since in DARS the operating pressure should be high because the cycle operates under Dalton's law principle based on partial pressures and the pressure in each point of the system is maintained constant using a gas auxiliary, the machine didn't run even when the pressure in the system was dropped to 5 bar.
2. From Figure 4.17. it can be realized that acetone needs a high operating temperature comparing with pure ammonia at the operating pressure of DARS. Thus acetone/$ZnBr_2$ is not a suitable binary solution for use as a low-temperature working solution in DARS comparing with other kinds of binary solutions which NH_3 is the refrigerant fluid of them.
3. Reducing the operating pressure of the cycle to less than 5 bar is not logical because of the very high value of circulation ratio at low pressures.

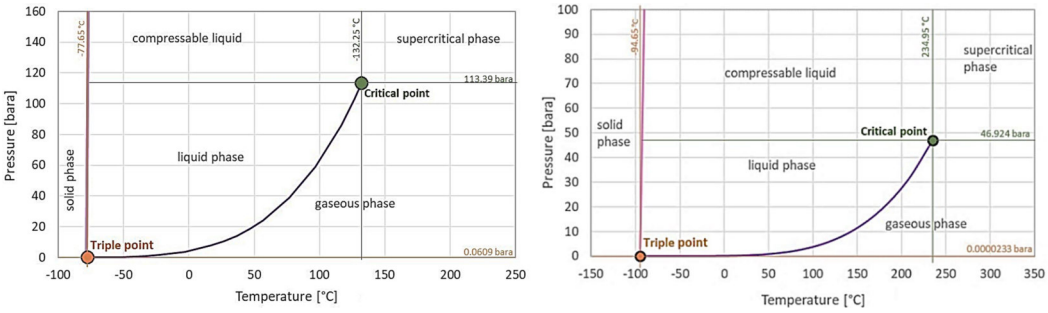

NH_3 phase diagram

Acetone phase diagram

Figure 4.17. Pressure-Temperature diagrams of pure acetone and pure ammonia, (Engineering ToolBox 2021)

4.4. The Valid Working Solution Characteristics

The NH_3/H_2O refrigeration working solution with 25 % concentration of NH_3 was prepared. The measured main parameters of this solution at 25 ^oC are presented as follows: density of 0.9150 (g cm^{-3}), viscosity 1.815 (mPa s), specific heat capacity 4134.15 (J g^{-1} K^{-1}), and thermal conductivity 0.550 (W m^{-1} K^{-1}). Firstly, the validation of utilizing the conventional working solution (without nanoparticles) in DARS was studied. Further similar samples of NH_3/H_2O were prepared for using it as a base-fluid then adding Fe_3O_4 nanoparticles. The obtained nanoferrofluid (Fe_3O_4-NH_3/H_2O) was prepared with different fraction mass concentrations (0,05, 0.1, 0.15, and 0.2 wt.% of Fe_3O_4 in NH_3/H_2O base-fluid with 25 % of $ZnBr_2$) using the two-step process (creation of the nanoparticle is prepared in a separated way from used working solution). The experiments were designed to see how effects of various concentrations of the nanoferrofluid mixture and to obtain the optimal concentrations of the nanoferrofluid components which will be used in DARS depending on its physical properties and visual inspection test. The most effective approach for enhancing nanoparticle suspension is prepared as follows; The nanoferrofluid samples are left in an ultrasonic device (bath type, 40 kHz, 160 W, model HY- 6 Lt D) produced by HI TEKNOLOJI LTD for 2 hours. Then three chemical surfactant substances (sodium dodecyl sulfate, poly vinyl pyrrolidone, and polyvinyl alcohol) were examined in a try to enhance the sonicated nanoferrofluid stability.

Although the enhancement of thermal conductivity increases as increasing nanoparticle concentration, where reaches 3.508 % at 0.2 (wt.%) of nanoparticles,

The nanoferrofluid has a high viscosity comparing with its base fluid and also comparing with other kinds of nanofluids with the same base-fluid. Furthermore, the specific heat capacity decreases with increasing the particles (Fe_3O_4) concentration. It is a logical consequence because of the low heat capacity value of the nanoparticles (0.653 J g^{-1} K^{-1}) compared with the specific heat capacity of NH_3/H_2O (4134.15 J g^{-1} K^{-1}), where higher concentration causes more agglomerations and bigger particles in the nanoferrofluid which drops the total heat capacity and that is also what was mentioned in the literature with other kinds of nanofluids, (Zhou and Ni, 2008; Sekhar and Sharma, 2015; Mohammed et al., 2020). On the other hand, from the visual inspection, it was found that PVP surfactant dissolves well in the solution and has a useful effect on the dispersion of the nanoparticles over time. Where after the sonication process particles start a late agglomeration comparing with other samples that have other surfactants, even comparing with the same concentration sample without surfactant. Depending on the above, the chosen concentrations of Fe_3O_4 nanoparticles in the NH_3/H_2O base-fluid to be examined in the cycle were 0.05 wt.% and 0.1 wt.% with addition 1 wt.% concentration of PVP surfactant.

4.5. The Effect of Using Various Placements of Permanent Magnets Around the Generator-Bubble Pump Component on Heat Transfer

In order to illustrate the effects of different installation of the permanent magnets around the generator-bubble pump component on the heat transfer using nanoferrofluid, the used magnet pieces are installed along the length of the generator-bubble pump external pipe at three different placements, starting from the bottom of the component to 7 cm, 16 cm, and 25 cm height, respectively, as is shown in Figure 4.18. For the three placements, 4, 8, and 12 pieces of the Neodymium Magnet (length 40 mm, Width 10 mm, Thickness 5 mm) respectively were used, (Magnet Market, 2021).

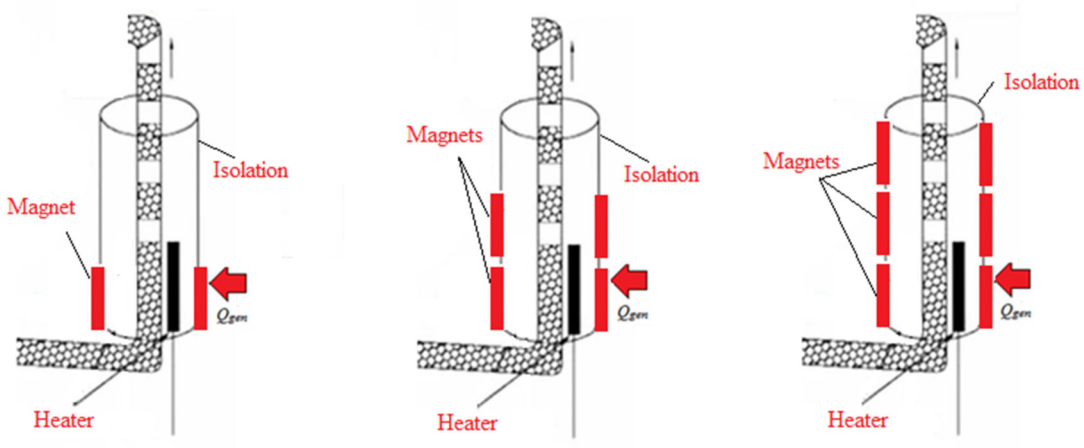

Figure 4.18. Schematic diagram of DARS with three different placements of the permanent magnets around the generator-bubble pump component

For every installation, the test procedure to be applied in this framework is defined as follows: the tested working solution in the system was Fe_3O_4-NH_3/H_2O nanoferrofluid with 0.05 wt.% nanoparticle concentration. The amount of energy for each application was supplied by an electrical heater its capacity equals 75 W. Permanent magnet pieces were installed regularly and at a constant radius (4 cm) on the isolation surface around the pipe of the generator-bubble pump pipe. The external magnetic field intensity was constant and equal to 220 mT, measured by (SJ200 Digital Gauss Meter Static Magnetic Field Tesla Tester with 0-200Mt-2000mT Adapter), Wu et al., (2010). Every test of the DARS with 7 cm and 16 cm magnet height continued for two hours. Whereas the test which had a 25 cm magnet height continued just for one hour.

The results can be represented as follows:

1. The effect of using an external magnetic field on the heat transfer in the generator bubble-pump component was significantly clear.
2. The best results were in the 16 cm magnet height test. Where this installation was chosen to use in the next experiments.
3. In the test of using the highest magnet, there was an overheated case and the temperature at point 3 (look Figure 4.17.) reached 200 ^{o}C. Thus, the cooling effect starts appearing at point 4 (the inlet of the condenser). Consequently, the cycle was in choked case after 35 minutes, so using this magnet prevents the cycle to run. This explains why this test continued for just one hour.

4. After equipping the DARS with the used nanoferrofluid in this step, the tests repeated several times in different periods for two days with the same working solution and the results showed almost the same values for every test, thus a good nanoparticle suspension stability for a long time with existing the external effect of the magnet.

4.6. Mechanistic Explanation of Heat Transfer Enhancement

The proportional motion among the nanoparticles and base-fluid is the major cause behind enhancement in heat transfer performance, where occasioned by the circulation of the nanoparticles, moving the heat along an oblique solution consequence extremely small convection created by the motion of the solution around the nanoparticles, (Pinto and Fiorelli, 2016).

On the other hand, using nanoferrofluid under influence of an external magnetic field causes appearing a macro-magnetic force and a magnetic–thermal effect in the nanoparticles. So, the obtained enhancement in heat transfer is not just only because of the small-size effect and rising in the effect of the heat exchanging surfaces of the nanoparticles. However, this phenomenon extremely related to a complex process of heat and mass transfer and no significant explanations exist in the literature for it.

Moreover, the expected enhancement in COP of DARS because of using this mechanism is not only related to heat transfer but also related to the enhancement of mass transfer, thus better values of the circulation ratio, Wu et al., (2010).

In fact, the obtained enhancement of the generator-bubble pump component performance and as a result in overall cycle performance by using the nanoferrofluid as an alternative for the conventional working solution under an external magnetic field has affected by combined various factors, and it may be optimized until a certain limit. This limitation can be briefed as follows, (Liu, 2004; Wu et al., 2010):

- Generally, nanomagnetic particles in the base-fluid become polarized under the effect of an external magnetic field. Thus the magnetic dipoles start to form and join to each other and align in a regular situation based on the magnetic field current.
- By rising the intensity of the magnetic field and at a certain value, the connection forces between the magnetic dipoles start to be stronger than the

thermal motion of them and form a steady chain structure. This phenomenon named **flux linkage**.

- After that, and due to the chain structure of the nanoparticle under the external magnetic field, the nanoferrofluid presents solid-state features. Thus it is able to transfer the shear stress. On the other hand, the connection between the flux linkages does not completely occur and has a so small distance between them, because of the polymer layer which is obtained by using the PVP surfactant during the nanoferrofluid preparation process.
- The nanomagnetic particles in the base-fluid are inhibited while the intensity of the magnetic field is upper than a certain value due to the above-mentioned flux linkage structure. So, the nanoparticles, in this case, cannot perform the positive required influence. Even cannot occur the random Brownian motion effect which exists without the magnetic field. That explains the choked case in the cycle which happened with 25 cm magnet height around the generator-bubble pump component.

4.7. Various Nanoferroflid Concentrations Effects Under the Same Conditions of DARS Cycle

Experiments were performed on nanoferrofluids of 0.05 wt.% and 0.1 wt.% Fe_3O_4 nanoparticles concentrations in 300 *ml* ammonia/water base-fluid with addition 1 wt.% concentration of PVP surfactant, which was equipped to DARS with and without an external magnetic field. Depending on the concentrations and presence or absence of the external magnetic field, the Experiments divided into five tests:

1. $DARS_{0.0\%.ref.}$ represents the test on DARS device using ammonia/water as a working solution without nanoparticles and in absence of magnets.
2. $DARS_{0.05\%}$ represents the test on using the nanoferrofluid of 0.05 wt.% nanoparticles concentration in absence of magnets.
3. $DARS_{0.05\%.Ma.}$ represents the test using the nanoferrofluid of 0.05 wt.% nanoparticles concentration in presence of the external magnetic field.
4. $DARS_{0.1\%}$ represents the test using the nanoferrofluid of 0.1 wt.% nanoparticles concentration in absence of the external magnetic field.

5. $DARS_{0.1\%.Ma.}$ represents the test using the nanoferrofluid of 0.1 wt.% nanoparticles concentration in presence of the external magnetic field.

Every test was repeated three times for ensuring the accuracy of tests results and every time the test ran 120 minutes. The obtained temperature values at the measuring points along the cycle, measured internal temperature in the cooled areas, and measured pressure over time for every DARS experiment are shown in Figures 4.19.–4.25.. Where the abscissas exemplify the experiment running time, whereas, the ordinates exemplify the temperature (^{o}C) of the necessary measurement points for the thermodynamic calculations of the cycle.

The detailed comparison of the illustrated temperature values in Figures 4.19.–4.25. shows the following notes:

- Although the early appearance of the cooling effect in the systems which run with nanoferrofluids in general, it takes a long time to reach the steady value comparing with the $DARS_{0.0\%.ref.}$. Where it has a sudden and major drop in this cycle till the steady case.
- Among the systems, the most late of the cooling effect appeared in $DARS_{0.1\%.}$ almost at minute 31. So, a higher suspension nanoparticle concentration results in a late appearance of the cooling effect. Whereas, the earliest appearance was in the $DARS_{0.1\%.Ma.}$ at the minute 20.
- The steady-state of the temperatures in different components is obtained early in $DARS_{0.0\%.ref.}$. While, it occurred late in the $DARS_{0.05\%}$.
- There was no necessity to perform the experiments for more than 120 minutes while the steady-state was reached in all systems maximum almost at minute 100 (evaporator temperature).
- The highest generator temperature (T_2) occurred in $DARS_{0.05\%}$ and the lowest one was in $DARS_{0.05\%.Ma.}$ at the same heater capacity.
- The highest evaporator entrance temperature (T_{6b}) occurred in $DARS_{0.05\%}$ and the lowest one was in $DARS_{0.05\%.Ma.}$ at the same running conditions.
- From Figure 4.24., it can be realized that the highest measured internal temperature in the cooled areas ($T_{in\text{-}amb.}$) occurred in $DARS_{0.05\%}$ and the lowest one was in $DARS_{0.05\%.Ma.}$.

- From Figure 4.25., it can be realized that the highest measured pressure values during the test over time ($P_{syst.}$) occurred in $DARS_{0.1\%.Ma.}$ and the lowest ones were in $DARS_{0.0\%.ref.}$.

In light of the previous notes, it can be briefed that:

- The significant influence of the external magnetic field is obvious in every aspect of the temperature and pressure values analysis.
- The presence of nanoparticles in the base-fluid causes rising in the pressure of the DARS. Also, the presence of the external magnetic field brings about more increases in the pressure value. Thus, higher nanoparticle concentration means higher overall cycle pressure due to the high viscosity of the nanoferrofluid. Furthermore, this increase occurs under the external magnetic field due to the chain structure of the nanoparticles.
- In the operation aspect of the cycle, it should be given attention that although the obtained enhancement in the cooling temperature by using the nanoferrofluid under the external magnetic effect, the taking off of the cycle needs longer time comparing with reference DARS, which runs just with conventional ammonia/water working solution, until reaching the steady-state of the temperatures of the different components.
- During the last analyses of the temperature and pressure values of the different systems, Although that the lowest evaporator and internal temperatures were in $DARS_{0.05\%,Ma.}$, the steady-state of the temperature of the internal cooled area appeared more clearly in $DARS_{0.1\%,Ma.}$.

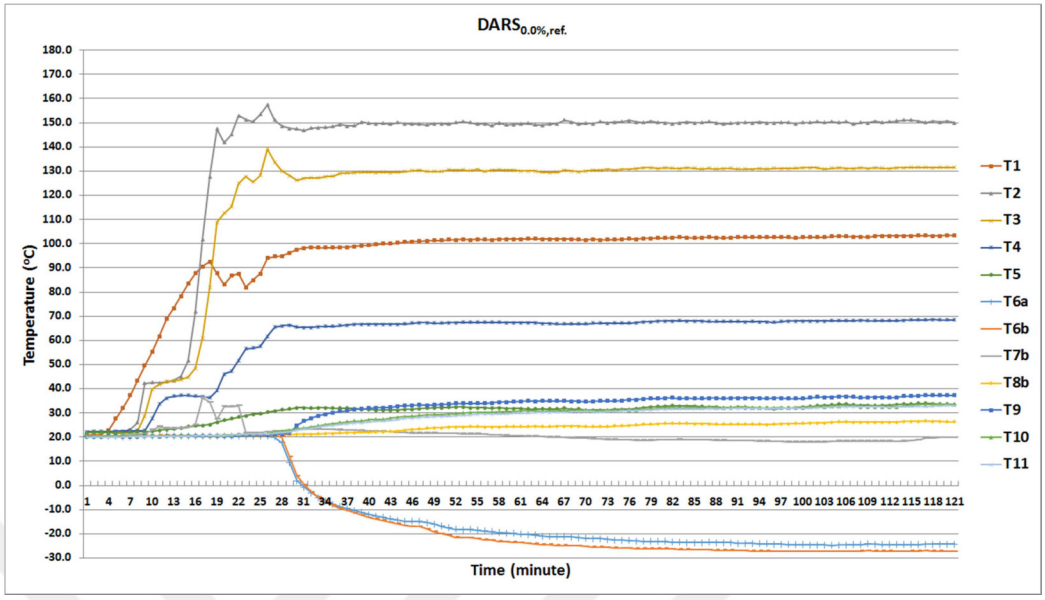

Figure 4.19. Measured temperatures in the $DARS_{0.0\%,ref.}$ at the measuring points of the cycle over time

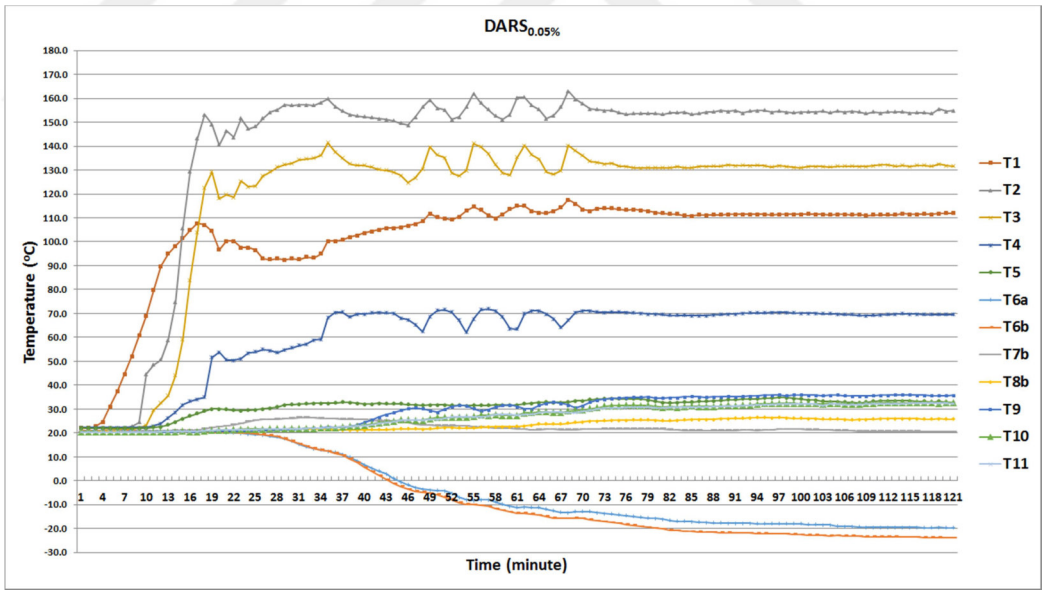

Figure 4.20. Measured temperatures in the $DARS_{0.05\%}$ at the measuring points of the cycle over time

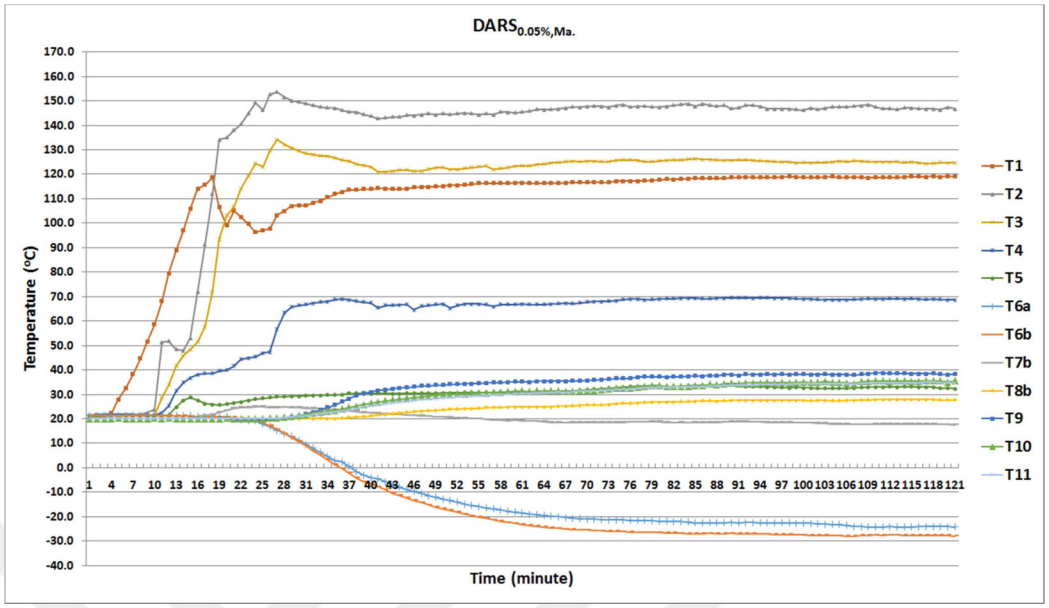

Figure 4.21. Measured temperatures in the $DARS_{0.05\%.Ma.}$ at the measuring points of the cycle over time

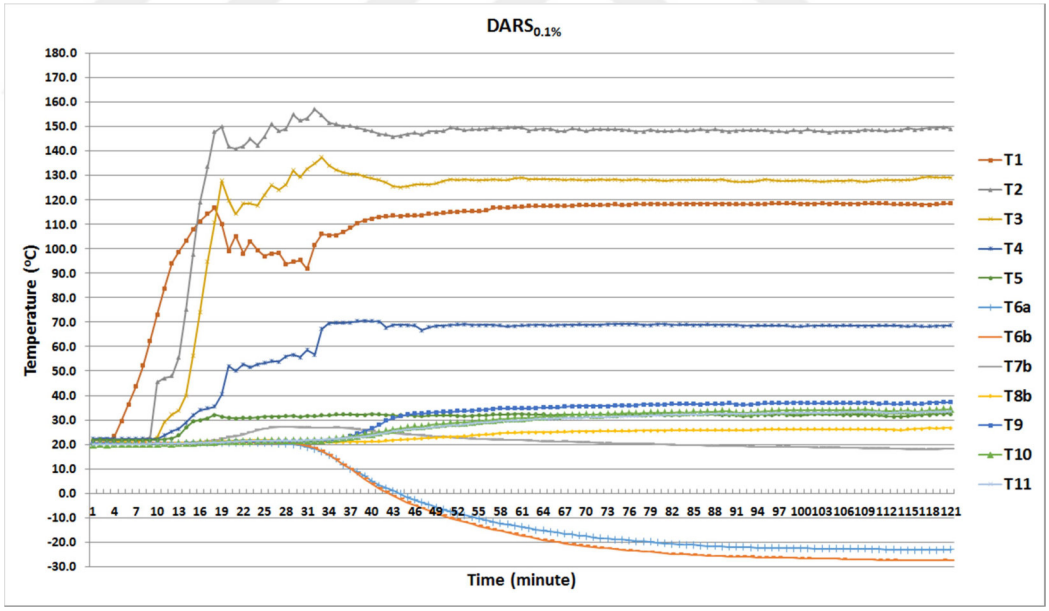

Figure 4.22. Measured temperatures in the $DARS_{0.1\%}$ at the measuring points of the cycle over time

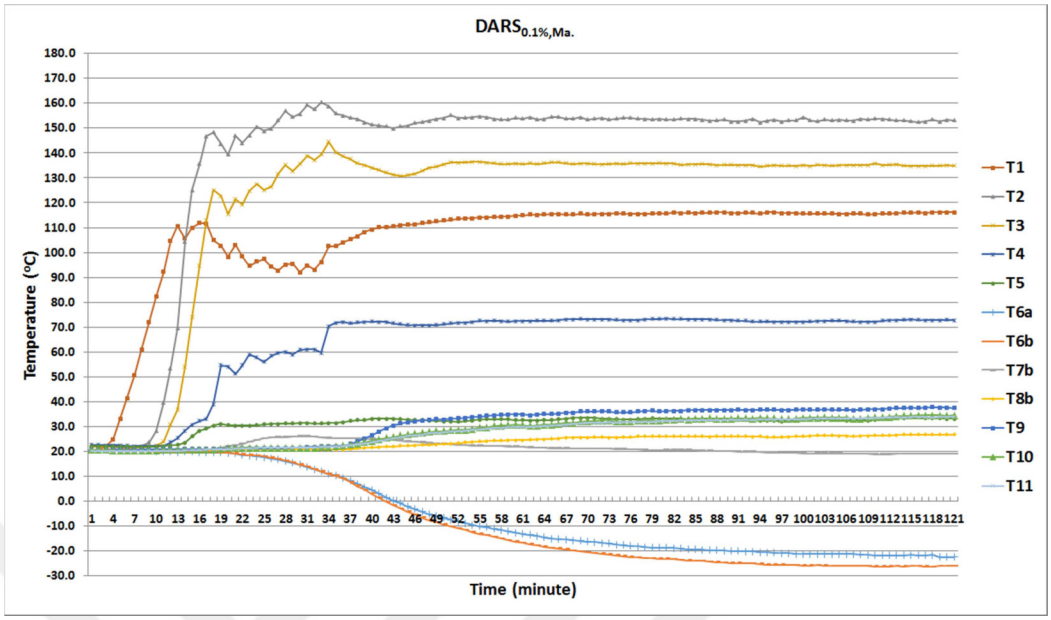

Figure 4.23. Measured temperatures in the $DARS_{0.1\%.Ma.}$ at the measuring points of the cycle over time

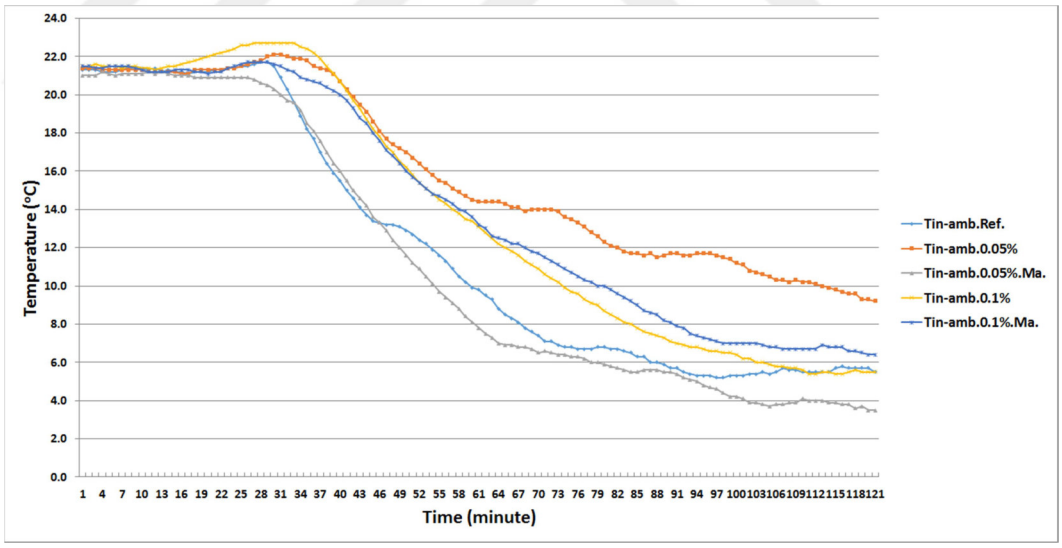

Figure 4.24. Measured internal temperature in the cooled areas of the $DARS_{0.0\%,ref.}$, $DARS_{0.05\%}$, $DARS_{0.05\%,Ma.}$, $DARS_{0.1\%}$, and $DARS_{0.1\%,Ma.}$ cycles over time

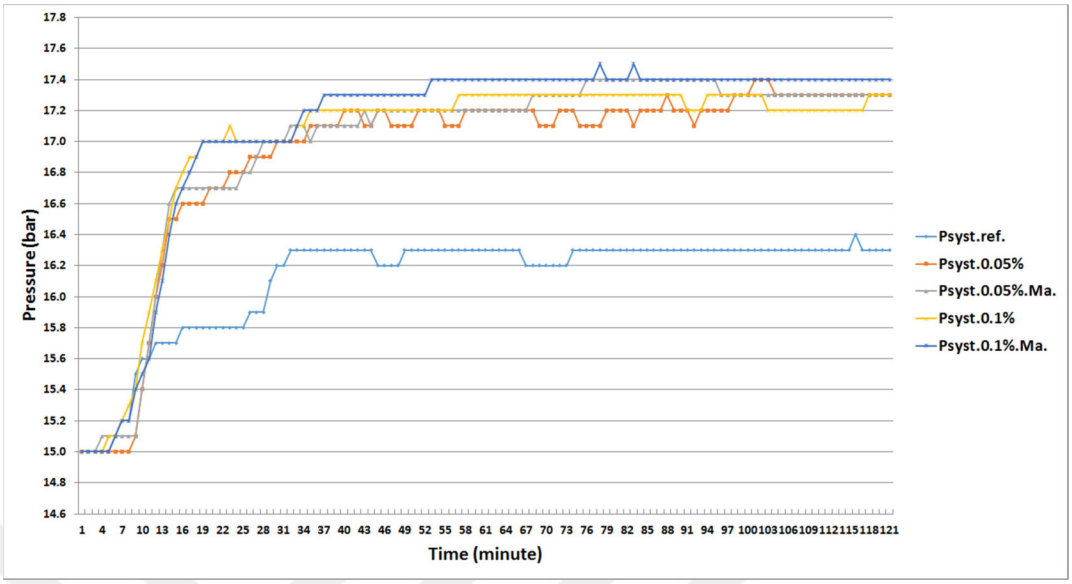

Figure 4.25. Measured pressure of the $DARS_{0.0\%,ref.}$, $DARS_{0.05\%}$, $DARS_{0.05\%,Ma.}$, $DARS_{0.1\%}$, and $DARS_{0.1\%,Ma.}$ cycles over time

4.8. Thermodynamic Analysis Results

In order to achieve optimal thermodynamic analyses, the values of the parameters listed in Table 4.8. for the $DARS_{0.0\%,ref.}$, $DARS_{0.05\%}$, $DARS_{0.05\%,Ma.}$, $DARS_{0.1\%}$, and $DARS_{0.1\%,Ma.}$ systems were obtained at minute 120, end of the test, and after a good period of the point that the cycles have reached the steady-state conditions.

It can be understood from Table 4.8. that the temperatures of the generator temperature measuring point from (T_1 ^{o}C) has a maximum value in and $DARS_{0.1\%,Ma.}$. On the other hand, the minimum value was in $DARS_{0.05\%,Ma.}$ and the lowest value of Evaporator entrance temperature of ammonia, (T_{6a} ^{o}C) in $DARS_{0.05\%,Ma.}$. These values have a major effect on generator and evaporator performances calculations, consequently, on the energy efficiency of the overall cycle. Also, it can be realized from Table 4.8. that the running pressure in the cycles rises.

Table 4.8. Measured parameters in the different tests at the measuring points of the cycle

Parameter	$DARS_{0.0\%,ref.}$	$DARS_{0.05\%}$	$DARS_{0.05\%,Ma.}$	$DARS_{0.1\%}$	$DARS_{0.1\%,Ma.}$
Bubble pump entrance temperature, $T_1=T_{1a}=T_{1b}$ (^oC)	103.3	112.0	119.0	118.6	116.2
Generator temperature, T_2 (^oC)	150.0	154.8	146.7	149.2	153.1
Bubble pump exit-rectifier entrance temperatures, T_3 (^oC)	131.5	131.6	124.7	129.1	134.9
Rectifier exit-condenser entrance temperatures, T_4 (^oC)	68.5	69.6	68.6	68.7	72.8
Condenser exit temperature, T_5 (^oC)	33.4	32.6	32.3	32.5	33.2
Evaporator entrance temperature of ammonia, T_{6a} (^oC)	-24.3	-19.6	-24.3	-23.0	-22.5
Evaporator entrance temperature, $T_6=T_{6b}=T_{6c}$ (^oC)	-27.2	-23.9	-28.0	-27.5	-26.0
Evaporator exit temperature, $T_7=T_{7a}=T_{7b}$ (^oC)	19.9	20.5	17.6	18.1	19.0
Absorber entrance	26.4	25.8	27.7	26.7	26.7

temperature, $T_8=T_{8a}=T_{8b}$ (^oC)					
Absorber exit temperature, $T_9=T_{9a}=T_{9b}$ (^oC)	37.3	35.8	38.2	37.3	37.5
SHX weak solution exit temperature, T_{10} (^oC)	33.6	32.7	35.6	34.3	34.5
SHX rich solution entrance temperature, T_{11} (^oC)	33.0	32.3	34.7	33.5	34.0
Internal-refrigerated area temperature, T_{in} (^oC)	5.5	9.2	3.5	5.5	6.4
Surrounding temperature, T_{out} (^oC)	21.5	21.5	21.5	21.5	21.5
Running pressure, P_r (bar)	16.3	17.3	17.3	17.3	17.4
Heater capacity, Q_{gen} (W)	75	75	75	75	75

As is mentioned previously, for modeling the overall cycle, then obtaining the other thermodynamic properties of the working solutions which are necessary to calculate the mass, ammonia mass, and energy balances equations, REFPROP 8.0 software was used. The calculated mass flow rates and mass concentration ratios in different components of the studied systems are given in Tables 4.9. and 4.10 as a result of representing the cycle using the measured data in Table 4.8. in the program and obtaining the entropy, and enthalpy properties values at the measuring points.

Table 4.9. Calculated values of (x) in the different systems at the measuring points of the cycle

Points	$DARS_{0.0\%,ref.}$	$DARS_{0.05\%}$	$DARS_{0.05\%,Ma.}$	$DARS_{0.1\%}$	$DARS_{0.1\%,Ma.}$
1a	0.2500	0.2500	0.2500	0.2500	0.2500
1b	0.2012	0.1976	0.2214	0.2131	0.2014
3	0.7330	0.7110	0.7750	0.7561	0.7268
3a	0.1910	0.1830	0.2165	0.2061	0.1912
4	0.9532	0.9542	0.9572	0.9558	0.9518
4a	0.4080	0.4186	0.4380	0.4271	0.4035
5	0.9532	0.9542	0.9572	0.9558	0.9518
6a	0.9532	0.9542	0.9572	0.9558	0.9518
6b (ig)	-	-	-	-	-
6c	0.9532	0.9542	0.9572	0.9558	0.9518
7a	0.9532	0.9542	0.9572	0.9558	0.9518
7b	-	-	-	-	-
8a	0.2012	0.1976	0.2214	0.2131	0.2014
8b	-	-	-	-	-
9a	-	-	-	-	-
9b	0.2500	0.2500	0.2500	0.2500	0.2500
10	0.2012	0.1976	0.2214	0.2131	0.2014
11	0.2500	0.2500	0.2500	0.2500	0.2500

Table 4.10. Calculated values of mass flow rates ($\dot{m}$) in the different systems at the measuring points of the cycle

Points	Flow rate $\dot{m}$ (kg s^{-1})				
	$DARS_{0.0\%,ref.}$	$DARS_{0.05\%}$	$DARS_{0.05\%,Ma.}$	$DARS_{0.1\%}$	$DARS_{0.1\%,Ma.}$
1a	1.9115E-04	1.8599E-04	3.3475E-04	2.7868E-04	2.1596E-04
1b	1.7875E-04	1.7311E-04	3.2171E-04	2.6484E-04	2.0198E-04
3	2.0808E-05	2.3601E-05	2.0079E-05	2.2244E-05	2.3709E-05
3a	1.7034E-04	1.6239E-04	3.1467E-04	2.5643E-04	1.9225E-04
4	1.2404E-05	1.2884E-05	1.3033E-05	1.3841E-05	1.3980E-05
4a	8.4040E-06	1.0717E-05	7.0461E-06	8.4030E-06	9.7288E-06
5	1.2404E-05	1.2884E-05	1.3033E-05	1.3841E-05	1.3980E-05
6a	1.2404E-05	1.2884E-05	1.3033E-05	1.3841E-05	1.3980E-05
6b (ig)	6.2515E-07	6.4933E-07	6.5685E-07	6.9761E-07	7.0459E-07

6c	1.3029E-05	1.3533E-05	1.3690E-05	1.4539E-05	1.4685E-05
7a	1.3029E-05	1.3533E-05	1.3690E-05	1.4539E-05	1.4685E-05
7b	6.2515E-07	6.4933E-07	6.5685E-07	6.9761E-07	7.0459E-07
8a	1.7875E-04	1.7311E-04	3.2171E-04	2.6484E-04	2.0198E-04
8b	6.2515E-07	6.4933E-07	6.5685E-07	6.9761E-07	7.0459E-07
9a	1.3029E-05	1.3533E-05	1.3690E-05	1.4539E-05	1.4685E-05
9b	1.9115E-04	1.8599E-04	3.3475E-04	2.7868E-04	2.1596E-04
10	1.9115E-04	1.8599E-04	3.3475E-04	2.7868E-04	2.1596E-04
11	1.7875E-04	1.7311E-04	3.2171E-04	2.6484E-04	1.9598E-04

4.8.1. Energy Analysis Results

According to the previous measured and calculated properties, the results of the energy analysis and circulation ratio of the studied five systems, including the energy analysis results of the generator, rectifier, condenser, evaporator, absorber, pipelines, reservoir, and solution heat exchanger components, and COP values are given in Table 4.11.

Table 4.11. The results of the energy and exergy analyses and circulation ratio of the tested different systems

Component	**$DARS_{0.0\%,ref.}$**	**$DARS_{0.05\%}$**	**$DARS_{0.05\%,Ma.}$**	**$DARS_{0.1\%}$**	**$DARS_{0.1\%,Ma.}$**
Q_{gen} (W)	75.000	75.000	75.000	75.000	75.000
Q_{rect} (W)	18.912	23.773	16.264	19.041	21.538
Q_{cond} (W)	13.954	14.509	14.701	15.560	15.924
Q_{evap}(W)	17.462	17.860	18.322	19.387	19.541
Q_{abs} (W)	1.171	0.413	8.675	5.244	1.871
Q_{SHX} (W)	37.106	31.603	39.697	35.221	31.804
$Q_{pip,r}$ (W)	21.319	22.562	13.985	19.321	23.404
COP	0.233	0.238	0.244	0.258	0.261
f	14.41	13.44	24.69	19.13	14.02

The main objective of DARS is to achieve the cooling effect thus absorbing the heat from the cooled area. In order to perform this effect, it is needful for supplying heat to the cycle through the generator and rejecting heat from the condenser and rectifier to the surrounding. Assuming that the positive direction is for rejection heat

to the ambient and negative direction is to the system, Figure 4.26. shows the comparison of heat transfer rates of the different cycle components between the studied five systems. It can be realized From Figure 4.26. that the highest heat transfer to the ambient in $DARS_{0.05\%,Ma.}$ was at the solution heat exchanger and equal to 39.697 W. Whereas, for $DARS_{0.0\%,ref.}$, $DARS_{0.05\%}$, $DARS_{0.1\%}$, and $DARS_{0.1\%,Ma.}$ were 37.106, 31.603, 35.221, and 31.804 W, respectively. Also, It can be realized that the lowest heat transfer to the ambient was at absorber in $DARS_{0.05\%}$ and equal to 0.413 W. Whereas, for $DARS_{0.0\%,ref.}$, $DARS_{0.05\%.Ma.}$, $DARS_{0.1\%}$, and $DARS_{0.1\%,Ma.}$ were 1.171, 8.675, 5.244, and 1.871 W, respectively.

At the same generator heat supplied to the studied systems, the highest heat transfer rate absorbed from the cooled area was in $DARS_{0.1\%,Ma.}$ and equal to 19.541 W. Whereas, for $DARS_{0.0\%,ref.}$, $DARS_{0.05\%}$, $DARS_{0.05\%.Ma.}$, and $DARS_{0.1\%}$ were 17.462, 17.860, 18.322, and 19.387 W, respectively.

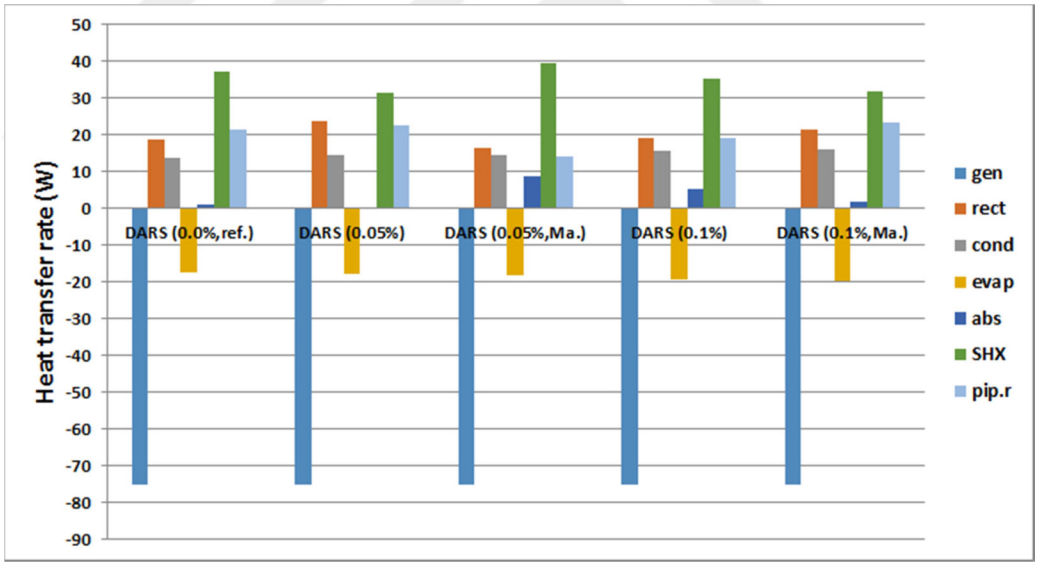

Figure 4.26. Comparative heat transfer rates values of the different components for the studied systems

Figure 4.27. shows the relative values of losses heat rates of the different components for the studied systems. Where 15 % of the supplied heat to the $DARS_{0.0\%,ref.}$ is wasted in the condenser to the ambient, whereas 21% in rectifier, 40% in SHX, 23% in pipelines and reservoir and 1% in absorber. In $DARS_{0.05\%}$, 16%, 34%, 26%, less than 1%, 24% and of the supplied heat is wasted in condenser, SHX, rectifier, absorber, and pipelines and reservoir, respectively. In $DARS_{0.05\%.Ma.}$,

it can be realized that a noticeable percentage of supplied heat is wasted in the absorber, almost 9% of the supplied heat. For other components of $DARS_{0.05\%.Ma.}$, 16%, 43%, and 17%, and 15% are wasted in condenser, SHX, rectifier, and pipelines and reservoir respectively. In $DARS_{0.1\%}$ and $DARS_{0.1\%.Ma}$, the major losses of heat were in SHX component with 37% and 33%, respectively. Whereas, the losses in the condenser were almost 17% in each $DARS_{0.1\%}$ and $DARS_{0.1\%.Ma}$,

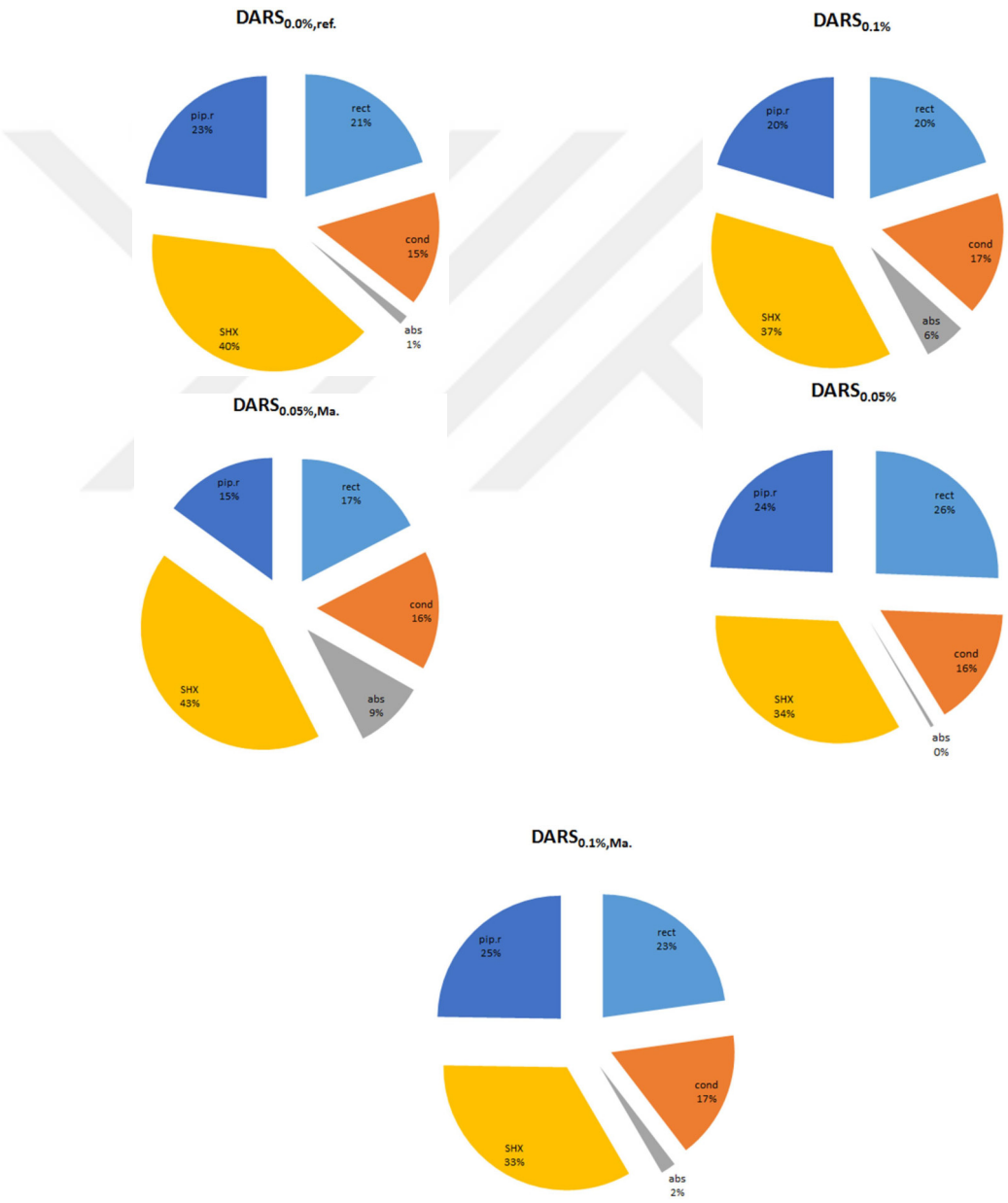

Figure 4.27. Relative values of heat transfer rates of the different components for the studied systems

The circulation ratio is defined as the mass flow rate of the coolant to the mass flow rate of the rich working solution thus, the highest value was in $DARS_{0.05\%Ma.}$, equal to 24.69 and the lowest one was in $DARS_{0.05\%}$ equal to 14.02 as it is shown in Table 4.11.

COP is defined as the ratio of the absorbed energy from the cooled area by the evaporator to the supplied heat to the generator. The highest energy performance was in $DARS_{0.1\%,Ma.}$ and equal to 0.261. While the other COPs of the $DARS_{0.0\%,ref.}$, $DARS_{0.05\%}$, $DARS_{0.05\%.Ma.}$, and $DARS_{0.1\%}$ were 0.233, 0.238, 0.244, and 0.258, respectively.

4.8.2. Exergy Analysis Results

Only energy analyses for the refrigeration system, in general, represent an incomplete image of the overall thermodynamic analyses. In light of this important principle, the exergy analyses were performed in this research including the destruction exergy for every component of DARS then calculating the ECOP which illustrates with COP the complete vision about the overall DARS performance. According to the working solutions properties, the results of the exergy analysis of the studied five systems are given in Table 4.12.

Table 4.12. The results of the exergy analyses of the tested systems

Component	$DARS_{0.0\%,ref.}$	$DARS_{0.05\%}$	$DARS_{0.05\%,Ma.}$	$DARS_{0.1\%}$	$DARS_{0.1\%,Ma.}$
$E_{dest,gen}$	2.116	1.862	1.265	1.368	1.616
$E_{dest,rect}$	1.068	1.450	0.924	1.081	1.176
$E_{dest,cond}$	0.139	0.074	0.063	0.068	0.130
$E_{dest,evap}$	0.233	0.179	0.270	0.254	0.242
$E_{dest,abs}$	11.039	10.280	25.474	19.659	13.449
$E_{dest,SHX}$	17.770	18.178	18.272	18.360	18.205
ECOP	0.110	0.096	0.214	0.185	0.150

It should be mentioned that the most effective exergy destruction in the exergy performance of the system is the generator destruction and the pipelines and reservoir exergy destruction was negligible, (Yıldız and Ersöz, 2013). From Table 4.12., the lowest value of the generator exergy destruction was in $DARS_{0.05\%,Ma.}$

From Figure 4.28. it can be understood that the exergy destruction losses of SHX in the $DARS_{0.0\%,ref.}$, $DARS_{0.05\%}$, $DARS_{0.05\%,Ma.}$, $DARS_{0.1\%}$, and $DARS_{0.1\%,Ma.}$ were 55%, 57%, 39%, 45%, and 52%, respectively. whereas, the exergy destruction losses of absorber in the $DARS_{0.0\%,ref.}$, $DARS_{0.05\%}$, $DARS_{0.05\%,Ma.}$, $DARS_{0.1\%}$, and $DARS_{0.1\%,Ma.}$ were 34%, 32%, 55%, 48%, and 39%, respectively. On the other hand, the exergy destruction of other components has no significant relative values comparing with the exergy destructions in SHX and absorber.

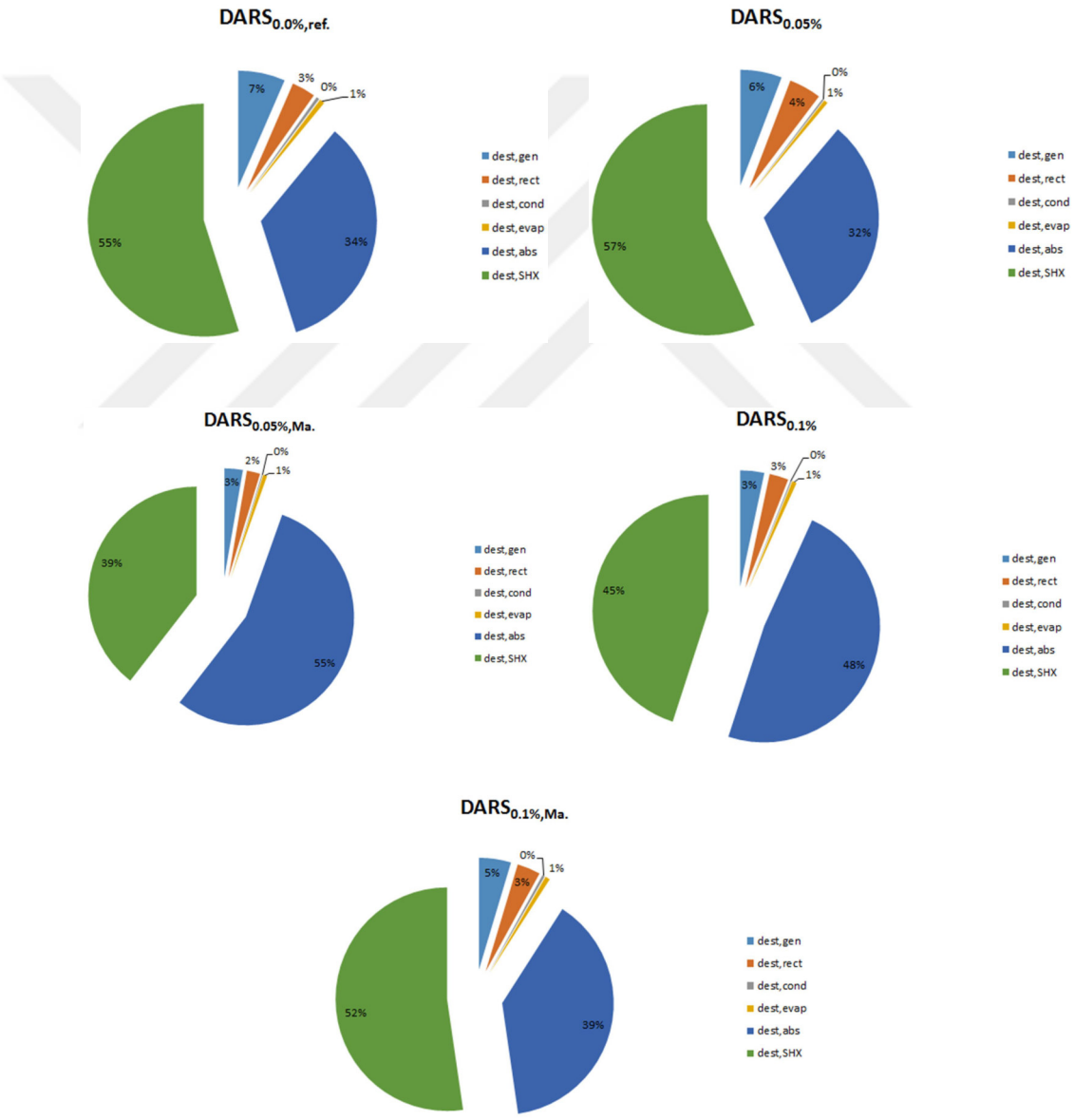

Figure 4.28. Relative values of exergy destruction of the different components for the studied systems

ECOP is defined as total outlet exergy to total inlet exergy. according to this definition the highest exergy performance was in $DARS_{0.05\%,Ma.}$ and equal to 0.214. While the other ECOPs of the $DARS_{0.0\%,ref.}$, $DARS_{0.05\%}$, $DARS_{0.1\%}$, and $DARS_{0.1\%,Ma.}$ were 0.110, 0.096, 0.185, and 0.150, respectively.

4.9. Comparative Discussion of Exergy and Energy Efficiencies

The results of comparing the energy efficiencies of the studied DARSs which run by the nanoferrofluids (with and without an external magnetic field) with the reference $DARS_{0.0\%.ref.}$ shows that the best system was $DARS_{0.1\%.Ma.}$ with enhancement reached to 10.72%. Whereas enhancements of COP in the $DARS_{0.05\%}$, $DARS_{0.05\%,Ma.}$, and $DARS_{0.1\%}$ were 2.14%, 4.50%, and 9.69%, respectively.

On the other hand, the achieved enhancements in the exergy efficiencies of the studied, $DARS_{0.05\%,Ma.}$, $DARS_{0.1\%}$, and $DARS_{0.1\%.Ma.}$ systems comparing with the reference $DARS_{0.0\%.ref.}$ were 48.59%, 40.54%, and 26.66%, respectively. Whereas, the $DARS_{0.05\%}$ illustrated a worse result than the reference system.

As is shown in Figure 4.29. and by adding the fact that $DARS_{0.1\%,Ma.}$ has the minimum value of the circulation ratio, it can be considered that the best system is $DARS_{0.1\%,Ma.}$ with enhancements in COP, ECOP, and *f* reached 10.72%, 26.66%, and 2.70%, respectively.

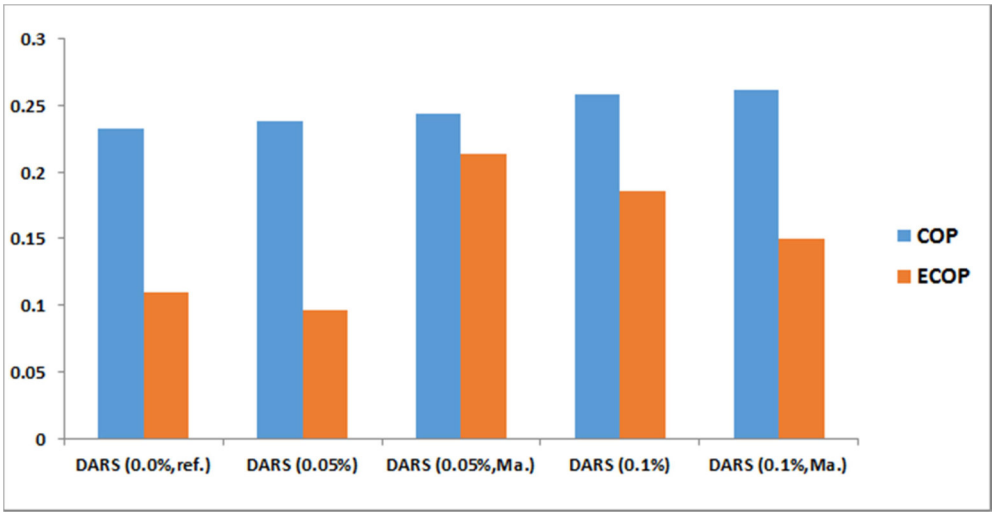

Figure 4.29. Comparative exergy and energy efficiencies of the different components for the studied systems

5. CONCLUSION AND RECOMMENDATIONS

5.1. Conclusion

As a part of the vision of energy-saving and environmental attention over the world, the effectiveness of the cooling system required to be enhanced, which might be performed by improving either the systems or the properties of refrigeration working solutions. Newly, the nanofluids or hybrid nanofluids have obtained a concern in several engineering areas because of their superior thermophysical properties, which might be surely utilized in refrigeration and air-conditioning devices by various roles for performance enhancement. This review illustrates a literature review of nanofluids in DARSs. Several investigation options such as different types of refrigeration working solutions as conventional solutions without added nanosize particles, then research on nanofluids and nanoferrofluids, and utilized various methods for enhancement of absorption processes are discussed. Moreover, a summary is achieved for an explanation of the refrigeration operation and components, DARS and bubble pump configurations, and modeling studies of DARS in the literature.

It can be concluded from the previous studies that the DARSs technology is attractive where it has advantages when contrasted to vapor compression systems of small refrigeration capacities because of non-mobile parts, avert noises, and has fewer prices. Though, it has been explained that DARSs have almost 40% less effective than conventional ARSs. From the different studies that were analyzed, it could result that the most critical parameters that influence the ECOP of the system are the flow cycle and operation heat. Commercially the most popular refrigeration working solution is NH_3/H_2O with hydrogen or helium as an auxiliary gas. Nevertheless, various solutions should be investigated to gain enhanced efficiency and locate various resources of supply energy, like solar energy. It is purposed to more detect this technology and encourage research interest and the investigation for energy efficiency. The kind, content, and of nanosize particles volume, temperature, as well as dispersion stability, are the critical parameters that influence the thermal conductivity of nanofluids. The thermal conductivity enhances considerably by

increasing the stabilities of nanofluids, which is obtained by adding chemical surfactants or proposing the exact selection refrigerant content in the mixture. A unique type of nanofluids is nanoferrofluids. Nanoferrofluids contain ferromagnetic nanoparticles that exhibit higher thermophysical properties contrasted to the conventional nanofluids. In literature, investigators are focusing on how to enhance the composition and properties of the refrigeration working solution. The utilization of nanofluids will enhance a vapor absorption operation and the evaporation as well as condensation heat transfer coefficients, which pushes to more built-in and agile refrigeration systems. Furthermore, expend less thermal energy with high energy efficiency. The investigation of utilizing nanoparticles with a working mixture includes the investigation of condensing and evaporating heat transfer events because of the phase changing operation in the cooling system which relies on several thermophysical properties. Enhancing these properties push us to enhancement in overall the system.

No previous study has tested the nanoferrofluids based on the studied binary working solutions as it is performed in this research. So this work can be considered an investigation of new nanoferrofluids and a continuation of the previous studies. Consequently, a thermal study with the valid nanoferrofluid at the low generator temperature has not been investigated before to improve the performance of DARS.

Thermophysical analyses were achieved for the mixture of (Fe_3O_4 - acetone/$ZnBr_2$) refrigeration working solution and examine its efficiency characteristics as a nanoferrofluid. There is no previous study that has tested the nanoferrofluid based acetone/$ZnBr_2$ as it is performed in this work. Where it shows an investigation of (Fe_3O_4 - acetone/$ZnBr_2$) as a nanoferrofluid containing the preparation, stability, structure, and properties. The reasons behind choosing Fe_3O_4 nanoparticles are that acetone is a good dispersivity medium for this kind of nanoparticles, also, their excellent thermophysical properties and magnetic property which give an ability to utilize them combined with applying an external magnetic field as a method for long and acceptable suspension stability of these nanoparticles in the base-fluid thus enhancement in the heat transfer process in the generator. As a multi-factor experimental study, the experiments are designed to perform a visual inspection of the suspension nanoparticles stability and thermophysical analysis of how the various concentrations of the new nanoferrofluid mixture components affect its different properties values (thermal conductivity, density, dynamic viscosity, and

specific heat capacity). The results elucidate that the studied nanoferrofluid has good dispersion and an enhancement in thermal conductivity that reaches 10.179 % at 0.2 (*wt.*%) of nanoparticle concentration. Also, by increasing nanoparticle concentration, the density increase, heat capacity decrease, as expected, and viscosity had a significant increase.

Also, the same thermophysical analyses were achieved for the mixture of nanoferrofluid (Fe_3O_4–NH_3/H_2O) and examine its efficiency characteristics as a refrigeration working solution by the same method. The reasons behind choosing this nanoferrofluid are that ammonia/water has the ability to be used under altitude running pressure (15 bar in diffusion absorption cycles) driven by low-temperature heat resources. This availability does not exist in most conventional working solutions whose absorbent is a salt, also, the excellent thermophysical properties of nanoferrofluid and its magnetic property which give an ability to utilize it combined with applying an external magnetic field as a method for long and acceptable suspension stability of these nanoparticles in the base-fluid thus enhancement in the heat transfer process in the generator of DARS. The results are represented as follows:

- The visual inspection analyses of stability elucidate that the Fe_3O_4 nanoparticles in the base-fluid have good dispersion and weak stability characteristics.
- PVP surfactant dissolves well in the solution and has a useful effect on the dispersion of the nanoparticles over time. Where after the sonication process particles start a late agglomeration comparing with other samples that have other surfactants, even comparing with the same concentration sample without surfactant.
- SEM analysis shows almost a typical and random distribution situation of the nanoparticles, without a magnetic field, in the base-fluid. And this distribution occurred after sonication because of just the nanoparticles' thermal motion.
- The density of the nanoferrofluid (at 25 °C) increases from 0.9150 to 0,9165 $g\ cm^{-3}$ with an increasing the concentration of the added nanoparticles from 0.0 to 0.2 *wt.*%. And also, Experimental measurements have almost identical values with the theoretical density.

- A significant increase in viscosity of mixture happened from 1.815 to 7.637 mPa.s with increasing concentration of Fe_3O_4 from 0 to 0.2 *wt.*%. Consequently, the nanoferrofluid has a high viscosity comparing with its base fluid. And also has a high viscosity comparing with another kind of nanofluid with the same base-fluid.
- By increasing nanoparticle concentration heat capacity decreases, as expected, because of the low heat capacity value of the nanoparticles (0.653 J g^{-1} K^{-1}) comparing with the specific heat capacity of NH_3/H_2O base-fluid (4134.15 J g^{-1} K^{-1}).

In presence of an external magnetic field affects the DARS generator, the validation of using new nanoferrofluids (Fe_3O_4-acetone/$ZnBr_2$ and Fe_3O_4-NH_3/H_2O) as working solutions were experimentally investigated. Then an experimental study of obtained enhancement in DARS' performance was presented by using the valid solution with helium as an inert gas. The experiments were performed on nanoferrofluids of 0.05 wt.% and 0.1 wt.% Fe_3O_4 nanoparticles concentrations in 300 ml ammonia/water base-fluid with addition 1 wt.% concentration of PVP surfactant, which was equipped to DARS with and without an external magnetic field. Depending on the concentrations and presence or absence of the external magnetic field, the experiments divided into five tests. According to the obtained results of the analyses, the following essential inferences can be drawn from this research:

- Although theoretically, the DARS can be started running with the chosen operation conditions under cycle pressure less than 10 bar, the experimental results presented that acetone/$ZnBr_2$ binary solution is not valid for use in DARS. Thus DARS was investigated only with NH_3/H_2O nanoferrofluid.
- Although the enhancement of thermal conductivity increases as increasing nanoparticle concentration in NH_3/H_2O base-fluid, where reaches 3.508% at 0.2 wt.% of nanoparticles, the high viscosity and low specific heat capacity of nanoferrofluid with high nanoparticle concentrations prevent use them in DARSs.
- The positive effect of using an external magnetic field on the heat transfer in the generator bubble-pump component was significantly clear in the experiments.

- The initial experiments of the magnet installation test showed that the best placement was in the 16 cm magnet height from the bottom of the generator-bubble pump component. Then this placement was chosen to use in the performed experiments.
- A good nanoparticle suspension stability for a long time with existing the external effect of the magnet.
- The presence of nanoparticles in the base-fluid causes rising in the pressure of the DARS. Also, the presence of the external magnetic field brings about more increases in the pressure value.
- Although that the lowest evaporator and internal temperatures occurred in $DARS_{0.05\%,Ma.}$, the steady-state of the temperature of the internal cooled area appeared more clearly in $DARS_{0.1\%,Ma.}$.
- Although the DARS had a major enhancement in $DARS_{0.05\%,Ma.,}$ it had high losses in the absorber and SHX, thus a very high circulation ratio value, and a low improvement in energy performance comparing with the best system.
- $DARS_{0.1\%,Ma.}$ was the best system with enhancements in COP, and ECOP, reached 10.72%, and 26.66%, respectively, and a decrease in f by 2.70%. Whereas, $DARS_{0.05\%}$ system has the lowest COP and ECOP comparing with the reference system

5.2. Recommendations

The performed review in this research has several scientific aspects that investigations in them are needed to be continued in the future. Since the enhancement of the efficiency by using nanofluids will enable the derivation of new projects as it will be initiated to improve efficiency with other refrigeration cycles which will be able to perform on many promising future applications. Recently, many improved compact kinds of heat exchangers are utilized like Shell and Tube kind heat exchangers, microchannel heat exchangers, plate type heat exchangers. But all of them have a secondary influence on the effectiveness of DARSs compared to the bubble pump importance. On the other hand, and in light of the previous studies the attempts to improving the design of bubble pump configuration become limited anymore, due to the simplicity of the bubble pump composition originally. Thus, the next investigations should focus on improving the stability of nanoparticles. Where,

although the high thermal conductivity of the nanofluids compared to the conventional working solutions, the main problem of nanoparticles is the tendency to agglomeration and sedimentation quickly over time and prevent good dispersion attempts of nanosize particles in the nanofluids.

In light of the previous results, the significant influences of using nanomagnetic particles in a conventional binary working solution as a base-fluid under an external magnetic field in DARSs as a new method to improve this kind of refrigeration cycles open new horizons for more investigations in this way to obtain better results. Especially that these refrigerators can be run by a low generator temperature by the solar energy or any kind of waste heat resources. Furthermore, the enhancements in the heat transfer and the suspension nanoparticles stability due to a simple installation of the cheap permanent magnets around the generator-bubble pump components encourage future interests to make this research with some developments able to be performed to existing DARSs in commercial applications.

REFERENCES

Abduwadood, S.S., and Akeel, M.A.M., (2012), "Experimental investigation of water vapour-bubble pump characteristics and its mathematical reconstruction". Engineering and Technical Journal. 30:1870–85.

Abe O., and Narita M., (1997), "Solid State Ionics" 101– 103 (1997) 103–109

Abu-Mulaweh, H.I., Mueller, D.W., Wegmann, B., Speith, K., and Boehne, B., (2011), "Design of a bubble pump cooling system demonstration unit". International Journal of Thermal and Environmental Engineering. 2:1–8.

Acuña, A., Velazquez, N., and Cerezo, J., (2013), "Energy analysis of a diffusion absorption cooling system using lithium nitrate, sodium thiocyanate and water as absorbent substance and ammonia as the refrigerant". Applied Thermal Engineering; 51:1273–81.

Aghayari R., Kerdegari M., Khosravi S., Kia A., Maddah H., and Khalaj A. H., (2015), "Synthesis and Thermo-physical Properties of Fe3O4 Nanofluid". Journal of Materials Science & Surface Engineering Vol. 2 (1), 2015, pp 109-113

Ajib S., and Karno A., (2008), "Thermodynamic analysis of an absorption refrigeration machine with new working fluid for solar applications", Heat Mass Transf. 45 (2008) 71–81

Ajib, S, and Karno, A., (2008), "Thermophysical properties of acetone/zinc bromide for using in a low temperature driven absorption refrigeration machine." Heat and Mass Transfer. 45(1):61–70.

Ali A., Zafar H., Zia M., Haq I. u., Phull A. R., Ali J. S., and Hussain A., (2016), "Synthesis, characterization, applications, and challenges of iron oxide nanoparticles". Nanotechnology, Science and Applications 2016:9 49–67

Al-Najjar S., (2002), "Untersuchung geeigneter Arbeitsstoffpaare fu ¨r Absorptionska ¨ltemaschinen unter Beru ¨cksichtigung der Wa ¨rmeprozessoptimierung". PhD thesis, TU Ilmenau, Januar

Aman J., Henshaw P., and Ting D.S.-K., (2018), "Performance characterization of a bubble pump for vapor absorption refrigeration systems". International Jornal of Refrigeration 85 (2018) 58-69

An L.H., Liu D.P., Chen Y.J., Yang L., Yang M., and Lin F.L., (2017). "Theoretical and experimental study on the lifting performance of bubble pump with variable crosssection lift tube", Appl. Therm. Eng. 111 (2017) 1265–1271.

Anand D.K. and Kumar B., (1987), “Absorption machine irreversibility using new entropy calculations”. Sol Energy; 39:243 56. 1987.

Angayarkanni, S.A., and Philip, J., (2015), "Review on thermal properties of nanofluids: recent developments". Adv Colloid Interface Sci. 225:146–76.

Angéla H., Márta S., Tóth I.Y., Bauer R.A., Judith M., István Z., and Etelka T., (2012) “Enhanced stability of polyacrylate-coated magnetite nanoparticles in biorelevant media”, Colloids and Surfaces B 94 (2012) 242–249.

Aphornratana S, and Eames IW., (1995), "Thermodynamic analysis of absorption refrigeration cycles using the second law of thermodynamics method". International Journal of Refrigeration 1995;18:244–52

Arivazhagan S., Murugesan S., Saravanan R., and Renganarayanan S., (2005), "Simulation studies on R134a—DMAC based half effect absorption cold storage systems", Energy Convers. Manage. 46 (2005) 1703–1713.

Arshi Banu P.S., and Sudharsan N.M., (2017), "Feasibility studies of singleeffect H2O-LiBr+LiI +LiNO3+LiCl vapour absorption cooling system for solar based applications", J Chem Pharm Sci 12 (2017) 1–7.

Augustin L.B., Golecha J., Shreenaath K.G.S., Swami V., and Suresh M., (2013), "Numerical studies on the performance of a bubble pump", Appl. Mech. Mater. 330 (2013) 203–208.

Azmi, W.H., Sharma, K.V., Mamat, R., Najafi, G., and Mohamad, M.S., (2016), "The enhancement of effective thermal conductivity and effective dynamic viscosity of nanofluids – a review". Renew Sustain Energy Rev. 53:1046–58.

Bai Y., Chen W., Xu C., Sun Q., Zhang B., and He Y., (2021), "Investigation on the thermal performances of [Na(TX-7)]SCN/NH3 absorption systems based on physical properties measurement of the working fluid". Applied Thermal Engineering, Volume 183, Part 2, 25 January 2021, 116175

Bashtovoi V.G., Challant G., and Yu V.O., (1993), "Boiling heat transfer in magnetic fluids", Journal of Magnetism and Magnetic Materials 122 (1993) 305–308.

Ben Ezzine, N., Garma, R., and Bellagi, A., (2010), "A numerical investigation of a diffusion-absorption refrigeration cycle based on R124-DMAC mixture for solar cooling". Energy. 35:1874–83.

Benhmidene A., Chaouachi B., Bourouis M., Gabsi S., (2011), "Effect of operating conditions on the performance of the bubble pump of absorption-diffusion refrigeration cycles", Thermal Sci. 15 (3) (2011) 793–806.

Benhmidene A., Hidouri K., Chaouachi B., Gabsi S., and Bourouis M., (2016), "Experimental investigation on the flow behaviour in a bubble pump of diffusion absorption refrigeration systems", Case Stud. Thermal Eng. 8 (2016) 1–9.

Benhmidene, A., Chaouachi, B., and Gabsi, S., (2010). "A Review of Bubble Pump Technologies". Journal of Applied Sciences. 10(16), 1806-1813.

Benhmidene, A., Chaouachi, B., Bourouis, M., and Gabsi, S., (2011), "Modelling of heat flux received by a bubble pump of absorption–diffusion refrigeration cycles". Heat and MassTransfer. 47:1341–7.

Bezerra M. A., Lemos V. A., Novaes C. G., de Jesus R. M., Souza Filho H. R., Araújo S. A., and Alves J. P. S., (2020). "Application of mixture design in analytical chemistry". Microchemical Journal., 152, 104336.

Bhattad A., Sarkar J., and Ghosh P., (2018) Improving the performance of refrigeration systems by using nanofluids: A comprehensive review, Renewable and Sustainable Energy Reviews 82 3656–3669.

Bierling B., Schmid F., and Spindler K., (2019), "Influence of different heating types on the pumping performance of a bubble pump". Heat Mass Transfer (2019) 55:67–79.

Bierling B., Schmid F., and Spindler K., (2019), "Influence of different heating types on the pumping performance of a bubble pump". Heat Mass Transfer (2019) 55:67–79

Bourouis M., Valle` s M., Medrano M., and Coronas A., (2005), "Performance of air-cooled absorption air-conditioning systems working with water-(LiBr + Lil + LiNO3 + LiCl)", Proc. Inst. Mech. Eng., Part E: J. Process Mech. Eng. 219 (2) (2005) 205–213, https://doi.org/10.1243/095440805X8601

Bourseau P, and Bugarel R., (1986), "Réfrigération par cycle à absorption–diffusion: comparaison des performances des systèmes NH3–H2O et NH3–NaSCN". International Journal of Refrigeration 1986;9:206–14

Cai D., He G., Tian Q., Bian Y., Xiao R., and Zhang A., (2015), "First law analysis of a novel double effect air-cooled non-adiabatic ammonia/salt absorption refrigeration cycle", Energy Convers. Manage. 98 (2015) 1–14.

Cai D., Jiang J., He G., Li K., Niu L., and Xiao R., (2016), "Experimental evaluation on thermal performance of an air-cooled absorption refrigeration cycle with NH3–LiNO3 and NH3–NaSCN refrigerant solutions", Energy Convers. Manage. 120 (2016) 32–43

Changwei, P., Weidong, W., Wei, S., Hua, Z., and Yong, T. K., (2012), "Mass transfer enhancement by binary nanofluids (NH3/H2O + Ag nanoparticles) for bubble absorption process". International Journal of Refrigeration Volume 35, Issue 8, Pages 2240-2247.

Chen, J., Kim K.J., and Herold K.E., (1996), "Performance enhancement of a diffusion absorption refrigerator". Int. J. Refrigeration, 19: 208-218.

Choi, S.U.S., (1995), "Enhancing thermal conductivity of fluids with nano-particles" [M]// Siginer, D. A., Wang, H. P. "Development and Applications of Non-Newtonian Flows", EFD. New York: ASME, 1995: 99−105.

Chuncheng Y., Xiufang B., Jingyu Q., Xiaolin Z., Kai Z., and Yanwen B., (2014), "An investigation of a viscosity-magnetic field hysteretic effect in nano-ferrofluid". Journal of Molecular Liquids. Volume 196, August 2014, Pages 357-362.

Conde-Petit M. R., (2004), "Thermophysical properties of NH_3-H_2O solutions for the industrial design of absorption refrigeration equipment. Formulation for industrial use". M. conde eng. -Switzerland/Switzerland. https://iifiir.org/en/fridoc/thermophysical-properties-of-nh3-h2o-solutions-for-the-industrial-design-3468

Cuenca Y, Vernet A, and Valle`s M., (2014), "Thermal conductivity enhancement of the binary mixture (NH3+LiNO3) by the addition of CNTs". Int J Refrig. 41:113–20.

Dammak, N., Chaouachi, B., Gabsi, S., and Bourouis, M., (2010), "Optimization of the geometrical parameters of a solar bubble pump for absorption-diffusion cooling systems". American Journal of Engineering and Applied Science. 3:693–8.

Decagon Devices, Inc. web-based product information accessed at: http://manuals.decagon.com/Manuals/13351_KD2%20Pro_Web.pdf last accessed November 2020.

Donate M., Rodriguez L., De Lucas A., and Rodrı´ guez J.F., (2006), "Thermodynamic evaluation of new absorbent mixtures of lithium bromide and organic salts for absorption refrigeration machines", Int. J. Refrig. 29 (2006) 30–35.

Elsafty, A., and Al-Dain, A.J. (2002), "Experimental investigation of performance enhancement by the use of additives in a vapor absorption cooling system", in: A.A.M. Sayigh (Ed.), World Renewable Energy Congress (WREC VII), Cologne, Germany, pp. 225–259.

El-Sayed YM., and Tribus M., (1985), "Thermodynamic properties of water-ammonia mixtures: theoretical implementation for use in power cycle analysis". ASME Publications 1985;1:89–95.

Engineering ToolBox – Resources. The phase diagram for ammonia, web-based product information accessed at https://www.engineeringtoolbox.com/ammonia-d_1413.html, last accessed January (2021)

Fan, J., and Wang, L., (2011), "Review of heat conduction in nanofluids". J Heat Transf. 133:1–14.

Farhanian D., Crescenzo G.D., and Tavares J. R., (2018), "Large-Scale Encapsulation of Magnetic Iron Oxide Nanoparticles via Syngas Photo-Initiated Chemical Vapor Deposition". Scientific REPORTS | (2018) 8:12223 | DOI:10.1038/s41598-018-30802-1

Fluke Corporation, Fluke 43B/003 Power Quality Analyzer web-based product information accessed at https://www.fluke-direct.com/product/fluke-43b-003-power-quality-analyzer. last accessed January (2021)

Gessner, T.R., Jader R., and Barbosa J.R., (2006), “Modeling absorption of pure refrigerants and refrigerant mixtures in lubricant oil”. International Journal of Refrigeration 29 (5), 773–780.

Gurevich B., Jelinek M., Levy A., and Borde I., (2015), "Performance of a set of parallel bubble pumps operating with a binary solution of R134a DMAC", Appl. Therm. Eng. 75 (2015) 724–730.

Gutiérrez, F., (1998), "Behavior of a household absorption diffusion refrigerator adapted to autonomous solar operation".Solar Energy. 40:17–23.

Han W., Chen Q., Sun L., Ma S., Zhao T., and Zheng D., (2014), Experimental studies on a combined refrigeration/power generation system activated by low-grade heat. Energy;74:59–66.

Han X.H., Wang S.K., He W., Hao N., Zeng Z.Y., Wang Q., and Chen G.M., (2015), "Experimental investigations on the pumping performance of bubble pumps with organic solutions", Appl. Therm. Eng. 86 (2015) 43–48.

Harraz A. A., Freemana J., Wanga K., MacDowellb N., and Markidesa C. N., (2019), "Diffusion-absorption refrigeration cycle simulations in gPROMS using SAFT-γ Mie". Energy Procedia 158 (2019) 2360–2365

Herold K.E., Radermacher R., and Klein S.A., (1996), “Absorption chiller and heat pumps”.1st ed. NewYork: CRC Boca Raton.

Herold KE, Han K, Moran MJ., and AMMWAT, (1988), "A computer program for calculating the thermodynamic properties of ammonia and water mixtures using a Gibbs free energy formulation". ASME Publications 1988;4:65–75.

Herold, K.E., (1996), "Diffusion-absorption heat pump". Final Report for Gas Research Institute. GRI-96/0271. Gas Research Institute, USA.

Herold, K.E., and Chen, J., (1993), "Diffusion-absorption heat pump". Annual Report for Gas Research Institute, GRI-93/0055. Gas Research Institute, USA. http://adsabs.harvard.edu/abs/1993umd..rept.....H

Herold, KE, and Chen, J. (1994) "Diffusion–absorption heat pump. Annual Report for Gas Research Institute", USA. Available from: http://adsabs.harvard.edu/abs/1994umd.. rept…..H.

Hodenius M.A., Niendorf T., Krombach G.A., Richtering W., Eckert T., Lueken H., Speldrich M., Günther R.W., Baumann M., Soenen S.J., De Cuyper M., and SchmitzRode T., (2008), "Synthesis, physicochemical characterization and MR relaxometry of aqueous ferrofluids", Journal of Nanoscience and Nanotechnology 8 (2008) 2399–2409

Hong H.X., Wu W.D., Sheng W., and Liu H., (2009), “Study on the dispersion stability influencing factors of nanofluids, in: T.X. Tao (Ed.)”, UECTC-RE’09–Proceedings of the Inaugural US–EU–China Thermophysics Conference—Renewable Energy, 28–30 May, Beijing, China, ID246, 2009

Hong T., Yanga H.S., and Choi C.J., (2005), “Study of the enhanced thermal conductivity of Fe nanofluids”, J. Appl. Phys. 97 (2005) 064311.

Hyteknoloji Limited, web-based product information accessed at: http://www.hyteknoloji.com/pdf/ultrasonik.pdf. last accessed November 2020.

Infante Ferreira, C.A., (1984), "Thermodynamics and physical property data equations for ammonia–lithium nitrate and ammonia–sodium thiocyanate solucions". Solar Energy. 32:231–6.

Iyoki S., and Uemura T., (1990), "Performance characteristics of the water lithium bromide-zinc chloride-calcium bromide absorption refrigerating machine, absorption heat pump and absorption heat transformer", Int. J. Refrig. 13 (1990) 191–196.

Jang SP., and Choi SUS., (2007) “Effects of various parameters on nanofluid thermal conductivity”. J Heat Transf. 2007;129:617–23.

Jemaa R. B., Mansouri R., and Bellagi A., (2018), "Experimental Analysis and Thermodynamic Modeling of a Diffusion-Absorption Refrigerator". Exergy for A Better Environment and Improved sustainability 1, Green Energy and Technology. Springer International Publishing AG, part of Springer Nature 2018

Jiang W., Li S., Yang L., and Du K., (2019), "Experimental investigation on performance of ammonia absorption refrigeration system with TiO2 nanofluid", Int. J. Refrig. 98 (2019) 80–88

Kamiyama S., and Ishimoto J., (1995), "Boiling two-phase flows of magnetic fluid in a nonuniform magnetic field", Journal of Magnetism and Magnetic Materials 149 (1995) 125–131.

Kang, Y.T., and Kim, J.K., (2006), "Comparisons of mechanical and chemical treatments and nanotechnologies for absorption applications". HVAC & R Research 12 (3b), 807–819.

Kaushik S., and Kumar R., (1985), "Thermodynamic study of a two-stage vapour absorption refrigeration system using NH 3 refrigerant with liquid/solid absorbents", Energy Convers. Manage. 25 (1985) 427–431.

Kaynakli, O., and Kilic, M., (2007). "Theoretical study on the effect of operating conditions on performance of absorption refrigeration system". Energy Convers Manage. 48(2):599–607.

Kaynakli, O., and Yamankaradeniz, R., (2007), Thermodynamic analysis of absorption refrigeration system based on entropy generation. Curr. Sci. 92, 427–479.

Keblinski, P., Pillpot, S. R., Choi, S. U. S., and Eastman, J. A., (2002), "Mechanism of heat flow in suspensions of nano-sized particles (nanofluids)" [J]. Int J Heat Mass Transfer. 45 (4): 855−863.

Keppler D., (2018), "Absorption chillers as a contribution to a climate-friendly refrigeration supply regime: Factors of influence on their further diffusion", Journal of Cleaner Production 172 1535e1544

Killion, J.D., and Garimella, S., (2001), "A critical review of models of coupled heat and mass transfer in falling-film absorption". International Journal of Refrigeration 24 (8), 755–797.

Kim G., Choi H. W., Lee G., Lee J. S., and Kang Y. T., (2020), "Experimental study on diffusion absorption refrigeration systems with low GWP refrigerants"Energy. Volume 201, 15 June 2020, 117626

Kim, J., Kang, Y. T., and Choi, C. K., (2004), "Analysis of convective instability and heat transfer characteristics of nanofluids" [J]. Phys Fluids. 16(7): 2395−2401.

Kim, J.K., and Kang, Y.T., (2006), "A review of heat and mass transfer analysis for absorption process". International Journal of Refrigeration and Air Conditioning 14 (4), 131–137.

Kim, J.K., Lee, J.K., and Kang, Y.T., (2007), "Absorption performance enhancement by nanoparticles and chemical surfactants in binary nanofluids". Int. J. Refrigeration 30, 50-57.

Kim, K.J., Chen J., Shi Z., and Herold, K.E., (1994), "Diffusion-absorption heat pump". Annual Report for Gas Research Institute, GRI-94/0080. Gas Research Institute, USA.

King H. H., Lowe Hall J., and Ware G. C., (1930), "A STUDY OF THE DENSITY, SURFACE TENSION AND ADSORPTION IN THE WATER-AMMONIA SYSTEM AT 20° C". J. Am. Chem. Soc. 1930, 52, 12, 5128–5135

Koehler WJ, Ibele WE, Soltes J, and Winter ER., (1987), "Entropy values of aqueous solution of lithium bromide and approximation equation". ASHRAE Transcations 1987;93:2379–87.

Koikea M., and Abeb. O., (2004), " Redox synthesis of magnetite powder under mixing-grinding of metallic iron and hydrated iron oxide". Graduate School of Science and Engineering, Ibaraki University, 4-12-1, Nakanarusawa, Hitachi, Ibaraki 316-8511, Japan

Kouremenos DA, and Stegou-Sagia A., (1988), "Use of helium instead of hydrogen in inert gas absorption refrigeration". International Journal of Refrigeration 1988;11: 336–41.

Kouremenos DA, Stegou-Sagia A, and Antonopoulos KA., (1994), "Three-dimensional evaporation process in aqua-ammonia absorption refrigerators using helium as inert gas. International Journal of Refrigeration 1994;17:58–67.

Koyfman, A., Jelinek M., Levy, A., and Borde, I., (2003), "An experimental investigation of bubble pump performance for a diffusion absorption refrigeration system with organic working fluids". Applied Thermal Engineering. 23:1181–94.

Kumar, D.S., and Elansezhian, R., (2014), "ZnO nanorefrigerant in R152a refrigeration system for energy conservation and green environment". Front Mech Eng; 9(1):75–80.

Lee G., Choi H. W., and Kang Y.T., (2020), "Cycle performance analysis and experimental validation of a novel diffusion absorption refrigeration system using R600a/n-octane"Energy, available online 13 November 2020, 119328

Lee H.-R., Koo K.-K., Jeong S., Kim J.-S., Lee H., and Oh Y.-S., (2000), "Thermodynamic design data and performance evaluation of the water+ lithium bromide+ lithium iodide+ lithium nitrate+ lithium chloride system for absorption chiller", Appl. Therm. Eng. 20 (2000) 707–720

Lee, J. K., Koo, J., Hong, H., and Kang, Y. T., (2010), "The effects of nanoparticles on absorption heat and mass transfer performance in NH3/H2O binary nanofluids" [J]. International Journal of Refrigeration, 33(2): 269−275.

Li D.X., He Q., and Li J.B., (2009), “Smart core/shell nanocomposites: intelligent polymers modified gold nanoparticles”, Advances in Colloid and Interface Science 149 (2009) 28–38.

Li Q., and Xuan Y.M., (2009), "Experimental investigation on heat transfer characteristics of magnetic fluid flow around a fine wire under the influence of an external magnetic field", Experimental Thermal and Fluid Science 33 (2009) 591–596.

Lin F.L., Liu D.P., Jiang D.Q., Yang L., and Zhao R.X., (2016) "An experimental study on the performance of guided bubble pump with multiple tubes", Appl. Therm. Eng. 106 (2016) 1052–1061.

Lin, L., Peng, H., and Ding, G., (2015)., "Dispersion stability of multi- walled carbon nanotubes in refrigerant with addition of surfactant". Appl Therm Eng. 91:163–71.

Linghui Z., and Junjie G., (2010), “Second law-based thermodynamic analysis of ammonia/sodium thiocyanate absorption system”, Renewable Energy 35, 1940–1946, 2010.

Liu J., Gu J., Lian Z., and Liu H., (2004), “Experiments and mechanism analysis of pool boiling enhancement with water-based magnetic fluid”, Heat Mass Transfer 41 (2004) 170–175.

Liu J.H., (2004), "Study of pool boiling heat transfer enhancement of magnetic fluid and its application in heat pipe and refrigeration system", Doctoral dissertation, Shanghai Jiaotong University, 2004

Magnet Market, web-based product information accessed at https://www.magnetmarket.com.tr/boy-40mm-x-en-10mm-x-kalinlik-5mm-neodymium-magnet-html last accessed January (2021)

Mahbubal I.M., Saidura R., and Amalinaa M.A., (2013), "Heat transfer and pressure drop characteristics of Al2O3-R141b nanorefrigerant in horizontal smooth circular tube", 5th BSME International Conference on Thermal Engineering, Procedia Engineering 56 (2013) 323 – 329.

Markhulia J., (2016), “Some Physical Parameters of PEG-modified Magnetite Nanofluids”. J. Pharm. Appl. Chem. 2, 33–37

Maxwell JC., (1904), “A treatise on electricity and magnetism”. 2nd ed. Cambridge: Oxford University Press; 1904

McLinden MO, Lemmon EW, and Jacobsen RT. (1998), "Thermodynamic properties for alternative refrigerants". International Journal of Refrigeration 1998;21:332–8

Mehyo M., Ozcan H., and HASSAN A. H. A., (2018), "Thermodynamic Analysis of a Power Plant Waste Heat Driven Absorption Refrigeration System", Proceedings of the 4th World Congress on Mechanical, Chemical, and Material Engineering (MCM'18) Madrid, Spain – August 16 – 18, 2018

Meissner, H. P., and Kusik, C. L., (1978), “Electrolyte activity coefficients in inorganic processing”, AIChE Symp. Ser. 173, vol. 74(1978)14-20.

Meissner. H.P., and Tester J.W., (1972), "Activity Coefficients of Strong Electrolytes in Aqueous Solutions", Ind. Eng. Chem. Proc. Des. Dev., 11, 128 (1972)

Merck KGaA, Darmstadt, Germany. web-based product information accessed at:https://www.sigmaaldrich.com/catalog/product/aldrich/518158?lang=en&region=TR&cm_sp=Insite-_-caSrpResults_srpRecs_srpModel_fe3o4-_-srpRecs3-3 . last accessed November 2020.

Misra, R.D., Sahoo, P.K., and Gupta, A., (2006), “Thermoeconomic evaluation and optimization of an aqua-ammonia vapour absorption refrigeration system”. International Journal of Refrigeration 29 (1), 47–59.

Mohammed H. I., Giddings D., Walker, G. S., and Power, H., (2018), "CFD assessment of the effect of nanoparticles on the heat transfer properties of acetone/ZnBr2 solution". Applied Thermal Engineering Volume 128, Pages 264-273.

Mohammed H. I., Giddings D., and Walker G. S., (2020), "Experimental investigation of nanoparticles concentration, boiler temperature and flow rate on flow boiling of zinc bromide and acetone solution in a rectangular duct", International Journal of Heat and Mass Transfer 130 (2020) 710–721

Mohammed H. I., Giddings D., and Walker G. S., (2020), "Thermo-physical properties of the nano-binary fluid (acetone–zinc bromide-ZnO) as a low temperature operating fluid for use in an absorption refrigeration machine". Heat and Mass Transfer, Springer-Verlag GmbH Germany, part of Springer Nature 2020.

Mohd Razif N.H., Bin Mamat A.M.I, Lias I., and Mohamed W.A.N.W, (2015), "Thermophysical Properties Analysis For Ammonia-Water Mixture of An Organic Rankine Cycle". Jurnal Teknologi (Sciences & Engineering) 75:8 (2015) 13–17

Narayankhekar K.G., and Maiya M.P., (1985), "Investigation on triple fluid vapour absorption refrigerator". International Journal of Refrigeration. 8:335–42.

Niu, X.F., Du, K., and Du, S.X., (2007), "Numerical analysis of falling film absorption with ammonia–water in magnetic field", Applied Thermal Engineering 27. 2059–2065.

Nourafkan E., Asachi M., Jin H., Wen D., and Ahmed W., (2019), "Stability and photo-thermal conversion performance of binary nanofluids for solar absorption refrigeration systems". Renewable Energy 140 (2019) 264-273

Nourafkana, E., Asachia, M., Gaoa, H., Razaa, G, and Wena, D., (2017), "Synthesis of stable iron oxide nanoparticle dispersions in high ionic media". Journal of Industrial and Engineering Chemistry 50 (2017) 57–71

Olle B., Bucak S., Tracy C.H., Bromberg L., and Hatton A.T., (2006), "Enhancement of oxygen mass transfer using functionalized magnetic nanoparticles", Industrial and Engineering Chemistry Research 45 (2006) 4355–4363.

Orhan B., and Güngör A., (2012), "Absorpsiyonlu ve Adsorpsiyonlu İklimlendirme Sistemleri Performans Değerlendirmesi", Tesisat Mühendisliği - Sayı 130, 2012.

Park YM, and Sonntag RE. (1990), "Thermodynamic properties of ammonia-water mixtures: a generalized equation-of-state approach". ASHRAE Transactions 1990;96:150–9

Patel J., Pandya B., and Mudgal A., (2017) "Exergy based analysis of LiClH2O absorption cooling system", Energy Procedia 109 (2017) 261–269.

Pfaff, M., , R., Maiya, M.P., and Srinivasan Murthy S., (1998), "Studies on bubble pump for a water-lithium bromide vapour absorption refrigerator". International Journal of Refrigeration. 21:452–62.

Philip, J., and Shima P.D., (2012), "Thermal properties of nanofluids". Adv Colloid Interface Sci. 183–184:30–45.

Pinto R.V., and Fiorelli F.A.S., (2016) Review of the mechanisms responsible for heat transfer enhancement using nanofluids. Appl Therm Eng;108:720–39.

Pitatowsky I., Rivera W., and Romero RJ., (2001), "Thermodynamic analysis of monomethylamine-water solutions in a single-stage solar absorption refrigeration cycle at low generator temperatures". Sol Energy Mater Sol Cells 70:287–300

Prasher R., and Phelan EP., (2006), “Brownian motion-based convective-conductive model for the effective thermal conductivity of nanofluids”. ASME J Heat Transf 2006;128:588–595

Ranjan G., Swarnendu S., and Puri I.K., (2004), "Heat transfer augmentation using a magnetic fluid under the influence of a line dipole", Journal of Magnetism and Magnetic Materials 271 (2004) 63–73.

Rasheed AK, Khalid M, Rashmi W, Gupta TCSM, and Chan A. (2016), "Graphene-based nanofluids, and nanolubricants -review of recent developments". Renew Sustain Energy Rev 2016;63:346–62.

Rizvi IH., Jain A., Ghosh SK., and Mukherjee PS., (2013), “Mathematical modelling of thermal conductivity for nanofluid considering interfacial nano-layer”. Heat Mass Transf. 2013;49:595–600.

Rodríguez-Muñoz J. L., and Belman-Flores J. M., (2014), “Review of diffusion–absorption refrigeration technologies”, Renewable and Sustainable Energy Reviews 30, 145–153.

Safarik, M., (2008), "Solar cooling projects with water–LiBr absorption chillers" (German). In: Fünftes symposium solares kühlen in der praxis. Hochschule für Technik Stuttgart, Band, vol. 89. p. 81–90.

Saidur, R., Kazi, S.N., Hossain, M.S., Rahman, M.M., and Mohammed, H.A., (2011), "A review on the performance of nanoparticles suspended with refrigerants and lubricating oils in refrigeration systems". Renew Sustain Energy Rev;15:310–23.

Saravanan R, and Maiya MP., (1998), "Thermodynamic comparison of water based working fluid combinations for a vapour refrigeration system". Appl Therm Eng;18:357–68.

Sarkar J., Ghosh P., and Adil A., (2015), “A review on hybrid nanofluids: recent research, development and applications”. Renew Sustain Energy Rev; 43:164–77.

Schmid F., Bierling B., and Spindler K., (2019), "Development of a solar-driven diffusion absorption chiller", Solar Energy 177 (2019) 483–493

Schweigler, C., Costa, A., Högenauer-Lego, M., Harm, M., and Ziegler, F., (2002), Entwicklung und Betrieb einer 10 kW H2O/LiBr- Absorptionska ltemaschine. Band Zweittes Symposium Solares Kühlen in der Praxis, HfT Stuttgart, 10–11, juni S:110–134

Sekhar Y. R., and Sharma K. V., (2015), “Study of viscosity and specific heat capacity characteristics of water-based Al_2O_3 nanofluids at low particle concentrations”. J ExpNanosci 10(2):86–102.

SHARMA A., (2015), “Level set method for computational multi-fluid dynamics: A review on developments, applications, and analysis”, Sadhana Vol. 40, Part 3, pp. 627–652. c Indian Academy of Sciences.

Shelton, S.V., White, S. (2002). "Bubble pump design for single pressure absorption refrigeration cycles". ASHRAE Transactions.108:1–10

Singh K. P., and Singh O., (2019), "Thermodynamic Investigation of Solar Energy-Driven Diffusion Absorption Refrigeration Cycle". Advances in Fluid and Thermal Engineering, Springer Nature Singapore Pte Ltd. 2019

Singh S., Sharma K., Lal K., and Mani Tripathi N., (2015), "To study the behaviour of nanorefrigerant in vapour compression cycle- a review". IJRET. Volume: 04 Issue: 04 | Apr-2015, Available @ http://www.ijret.org

Smirnov, G.F., Bukraba, M.A., Fattuh, T., Nabulsi, B., (1996). "Domestic refrigerators with absorption-diffusion units and heat transfer panels.international journal of Refrigeration".19:208–18.

Sohel Murshed S.M., (2011), "Determination of effective specific heat of nanofluids". Journal of Experimental Nanoscience.Vol. 6, No. 5, October 2011, 539–546

Solangi, K.H., Kazi, S.N., Luhur, M.R., Badarudin, A., Amiri, A., Sadri, R., Zubir, M.N.M., Gharehkhani, S., and Teng, K.H., (2015), "A comprehensive review of thermo-physical properties and convective heat transfer to nanofluids". Energy. 89:1065–86.

Soo. W.JO., Sherif S.A., and Lear W.E., (2013), "Numerical simulation of saturated flow boiling heat transfer of ammonia-water mixture in bubble pumps for absorption–diffusion refrigerators", ASMJ.Therm. Sci. Eng. Appl. 6 (2013).

Sozen A., (2001), "Effects of heat exchangers on performance of absorption refrigeration system". Energy Convers Manage;42:1699–716

Sözen A., Özbaş, E., Menlik, T. İskender, Ü., Kılınç, C, and Çakır, M. T., (2015), "Performance investigation of a diffusion absorption refrigeration system using nano-size alumina particles in the refrigerant", International Journal of Exergy, Vol. 18, Issue 4, pp. 443-461.

Sridhara, V., and Satapathy, L.N., (2015), "Effect of nanoparticles on thermal properties enhancement in different oils – a review". Crit Rev Solid State Mater Sci. 40:399–424.

Srinivas K., Rajagopal M., and Suresh A.K., (2007), "Synthesis, characterization and testing for ferrofluids for mass transfer intensification", International Journal of Refrigeration 5 (2007) 1913–1928.

Steiu S., Salavera D., Bruno J.C., and Coronas A., (2009), "A basis for the development of new ammonia–water–sodium hydroxide absorption chillers", Int. J. Refrig. 32 (2009) 577–587.

Stierlin, H., Wassermann U., Dorfler W., and Bosel J., (1994), "Messungen an Diffusions-Absorptions-Warmepumpen (DAWP) (data recording on Diffusion-Absorption Heat Pumps (DAHP)". Report, Bundesamt fr Energiewirtschaft (BEW 92-019), Switzerland.

Stierlin, H.C., and Ferguson, J.R., (1990), "Diffusion absorption heat pump (DAHP)". ASHRAE Trans., 96: 3319-3328.

Sun D.-W., (1998), "Comparison of the performances of NH3-H 2O, NH3-LiNO3 and NH3-NaSCN absorption refrigeration systems", Energy Convers. Manage. 39 (1998) 357–368.

Sun DW., (1998), "NH3–LiNO3 and NH3–NaSCN absorption refrigeration system Comparison of NH3–H2O". Energy Convers Manage 1998;39:358–67

Sundar L., Singh M., and Sousa A., (2013), "Investigation of thermal conductivity and viscosity of Fe_3O_4 nanofluid for heat transfer applications". Int.Commun. Heat Mass Transf. 2013, 44, 7–14

Takahashi M., Shinbo K., Ohkawa R., Matsuzaki M., and Inoue A., (1993), "Nucleate pool boiling heat transfer of magnetic fluid in a magnetic field", Journal of Magnetism and Magnetic Materials 122 (1993) 301–304

Teja A. S. (1983) "Simple method for the calculation of heat capacities of liquid mixtures". J. Chem. Eng. Data 1983, 28, 83-85

Thermo Fisher Scientific Inc. web-based product information accessed at: https://www.thermofisher.com/order/catalog/product/379-0600#/379-0600. last accessed November 2020.

Thomsen, K., (2009)., "Electrolyte Solutions: Thermodynamics, Crystallization, Separation methods". https://doi.org/10.11581/dtu:00000073

Tiwari, A.K., Ghosh, P., and Sarkar, J., (2012), "Investigation of thermal conductivity and viscosity of nanofluids". J Environ Res Dev. 7(2):10.

Tsai T. H., Kuo L. S., Chen P.H., and Yang C.T., (2009), "Thermal Conductivity of Nanofluid with Magnetic Nanoparticles". PIERS ONLINE, VOL. 5, NO. 3, 2009.

Vajjha RS., and Das DK., (2009), "Experimental determination of thermal conductivity of three nanofluids and development of new correlations". Int J Heat Mass Transf. 2009;52:4675–82.

Vemuri, S., Kim, K.J., and Kang, Y.T., (2006), "A study on effective use of heat transfer additives in the process of steam condensation". International Journal of Refrigeration 29 (5), 724–734.

Von Platen, B.C., and Munters, C.G., (1928), "Refrigerator", US Patent 1, 685 - 764.

Wang L., and Herold, K.E., (1992), "Diffusion-absorption heat pump". Annual Report for Gas Research Institute, GRI-92/0262. Gas Research Institute, USA.

Wang S., Liu Y., Chen Y., Wang Q., Xu X., Chen G., and Deng S., (2019), "Experimental investigations on the temperature lift performance of a novel diffusion absorption heat transformer". Energy 170 (2019) 906-914

Won S., Chung H., and Lee H., (1991), "Simulation and thermodynamic design data study on double-effect absorption cooling cycle using water-LiBr-LiSCN mixture", Heat Recov. Syst. CHP 11 (1991) 161–168

Won S., and Lee W., (1991), "Thermodynamic design data for double effect absorption heat pump systems using water-lithium chloride—cooling", Heat Recov. Syst. CHP 11 (1991) 41–48.

Wu W.D., Pang C.W., and Sheng W., (2010), "Enhancement on NH_3/H_2O bubble absorption in binary nanofluids by mono nano Ag", Journal of Chemical Industry and Engineering (China) 61 (2010) 1112–1117.

Wu, W. D., Liu, G., Chen S. X., and Zhang, H., (2013), "Nanoferrofluid addition enhances ammonia-water bubble absorption in an external magnetic field", Energy and Buildings 57. 268–277.

Xu J., Yu B., Zou M., and Xu P., (2006), “A new model for heat conduction of nanofluids based on fractal distributions of nanoparticles”. J Phys D Appl Phys. 2006;39:4486–90

Xuan Y., and Li Q., (2000), “Heat transfer enhancement of nanofluids”, International Journal of Heat Fluid Flow 21 (2000) 58–64.

Xuehu, M., Fengmin, S., Jiabin, C., and Yang, Z., (2007), "Heat and mass transfer enhancement of the bubble absorption for a binary nanofluid". Journal of Mechanical Science and Technology 21. 1813-1818.

Yang L., Du D., and Zhang, X., (2012), "Influence factors on thermal conductivity of ammonia-water nanofluids", J. Cent. South Univ.19: 1622−1628

Yang, L., Du, K., Zhang, X., and Cheng, B., (2011), "Experimental study on enhancement of ammonia-water falling film absorption by adding nano-particles" [J]. International Journal of Refrigeration. 34(3): 640−647.

Yıldız, A., and Ersöz M.A., (2013), "Energy and exergy analyses of the diffusion absorption refrigeration system", Energy xxx (2013) 1-9

You, S. M., Kim, J. H., and Kim, K. H., (2003), "Effect of nanoparticles on critical heat flux of water in pool boiling heat transfer" [J]. Appl Phys Lett. 83 (16): 3374−3376.

Yu W., Xie H.Q., Chen L.F., and Li Y., (2010), "Enhancement of thermal conductivity of kerosene-based Fe3O4 nanofluids prepared via phase-transfer method", Colloids and Surfaces A 335 (2010) 109–113

Zemaitis J.F., Clark D.M., Rafal M., and Scrivner N.C., (1986), "Handbook of aqueous electrolyte thermodynamics". New York: American Institute of Chemical Engineers;1986.

Zhang L.Y., Wu Y.Y., Zheng H.F., Guo J.G., and Chen D.S., (2006). "An experimental investigation on the performance of bubble pump with lunate channel for absorption refrigeration system", Int. J. Refrig. 29 (5) (2006) 815–822.

Zhang S., Wu J.Y., Tse C.T., and Niu J.L., (2012), “Effective dispersion of multi-wall carbon nano-tubes in hexadecane through physiochemical modification and decrease of supercooling”, Solar Energy Materials and Solar Cells 96 (2012) 124–130.

Zhou S., Zhao X., Cai D., Deng J., Gao Y., and He G., (2021), "Experimental evaluation on flow boiling heat transfer of R290/POE-oil working fluid for absorption refrigeration in smooth horizontal tubes". International Journal of Thermal Sciences Volume 159, January 2021, 106641

Zhou S.Q., and Ni R., (2008), “Measurement of the specific heat capacity of water-based Al_2O_3 nanofluid”. ApplPhysLett 92(9):093123.

Zhu L., Gu J., (2009), "Thermodynamic analysis of a novel thermal driven refrigeration system", World Acad. Sci., Eng. Technol. 56 (2009) 351–355.

Ziegler B., and Trepp C., (1984), "Equation of state for ammonia-water mixtures". International Journal of Refrigeration 1984;7:101–6.

Zohar A, Jelinek M, Levy A, and Borde I. (2005), "Numerical investigation of a diffusion absorption refrigeration cycle". International Journal of Refrigeration 2005;28: 515–25

Zohar, A., Jelinek, M., Levy, A., and Borde, I., (2008). "The influence of the generator and bubble pump configuration on the performance of diffusion absorption refrigeration (DAR) system". International Journal of Refrigeration. 962-969.

Zohar, A., Jelinek, M., Levy, A., and Borde, I., (2009), "Performance Diffusion Absorption refrigeration cycle with organic working fluids". International Journal of Refrigeration. 32:1241–6.